

Using Pneumatic Dryer in the Pharmaceutical Industry – A Feasibility Study

Verwendung von pneumatischen Trocknern in der pharmazeutischen
Industrie –
Eine Machbarkeitsstudie

Master Thesis

Masterarbeit in der Studienrichtung
Verfahrenstechnik an der Technischen Universität Graz

Submitted July 2013

Name: Jakob Dominik Redlinger-Pohn, BSc.

Adress: Kirchengasse 16
4802 Ebensee

Mat. No.: 0730355

Advisor: Dipl.-Ing. Diana Dujmovic¹

Scientific Director: Univ.-Prof. Dipl.-Ing. Dr.techn. Johannes G. Khinast^{1,2}

¹ResearchCenter Pharmaceutical Engineering GmbH

²Institute for Process- and Particle Engineering, Graz University of Technology

Declaration

The work presented in this diploma thesis is to the best of my knowledge and belief, original, except as acknowledged in the text. This material has not been submitted, either in the whole or in part, for a degree at this or any other university

Place, Date

Signature

Eidesstattliche Erklärung

Ich erkläre an Eides Statt, dass ich die vorliegende Arbeit selbstständig und ohne fremde Hilfe verfasst, andere als die angegebenen Quellen nicht benutzt und die den benutzten Quellen wörtlich und inhaltlich entnommenen Stellen als solche kenntliche gemacht habe. Ich versichere, dass ich dieses Masterthema bisher weder im In- noch im Ausland in irgendeiner Form als Prüfungsarbeit vorgelegt habe.

Ort, Datum

Unterschrift

Acknowledgement

K1 Competence Center „RCPE” acknowledge support from the „K1-Project A3.11” supported by the COMET-programme of the Austrian Research Promotion Agency (FFG) - initiated by the Federal Ministry of Economy, Family and Youth (BMWFJ) and the Federal Ministry of Transport, Innovation and Technology (BMVIT). Funded by FFG, Land Steiermark and Steirische Wirtschaftsförderung (SFG).

Personal I acknowledge the support from the RCPE laboratory staff which performed the analytical measurements for this project.

Abstract

The spin-flash dryer (SFD) is a pneumatic dryer capable of handling a large variation of feed composition. In the SFD particles are dried in an agitated fluidized bed and ejected when dry. In the chemical industry the SFD is well implemented in production processes. To answer the demand of the pharmaceutical industry for new production processes the SFD was investigated mathematically, experimentally and with statistical analyses. The goal was to answer whether the SFD is of use for pharmaceutical drying operation or not.

A full fractional experimental plan was set up by use of design of experiments. Drying settings were investigated using adipic acid and ibuprofen as model substances. The influence of energy via heat was investigated with an extra set of experiments using lactose as the model substance. The importance of not exceeding critical material temperature during drying was shown for ibuprofen. Important product attributes are the residual moisture and the material damage. For all experiments the residual moisture was well below acceptable limits of 2wt%. Additional experiment conducted with flour led to unacceptable results. The feed formed dough couldn't be dried as consequence of its structure. Material damage was observed for all experiments. The extent depends on the material size, the agitator speed and the drying-air throughput. By SEM analyses debris or actual particle breakage could be identified. In addition changes of pore structure was found for adipic acid. Material residues had been found in the dryer during experiments. The amount of residue depends on the dryer settings as well as on the material itself. Different agitator concepts are suggested to minimize the material residues on the wall.

In the mathematical calculation the dryer performance for various feed flux and feed composition was investigated. For adipic acid the operational field was calculated. In agreement with the experimental results the feed conditions always led to residual moisture below the limit. It could be shown that the relative humidity of the inlet air has a significant impact on the operational field and the drying kinetics. Drying operations containing toxic solvents or particles can be calculated with these equations. The critical particle size in dependence on the air throughput was calculated. It shows that material breakage exhibited for adipic acid particles also results from the fact that feed particles are bigger than the critical particle size.

Concluding, it could be shown in this work, that the SFD can be used for drying in the pharmaceutical industry but with restriction in particle size and feed consistency.

Kurzfassung

Der Spin-Flash Dryer (SFD), ein pneumatischer Trockner mit rotierender Wirbelschicht zeichnet sich vor allem durch eine breite Feed Zusammensetzung aus. Dadurch findet er in der chemischen Industrie weite Verbreitung. Als Antwort auf die Forderung der pharmazeutischen Industrie nach neuen Prozessen wird der SFD mittels Experiment, statistischer Auswertung und durch mathematische Formulierung beschrieben. Das Ziel der Arbeit ist heraus zu finden ob der SFD für die pharmazeutische Industrie geeignet ist.

Dafür wird ein voll fraktioneller Versuchsplan mittels Design of Experiment erstellt. Der Einfluss von Trocknungseinstellungen wurde anhand der Modellschichten Adipinsäure und Ibuprofen untersucht. Der Einfluss der Trocknungsenergie wurde mit Laktose untersucht. Negative Auswirkungen von Temperaturen höher als kritische Materialwerte wurden anhand von Ibuprofen gezeigt. Für alle Experimente konnte eine Restfeuchte unterhalb des Grenzwertes von 2% erreicht werden. Experimente mit Mehl, welches einen teigigen Feed formte, zeigten, dass solche Produkte nicht getrocknet werden können. In allen Experimenten wurde Materialbruch beobachtet. Das Ausmaß hing dabei von der Partikelgröße, dem Luftdurchsatz und der Rotorgeschwindigkeit ab. Durch REM Untersuchung wurde festgestellt ob es sich um Partikelbruch oder Absplittungen handelt. Zusätzlich wurde für Adipinsäure Veränderungen in der Porenstruktur festgestellt. Für alle Versuche wurden Anlagerungen an der Trocknerwand festgestellt. Die Menge hing dabei von den Trocknungseinstellungen und dem Material selbst ab. Durch Überarbeitung des Rotorkonzeptes könnten diese Materialablagerungen verringert werden.

In der mathematischen Beschreibung wurde die Trocknerperformance in Abhängigkeit des Feedrate und der Feedzusammensetzung untersucht. Übereinstimmend mit den Experimentergebnissen ergaben sich für Adipinsäure Restfeuchten kleiner dem Limit im untersuchten Bereich. Die Feuchte der Trocknungsluft hat dabei signifikanten Einfluss auf die erzielbare Restfeuchte. Die Berechnungen lassen sich auch auf problematischen Trocknungsvorgängen mit toxischen Substanzen anwenden. Die Abhängigkeit der Grenzkorngröße vom Luftdurchsatz wurde gezeigt. Dabei war zu erkennen, dass Bruch vor allem von größeren Partikeln auf zu geringe Gasgeschwindigkeiten zurückzuführen ist.

In der Arbeit konnte gezeigt werden, dass sich der SFD für Trocknungsaufgaben in der pharmazeutischen Industrie eignet, jedoch mit Einschränkungen in der Feed Beschaffenheit sowie Partikelgröße.

Table of Content

1. Introduction	1
1.1. Opportunities for Engineers.....	1
1.2. API Isolation Processes and Solid Production	2
1.3. Dryer Selection	4
1.4. Aim of this Work.....	6
1.5. Thesis Outline.....	7
2. Spin-Flash Dryer	8
2.1. The Drying Process Step-by-Step [8], [9]	9
3. Material and Methods.....	11
3.1. Spin-Flash Dryer 47 (SFD47) from Anhydro/SPX.....	11
3.1.1. Components of the SFD 47.....	11
3.1.2. Control of the SFD 47.....	13
3.2. Design of Experiment (DoE).....	14
3.2.1. Experimental Set-Up.....	14
3.2.2. Worksheet: Main process DoE	15
3.2.3. Additional Investigation of the Drying Energy.....	18
3.2.4. Lab work.....	18
3.2.5. Analyses.....	18
3.3. Additional Experiments	19
3.4. On-Line Measurement	19
3.4.1. Temperature and Pressure.....	19
3.4.2. Residual Moisture	19
3.5. Off-Line Measurement	20
3.5.1. Residual Moisture	20
3.5.2. Particle Size Distribution (PSD)	21
3.5.3. Particle Surface Area	22
3.5.4. Scanning Electron Microscope (SEM) images	22

3.5.5.	Production Rate.....	22
3.6.	Materials	23
4.	Experimental Work.....	26
4.1.	Preliminary Experiments	26
4.1.1.	Drying of Pump Able Liquid Suspensions.....	26
4.1.2.	Feed composition	28
4.1.3.	Feed Rate Calibration	30
4.2.	Laboratory Work	31
5.	Experimental Results, Statistical Analysis and Discussion	33
5.1.	Results for Adipic Acid	33
5.1.1.	Process description	33
5.1.2.	Measured Results	34
5.1.3.	DoE Analyses	37
5.1.4.	Result Summary of Adipic Acid.....	43
5.2.	Results for Ibuprofen	44
5.2.1.	Process description	44
5.2.2.	Measured Results.....	45
5.2.3.	DoE Analyses	47
5.2.4.	Result Summary of Ibuprofen.....	48
5.3.	Results for Drying Energy (Lactose).....	49
5.3.1.	Process description	49
5.3.2.	Measured Results	50
5.3.3.	DoE Analyses	53
5.3.4.	Result Summary of DoE Heat Influence (Lactose).....	54
5.4.	Additional Experiments	55
5.4.1.	Influence of Surfactants	55
5.4.2.	Drying above the melting point	57
5.4.3.	Drying of Benzoic acid	58
5.4.4.	Drying of Salicylic Acid	60

5.4.5.	Drying of Acetyl Salicylic Acid.....	62
5.4.6.	Drying of Flour	64
5.4.7.	Summary of additional experiments	66
5.5.	Discussion and Conclusion of the Experimental Study.....	67
6.	Theoretical Description of the SFD 47	70
6.1.	Drying of Particles	70
6.2.	Balance Area.....	71
6.3.	Mass and Energy Balances	72
6.3.1.	Mass balance.....	72
6.3.2.	Energy balance.....	74
6.3.3.	Application of the Material and Energy Balances	77
6.3.4.	Sorption Isotherm	80
6.3.5.	Drying capacity.....	82
6.3.6.	Summary of Mass and Energy Balances.....	85
6.4.	Drying Kinetics and Evaporation Rate	86
6.4.1.	Heat-transfer coefficient	87
6.4.2.	Free Particle Surface for Evaporation.....	90
6.4.3.	Calculation.....	91
6.4.1.	Summary of Drying Kinetics and Evaporation Rate.....	95
6.5.	Particle Motion	96
6.5.1.	Solid Unit Operations	96
6.5.2.	Critical particle size $d_{p,crit}$	97
7.	Summary and Outlook.....	99
8.	List of Figures	106
9.	List of Tables.....	111
10.	Appendix	113
10.1.	Data	113
10.2.	Process data documentation	113

10.3.	List of all experiments	113
10.4.	List of DoE results	116
10.4.1.	Adipic acid.....	116
10.4.2.	Ibuprofen.....	117
10.4.3.	Heat Influence (Lactose).....	118
10.5.	Result Data of Additional Experiments	118
10.6.	List of DoE analyses	119
10.6.1.	DoE analyses adipic acid	119
10.6.2.	DoE analyses for Ibuprofen	121
10.6.3.	DoE analyses for heat influence (Lactose).....	122
10.7.	Comparison of Calculated Outlet Temperature to Experimental Data	124
10.8.	MatLab Code for equilibrium residual moisture.....	126
10.9.	MatLab Code for evaporation rate and drying time.....	127

Abbreviations

API	Active pharmaceutical ingredient
DoE	Design of Experiment
DSC	Differential scanning calorimetry
FDA	U.S. Food and Drug Administration
NIR	Near-infrared spectroscopy
PAT	Process Analytical Technology
PSD	Particle size distribution
R&D	Research and development
QBD	Quality by Design
SFD	Spin-flash dryer

Nomenclature

Symbol	SI – Unit	Definition
A_T	-	Ration of outlet gas temperature to solid temperature
c_D	-	Drag coefficient
c_p	J/(kg*K)	Specific heat capacity at constant pressure
D	m	Diameter
d_p	m, μm	Diameter of spherical particles
d_p^*	-	Dimensionless diameter of spherical particles
E	J/s, W	Heat flux, energy losses
E	W/m ²	Specific heat energy flux
F_{air}	kg/s	Air throughput
F_{solid}	kg/s	Feed rate
G	kg/s	Dry gas mass flow rate
G	m/s ²	Acceleration due to gravity, 9.81 m/s ²
H	J/kg	Enthalpy of pure substance
H	J/s, W	Enthalpy flux
h_{vl}	J/kg	Latent heat of vaporization
h_{X+1}	J/kg	Specific enthalpy of dry solid mass flow rate
h_{Y+1}	J/kg	Specific enthalpy of dry gas mass flow rate
J	kg/(m ² *s)	Specific mass flux of evaporating water, evaporation rate
K	1/Pa	Ratio of adsorption rate and desorption rate
L	m	Height of dryer

Symbol	SI – Unit	Definition
L	-	Ratio of dry solid mass flow rate and dry gas mass flow rate = S/G
L	m	Characteristic length
M	kg	Mass, Body weight
MM	kg/kmole	Molar mass
N	-	Number of particle size fractions in particle size distribution
N	rps, 1/s	Number of rotor revolutions, Agitator speed
P	W	Mechanical power
P	Pa	Total pressure
p_i	Pa	Partial pressure
P_{water}^S	Pa	Saturated partial water vapor pressure
q_3	-	Particle size density distribution
Q_3	-	Cumulative particle size distribution
R	m	Radius
R	J/(mole*K)	Molar gas constant, 8.314
S	kg/s	Dry solid mass flow
T	K	Absolute temperature
T	s	Time, Particle residence time
T_{drop}	°C	Wet-bulb temperature
T_{room}	°C	Room temperature
u_t	m/s	Terminal particle velocity
u_t^*	-	Dimensionless terminal particle velocity
V	m ³ /s	Dry gas volume flow rate
V	m/s	Gas velocity
W	kg/s	Mass flux of evaporating water
w_{solid}	-	Solid content on wet basis
X	m, μm	Particle size
X	kg _{water} /kg _{solid}	Liquid water content on dry basis
X	-	Number of surface locations with water adhering (Langmuir equation)
X_0	-	Number of available locations on the surface (Langmuir equation)
Y	kg _{water} /kg _{air}	Vapor water content on dry basis

Greek Symbols

Symbol	SI – Unit	Definition
α	W/(m ² *K)	Heat-transfer coefficient
ϕ	-	Particle form ratio
η	Pa*s	Dynamic viscosity
φ	-, %	Relative humidity
λ	W/(m*K)	Thermal conductivity
ρ	kg/m ³	Density

Dimensionless Groups

Symbol	Definition	Equation
Nu	Nusselt number	$Nu = \frac{h*L}{\lambda}$
Re	Reynolds number	$Re = \frac{d*u*\rho_g}{\eta_g}$
Pr	Prandtl number	$Pr = \frac{c_p*\eta}{\lambda}$

1. Introduction

In the near future years the pharmaceutical industry will undergo two major developments [1].

- 1) The worldwide prescription drug sales are forecasted to grow by 3.1% per year between 2011 and 2018. In comparison the growth of prescription drug sales in the early 21st century was around 9% dropping in 2009.
- 2) The pharmaceutical industry has to face major patent expiration in the years ahead. In 2012 a large number of blockbusters expired resulting in \$33bn of sales being lost.

In addition research proved to become more challenging [2]:

- 1) Cures for straight forward diseases are already found leaving more complex diseases (like HIV/Aids) to deal with. For them it is more difficult and by that also more expensive to find new promising cures.
- 2) Requirements by the authorities (such as FDA, EMA) to bring a new medical product on the market rose.

The outcome of these two developments in pharmaceutical research and development (R&D) is a lower clinical success rate. For the industry this development means that it will become more troubling and expensive to develop new drugs. This is coupled with forecasted healthcare costs for society and the public health care system.

1.1. *Opportunities for Engineers*

Searching for opportunities to decrease their expenses, pharmaceutical companies look at tools developed by chemical engineers for other sectors of the chemical industry like simulation tools for the optimization of distillation processes or reaction processes [2]. Enhanced process understanding can lead to significant cost reduction in drug production [3]. Extensive knowledge of available manufacturing processes allows easier and more accurate process definition for new drugs. This leads to shorter R&D time and simultaneously to a reduction in R&D costs. In addition deeper process understanding also allows better process control and thus leads to reduced production costs and reduced amount of waste products.

Chemical engineering can also contribute to satisfy customer demands, seeking safe, convening and reliable products. Successful examples from the particle engineering are e.g. an improved dry powder inhaler providing higher drug dose consistency and new concepts in oral dosage forms.

Seeing the benefit of process understanding on drug quality and being emphasized by academics and consultants, the U.S. Food and Drug Administration (FDA) launched their GMP (good manufacturing practice) program [4]. FDA encouraged companies to increase their process understanding by using process analytical technology (PAT) for online monitoring of processes and Quality by Design (QbD) to design processes required by the product. Benefits for the pharmaceutical industry are a greater freedom to modify operation parameters within a defined operation space after launching a product.

1.2. API Isolation Processes and Solid Production

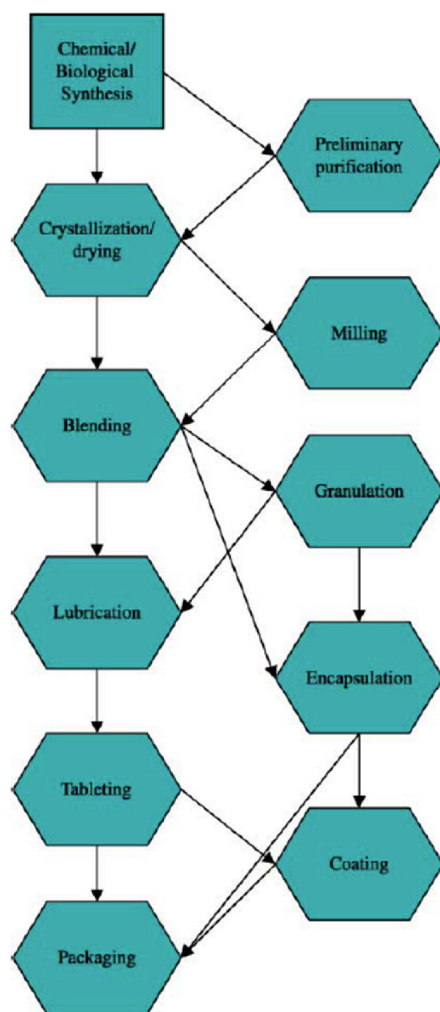


Figure 1-1: Production route of oral dosage forms [5].

its properties, like changes in crystal structure or degradation. The goal by crystallization and the following drying step is to achieve a stable product of high purity.

In figure 1-2 three routes of solid production are presented. In contrast to the process description above, there is no separate crystallizing and drying step for route 1, spray drying.

The dominating process to isolate and purify active drug substances called active pharmaceutical ingredient API is crystallization. Especially for the production of oral dosage form, which comprised roughly 80% of U.S. pharmaceutical consumption in 2002, crystallization is the first step in-line followed by several additional steps aiming to purify the API and increase its stability [5]. Several of such steps are listed in figure 1-1. As can be seen in the figure, the crystallization process is coupled with a drying process. This process step has a significant impact on the API quality. The product properties after the drying process are considered regulatory specifications [6]. The important product quality properties are the amount of residual solvent and residual moisture. Residual solvents are organic solvents from the production process which often are toxic. The impact of the residual moisture is mostly on the API stability. Depending on the API nature, the API can undergo different mechanisms, changing

However, as spray drying is a process implemented in the pharmaceutical industry, it is presented for the sake of completeness.

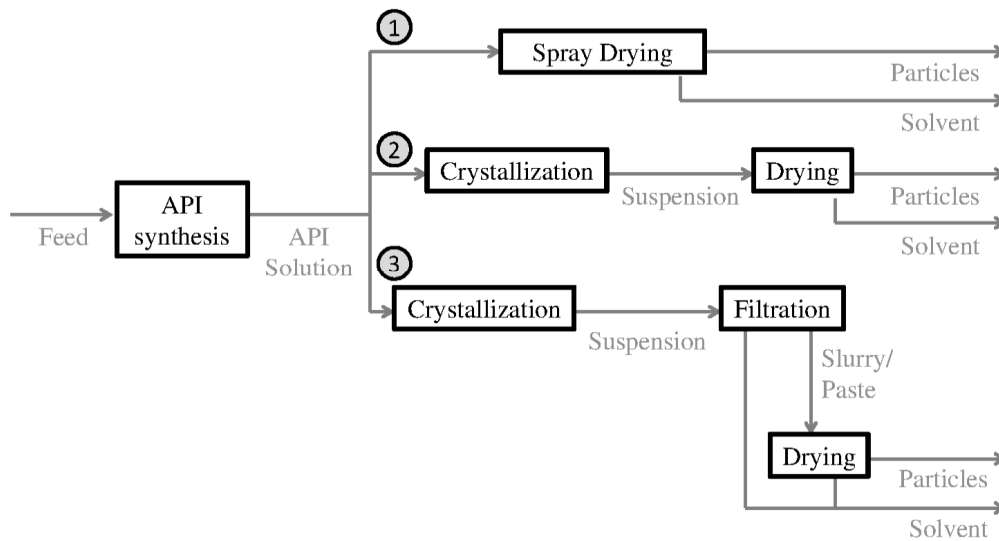


Figure 1-2: Pathways for producing API solids in the pharmaceutical industry.

In route 1, the API is directly dried out of solution by spray drying. Using spray drying, the solution is atomized and the drops are dried in a hot air stream. As the solvent is removed completely, all dissolved substances, impurities and API are crystallized. The impurities then will be found in the final product.

In route 2, the API is first crystallized and dried out of the suspension. This allows fulfilling of product requirements such as purity and stability. Furthermore it is possible to produce crystals or particles with defined crystal structure or particle size distribution using different crystallization settings.

In Route 3, crystallization is carried out like in route 2. But in the downstream of the crystallization the suspension is first filtered and then dried. Using filtration, the moisture is removed by mechanical force. Pressure difference between two sides of a phase separating filter cloth forces the liquid on the side of reduced pressure and retains the solids. Furthermore, the suspension can be washed by removing the mother liquor. As the mother liquor or supernatant is forced to flow through channels between solid particles building up a cake, the flow resistance increases and leads to a filtration stop. No completely dry product can be achieved solely by filtration. Mechanical removal of water is cheaper than evaporating the fluid which needs thermal energy.

Using thermal drying in conjunction with filtration can achieve drier products. The driving force here is the concentration difference for example of water between the drying air and the

solid surface. Depending on the saturation of the drying air (given by its relative humidity) solids can be bone dried (moisture = 0). For drying at high temperature heat recovery is used to reduce the energy cost. Pharmaceutical products which tend to be heat sensitive are dried at low temperature. Here heat recovery is not so efficient.

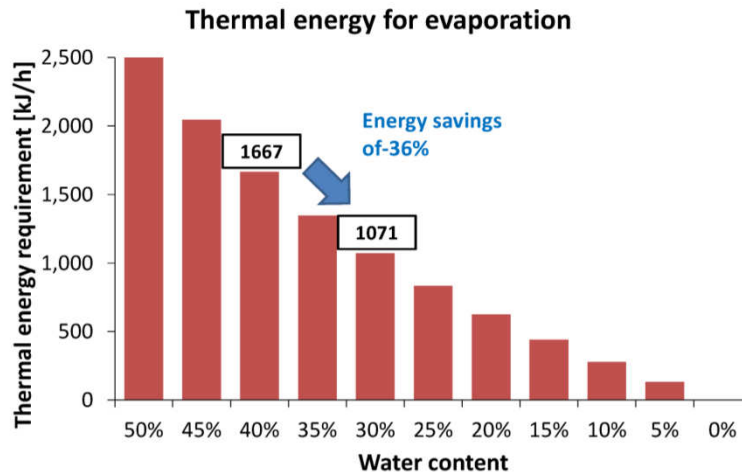


Figure 1-3: Thermal energy requirement to dry 1 kg/h solid with a given amount of water.

In figure 1-3 the energy required to bone dry solid material with given water content is shown. The solid stream is 1 kg/h and the latent heat of evaporation is 2500 kJ/h. It is illustrated that a large amount of energy can be saved for material with reduced water content. For example reducing the water content from 40wt% to 30%, which is a reduction of water content of 25% saves 36% of energy.

The maximum achievable solid content after filtration depends on the filtration process chosen and the properties of the solid particles such as particle size distribution, particle shape or affinity to the fluid. Designing a multi-purpose API production process changing feed composition has to account for the dryer feed. Typically product moisture of dryer feed after filtration is in the range of 5wt% to 50wt% but can be higher [6].

1.3. Dryer Selection

Developed for the chemical industry a large variety of dryers are on the market, most with adaptations to make them suitable for pharmaceutical production. Choosing a dryer for the solid production, the optimum feed water content as well as side effects, such as agglomeration and attrition have to be considered. Both of them result in a change of particle size and particle shape that can have an impact on later production steps or the drug dissolution. Also the drying time and possible material residues remaining in the dryer have to be considered.

A widely used drying system in the chemical industry is pneumatic or flash drying [7]. There the feed is dispersed in a hot air stream leading to large surface area benefitting the heat and mass transfer. High evaporation rate and short drying time are typical characteristics of a pneumatic dryer. This makes the dryer especially interesting for drying of heat sensitive

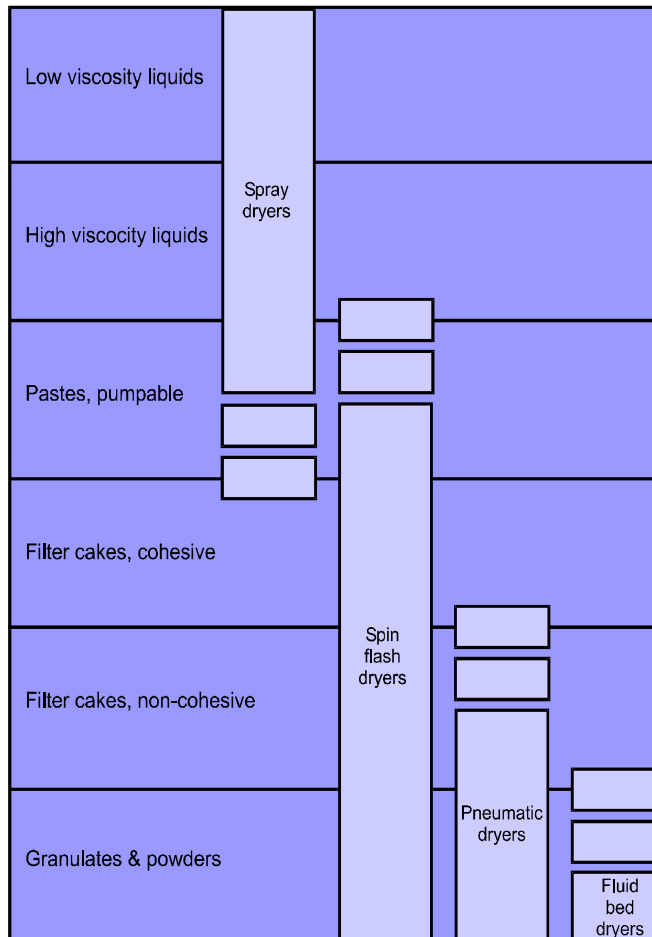


Figure 1-4: Solid dryer with dispersed particle and their hand able feeds [11].

materials. But they are also known for causing attrition. For products with bad drying kinetics, high levels of residual moisture could be the result and the product has to be recirculated into the drying process. The spin-flash dryer, a further development of the conventional pneumatic dryer has an integrated recirculation system. For that the spin-flash dryer has great potential to dry large variation of feed with different composition making it perfect for the needs described above. The spin-flash dryer is known by the standard literature ([8], [9]) and successfully used in the chemical industry for years [8]. The principle drying mechanisms are known and the dryer was successfully adapted to different types of products. Dryers designed for use in the pharmaceutical

industry are also available on the market [9]. However the design of the spin-flash dryer and the adaption of the apparatus on the product specification are still empirical. Pilot plant experiments have to be performed. The dryer is then optimized for one product type leaving its capability to dry another product doubtful.

Summing up the advantages of the spin-flash dryer, it's capability of drying various feeds consistently and heat sensitive materials as well as the short residence time the spin-flash dryer seems promising for drying pharmaceutical products. However further investigations are necessary to describe the dryer properly.

1.4. Aim of this Work

This work aims to increase the knowledge about the spin-flash dryer and investigate the feasibility of using the spin-flash dryer in pharmaceutical processes.

Predefined product requirements are

- residual moisture less than 2wt%,
- a minimum change in particle size distribution or at least a prediction of changes in the particle size distribution.

Predefined process settings are

- drying temperature equal or smaller than 80°C,
- low mass feed rates in the range of 1 kg/h (or less) to 5 kg/h,
- a variation in feed moisture.

The dryer will be investigated with statistical methods and design of experiment. Predictive models for the dryer type on hand can be generated from this analysis enabling the estimation of drying behavior for additional drying settings.

In addition it will be tested with principle equations known from drying operations to evaluate the spin-flash dryer and show its drying potential.

The outcome of this work will be the answer if required limits in residual moisture, the main target value can be met and which adaptations have to be made to make the spin-flash dryer fit for pharmaceutical usage.

1.5. Thesis Outline

In chapter 2 (Spin-Flash Dryer) the spin-flash dryer is introduced and its working principles are explained.

Chapter 3 (Material and Methods) explains the used dryer SFD 47 from Anhydro/SPX (Denmark) and its components. The concept of design of experiment (DoE) and how it was used for this study are explained. The analytical methods and the model substances for this study are listed.

In chapter 4 (Experimental Work) preliminary experiments, conducted to establish the dryer limitations and working behavior are presented. Following the dryer start-up and the drying experiment are described.

Chapter 5 (Experimental Results, Statistical Analysis and Discussion) offers the results of the experimental study. For the DoE analysis the result for every set of experiment is described followed by result data and statistical analysis. In the summary statistical models describing the effects of the used materials will be presented. In the second part of chapter 5 the additional conducted experiments with their results are presented. The chapter closes with a conclusion about the experimental study and the answer if the SFD 47 is capable of matching the requirements.

Chapter 6 (Theoretical Description of the SFD 47) shows how the dryer can be modeled using existing equations. The material and energy balance is solved and the data is compared to the experimental data from chapter 5. Building up on the equations the drying capacity and the drying time for an idealized system of spherical particles is calculated. Closing the material damage in dependence of particle size and air throughput is discussed.

Chapter 7 (Summary and Outlook) sums up the results from chapter 5 and chapter 6 and gives an outlook for further investigation which should be performed to describe the particle motion in the SFD.

2. Spin-Flash Dryer

In pneumatic drying solid or high viscous fluid feed is dispersed in a hot air stream of high velocity [7]. As the material is conveyed with the air the particles dry. The particles are later removed from the air stream by solid/gas separation (e.g. cyclone or cartridge filter).

As the particles are dispersed in the air stream the free particle surface in contact with the drying air is higher compared to other conventional dryer such as belt dryer. In addition the heat and mass transfer coefficient is enhanced by turbulent flow of the air. These two effects lead to high evaporation rates rapidly reducing the weight of the particles. The particles become fast airborne which leads to a short residence time of the particles (within seconds). The residence time can be adjusted in some degrees by a variable cross-sectional area [9]. Due to the water evaporation the temperature of the drying air reduces. The temperature of the air transporting the particles out of the drying zone is lower than the initial drying temperature. Both effects make the pneumatic dryer theoretically ideal for drying heat sensitive material.

However due to the short drying time, only free surface water or surface moisture can be removed whilst moisture bound in pores remains. If the residual moisture of the product is too high the product can be recycled into the drying process increasing the overall drying time. However, pore moisture cannot be removed completely by use of pneumatic dryers.

In addition sticky feed cannot be dispersed at the point of feed and will not dry properly in pneumatic dryers.

The spin-flash dryer SFD (also called an agitated flash dryer) operates under the same principles. Instead of a long pipe where particles are dried, the SFD has a rotor at the bottom of a vertical, short cylindrical pipe producing an agitated fluidized bed in which the particles are dried. Due to the rotor the particles are agitated and kept in motion allowing smaller gas velocity as compared to the pneumatic dryer. Particles are first dried in the agitated fluidized bed and then removed from the bed by following the air stream once airborne. This effect can be seen as internal recirculation reducing the disadvantage of pneumatic dryer having higher residual moisture.

The agitator disintegrates the feed supporting a fast increase of drying surface. In addition the agitator operated at optimal rotational speed supports a homogenous fluidized powder bed without bubbles or channels leading to maximal drying rate [10], [11], [12].

As shown in figure 2-1 the SFD consists primarily of 4 major components, the feed system (4), the drying chamber (1), the heater (2) and the exhaust air system (6) with the fan (3) to provide the air stream.

Following the steady-state drying process for the spin-flash dryer is outlined. During start-up the internal particle recirculation first has to be established and by that the process differs from steady-state production. The start-up procedure will be explained for some practical cases in chapter 4.2, page 31.

2.1. The Drying Process Step-by-Step [8], [9]

1. Feed is introduced into the feed vat (4). The feed vat can act as buffer. The agitation rotor of the feed vat homogenizes the feed. If the feed is solid like for filter cakes it will disintegrated. The feed is then extruded into the drying chamber (1).
2. In steady-state the feed entering the drying chamber is coated with fine and dry particles preventing the feed lumps sticking to the wall when falling into the dryer. Feed lumps and particles are drawn in green in figure 2-1.

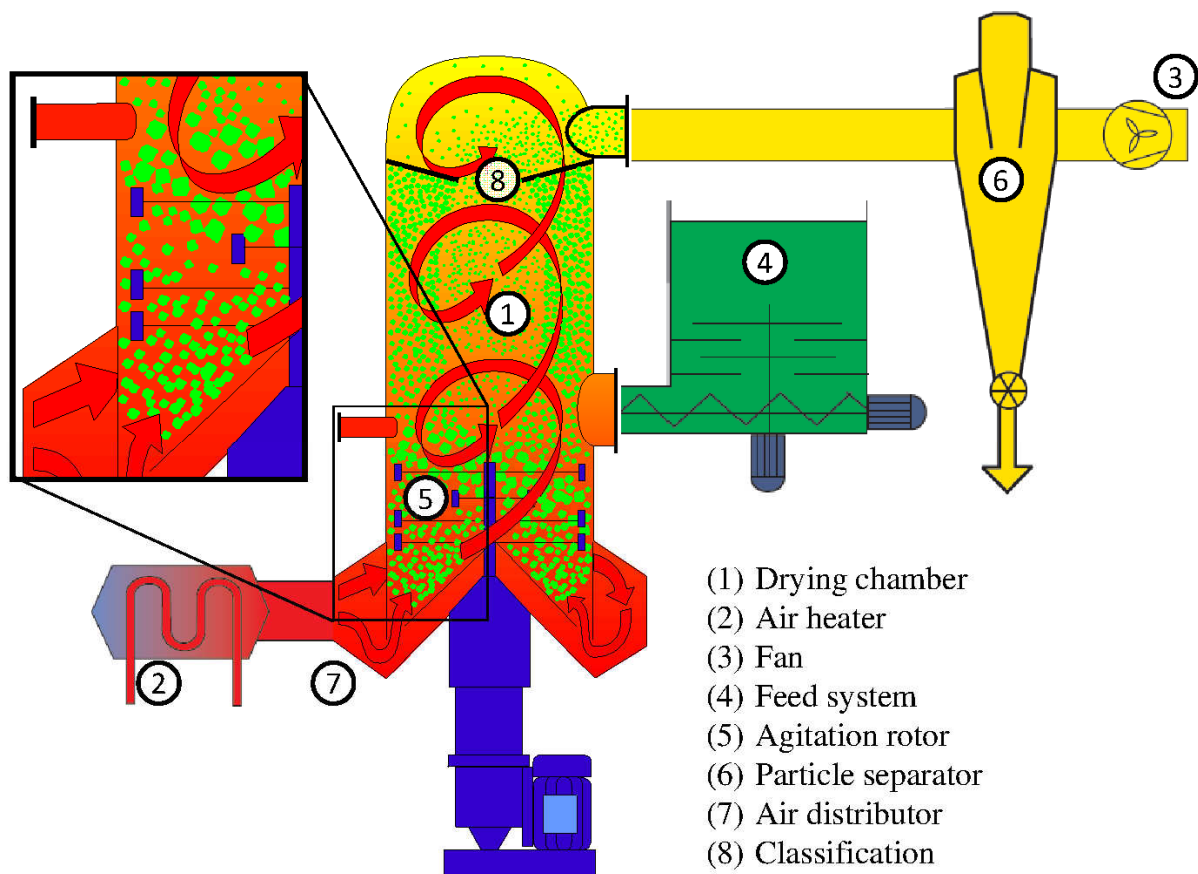


Figure 2-1: SFD consisting of the drying chamber, air heater, feeder and particle separator. Figure adapted from literature [7].

3. As the feed lumps are too heavy to follow the air stream upwards they fall down and pass through the agitator rotor blades. As shown in the detail view in figure 2-1, the lumps are reduced in size due to the mechanical action of the agitator (5) by attrition.
4. Rotating in the agitated fluidized bed at the bottom, the lumps and particles are dried by the hot air stream entering the dryer at the bottom.
5. The air stream first is heated (2) and enters the SFD tangentially at the bottom, passing through a small gap (7). By passing through the gap the air stream is distributed homogeneously along the circumference. The established flow pattern, a helical upwards flow is controlled by the air velocity and the classifier.
6. In the agitated fluidized bed particles or lumps are extensively mixed with the hot drying air improving the heat and mass transfer. The drying takes place at the surface of the particles and lumps which are reduced in size over time by the above mentioned mechanisms. By these steps (disintegration, attrition and drying) the particles in the fluidized bed become lighter over time.
7. Particles light enough then become airborne and leave the agitated fluidized bed. Following the air stream upwards they pass the feed entrance eventually covering fresh feed entering the dryer. Therefore a balanced fluidized bed is formed containing raw material and finished product.
8. Following the air stream further upwards the particles move along the wall in a helical way leading to higher particle concentrations on the wall.
9. At the end of the pipe the particles have to pass through a classifier (8). Heavier particles have more difficulty passing through the classifier and preferentially fall back into the dryer. Smaller and lighter particles follow the air stream and are removed by a particle separator (6).
10. The air stream then passes through a fan which sucks the air and the particles through the dryer.

The whole drying process is operated under low pressure preventing particles or evaporated solvent from leaking. This makes the SFD ideal for problematic substances which API's often can be.

The evaporation rate is typically in the range of 70 kg/(m²*h) to 300 kg/(m²*h). The residence time of particle spans from 5 s to 500 s [8]. Influences on the residence time might have the particle size, moisture load or consistency of the feed.

3. Material and Methods

3.1. Spin-Flash Dryer 47 (SFD47) from Anhydro/SPX

The spin-flash dryer SFD 47 (figure 3-1) was developed by the company Anhydro/SPX (Denmark) for pilot studies and small-scale production [9] and [13]. The drying chamber has a length of 937 mm and a diameter of 200 mm. The agitator is a rotor with 3 non-pitched blades. The feed vat can hold a volume of 42 L and the feed is transported into the dryer by a single screw. The range for production inlet temperature is 150°C to 350°C with an outlet temperature of 90°C. However as explained the drying temperature maximum in this study is 80°C. A cyclone is used for particle separation from the exhaust gas. The smallest removable size by the cyclone is 5 µm. The particles are collected in a basket which has to be emptied manually. The following detailed (table 3-1) description of the plant is from Anhydro “Original Operation and Maintenance Instructions Anhydro Small Scale Spin Flash Dryer Type SFD 47” [13].

3.1.1. Components of the SFD 47

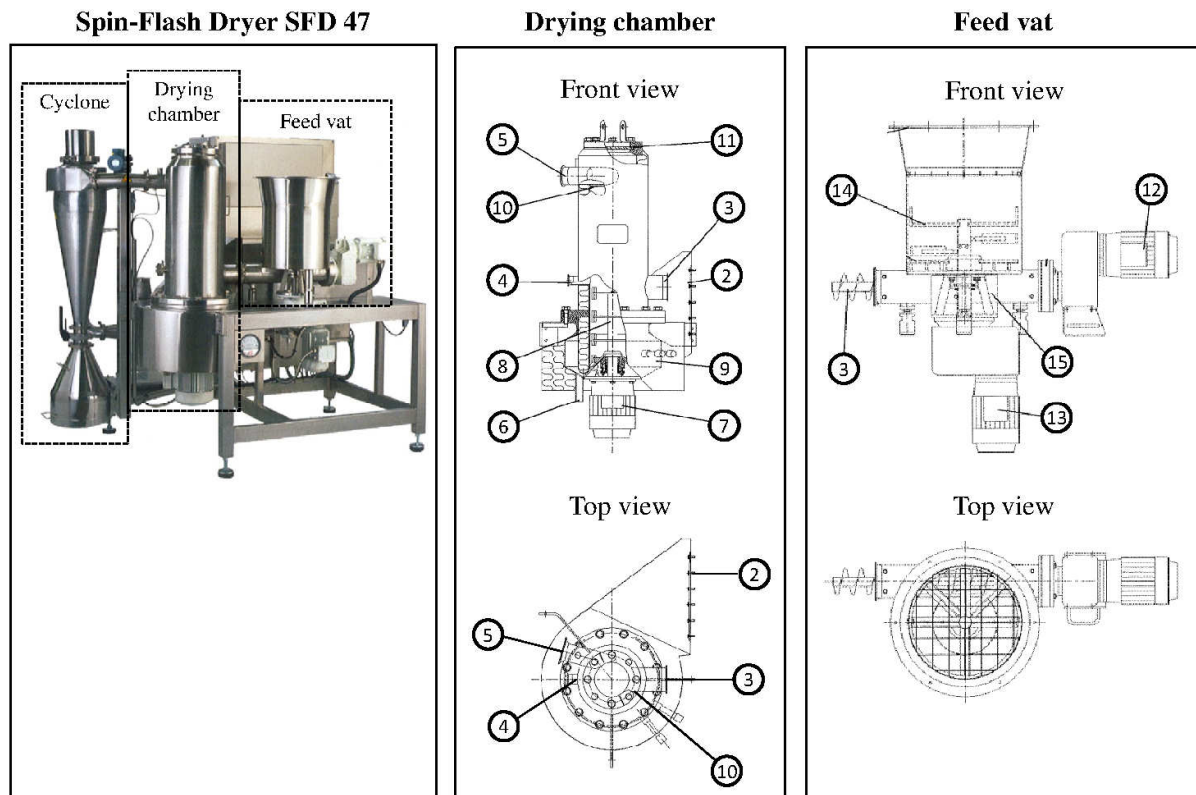


Figure 3-1: Spin-Flash Dryer SFD47 from Anhydro/SPX used for the feasibility study. According components are listed in table 3-1 [13].

Table 3-1: Main components of the drying unit SFD 47 [13].

Drying chamber		
(1)	Drying chamber	Heart component of the SFD 47 unit. Its height is 937 mm and its diameter is 200 mm. For insulation Vermiculite grade 3 is used. The insulation thickness is 47.5 mm.
(2)	Hot air inlet	Filtered and heated air is led into the air distributor.
(3)	Feed screw	Conveys non pump-able feed from the feed vat into the drying chamber. The speed of the feed screw is adjustable between 10 rpm to 41 rpm. The advised minimum speed is 10% of maximum speed which is 13.1 rpm. The feed speed used in this study is in the range from 10 rpm to 11.6 rpm.
(4)	Inlet for fluid feeds	Pump-able feed can be introduced into the drying chamber via a small connection pipe.
(5)	Powder duct flange	Connects the drying chamber with the cyclone. Position for the outlet temperature measurement.
(6)	Drain	Drain for emptying and cleaning the drying chamber and the feed vat.
(7)	Motor	Provides the necessary power to produce an agitated fluidized bed and to disintegrate feed lumps. Maximum power of 1100 kW and maximum rotation speed of 1400 rpm.
(8)	Agitator (Rotor)	Disintegrates the moist feed lumps and provides an even product layer (agitated fluidized bed). Scraper can help to clean the inner surface of the drying chamber.
(9)	Air distributor	Circular chamber where the hot air is set into rotation by a tangential inlet. The hot air is forced through a small gap at the bottom. Due to the high velocity, the air is distributed evenly across the gap. The insulation thickness of the air distributor is 100 mm.
(10)	Classifier	Aperture which prevents wet lumps or big and heavy particles from leaving the drying chamber. Two apertures with opening diameters of 60 mm and 80 mm were used.
(11)	Sight glass	Enables inspection of the SFD and optical process monitoring.
Feed vat		
(4)	Feed screw	See above.
(12)	Feed screw gear motor	Drives the feed screw and is always controlled by a frequency converter.
(13)	Agitator gear motor	Drives the feed vat agitator.

- | | |
|------------------------|---|
| (14) Feed vat agitator | Homogenizes the feed. Solid feed like filter cakes are broken up. Conveys the feed into the feed screw. |
| (15) Brackets | Support the feed vat. Optional weighing cells can be installed for monitoring the mass feed rate. Not installed for this study. |

3.1.2. Control of the SFD 47

The SFD can be controlled via a panel mounted on the side of the SFD. The main process parameters are adjustable as well as the controller settings. The SFD can be operated in automatic mode. The outlet temperature of the exhaust gas is measured after the drying chamber (TIC). The pressure drop over the drying chamber (PI) and over the cyclone (PIC) is also measured. Using near infrared spectroscopy (NIR) the residual moisture of the powder product is measured after the cyclone (QI). The NIR measurement was carried out separately and is no standard equipment of the SFD 47.

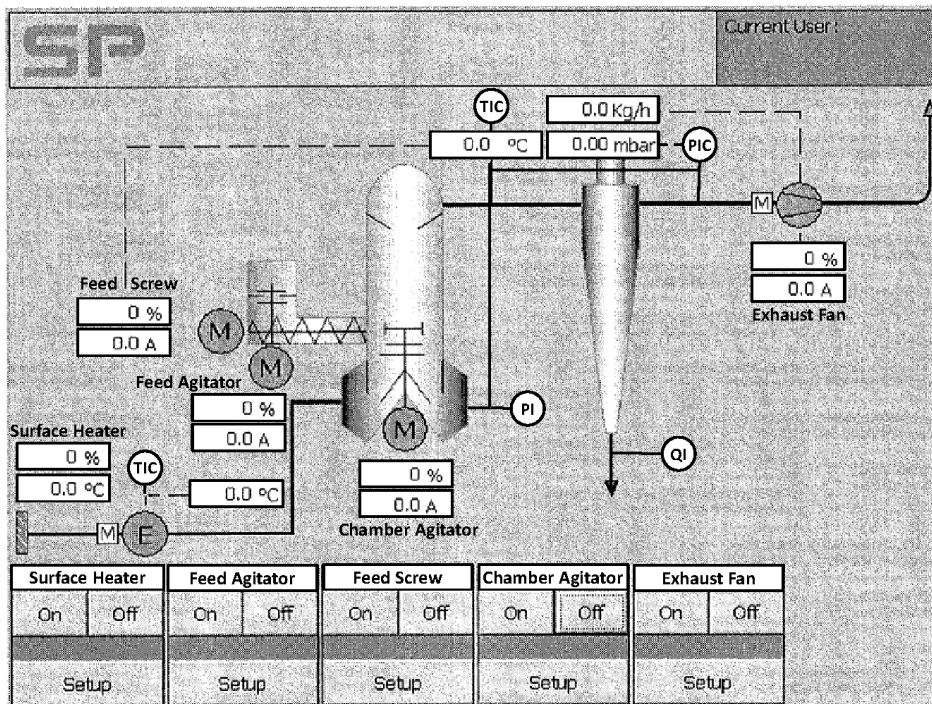


Figure 3-2: Control panel of the SFD 47 with measurement points are indicated. Adapted from [13].

To operate the SFD in automatic mode, an outlet temperature meeting target product quality has to be set. The velocity of the feed screw is adjusted to maintain the outlet temperature. However in this feasibility study the feed rate was set and the outlet temperature as well as the residual moisture was monitored. The inlet air is heated by a surface heater and the desired air temperature can be set. A stable inlet air temperature is necessary, which may be difficult for

low inlet temperatures, without overheating the heater. For operating the fan in automatic mode the pressure drop over the cyclone is measured. Fan speed is used to control gas flow rate, measured by the pressure drop.

3.2. Design of Experiment (DoE)

Design of Experiment (DoE) is a tool or concept used to define a set of experiments by use of statistical methods. The goal is to increase the information output of a set of experiments at a minimum number of experiments which have to be conducted.

Defined process parameters are varied simultaneously to determine not only the influence of one process parameter on the target value but also how interactions of process parameters will influence the target value. The results also allow a comparison of the effect to the noise. Prediction of the target value depending on the process parameter can be calculated.

For this feasibility study the software Modde V9.1 from Umetrics (Umetrics Inc./USA) was used to set up the experimental plan and to evaluate and interpret the experimental results [14]. The following 7 steps lead to a statistical predictive model for the SFD.

Table 3-2: 7 steps to generate a statistically predictive model by use of DoE.

1) Define factors	Experimental Set-Up chapter 3.2.1 (below)
2) Define responses	
3) Create Design	
4) Perform Experiments	Lab work chapter 4.2, chapter 31
5) Make model	Analyses chapter 5.1.3, page 37
6) Interpret Model	
7) Use Model	

3.2.1. Experimental Set-Up

In the experimental set-up the existing knowledge of the process and the quality targets of the products are taken to create a worksheet for the experimental study.

Process values which can affect critical product properties are named factors. For example for drying this can be the residual moisture. Hereby it is of interest how they could affect the target value and in what magnitude. Factors considered might be controllable or uncontrollable like room humidity or room temperature. Preparing the worksheet it is possible

to define parameters as controllable, uncontrollable or constant. Thereby the last two are not varied but recorded during the experiment.

With the theoretical knowledge about the process steps (chapter 2, page 8) the following factors listed in table 3-3 can be identified for the SFD 47. Note that these are first theoretical assumptions. The influence has to be verified by the experiment.

Table 3-3: Assumed factors for the SFD 47.

Product properties / responses	→	Process parameters / factors
Particle size	→	Agitator or rotor speed
Particle size	→	Air velocity, air stream
Particle size	→	Classifier dimensions
Residual moisture	→	Outlet temperature
Residual moisture	→	Feed rate
Residual moisture	→	Air throughput

The responses are critical product quality parameters to be controlled within a pre-defined range. These values have to be measured and documented for the DoE analyses. For the drying example these can be the residual moisture or the particle size distribution of the product.

With all this information a worksheet can be created. Using Modde it is possible to choose between three different models. Depending on the model the number of experiments and the output information varies. The model options are: a linear model (for screening and robustness tests) an interaction model (for screening) and a quadratic model (for optimization).

The DoE worksheets for this work were predefined and were not part of this work. However, a short explanation about the chosen factors and the range of variation will be given following.

3.2.2. Worksheet: Main process DoE

In this work the influence of factors as well as interacting influence of factors on the responses should be investigated. For that task the interaction model was chosen. In this model for every factor a low and a high value are chosen (full factorial design). Then every factor with its value is correlated to another factor. Automatically center points were placed at

the corresponding mean values. Experiments are performed once for every variation of the setting and are repeated thrice for the center points to get knowledge about the reproducibility. This leads to a total of 19 single experiments for a full DoE study.

Factors of the DoE

Table 3-4: Factors for the SFD DoE.

Factor	Type	Low	High	Center points
Air throughput	Controlled	200 kg/h	400 kg/h	300 kg/h
Agitator speed	Controlled	420 rpm	1400 rpm	910 rpm
Classifier size	Controlled	60 mm	80 mm	60 mm
Feed rate	Controlled	1 kg/h	3 kg/h	2 kg/h
Air temperature	Constant	70°C for ibuprofen / 80° for adipic acid		
Model substance	Constant	ibuprofen and adipic acid		
Solid content	Constant	self-adjusted (see chapter 4.1.2, page 28)		

Air throughput: As the dryer was coupled to the central exhaust system already, a minimum air throughput varying around 120 kg/h was previously established. To guarantee constant minimum air throughput for all experiments 200 kg/h was chosen as the low value. The high value of 400 kg/h is the upper limitation of the SFD fan.

Agitator speed: The maximum speed of 1400 rpm was chosen as the high value. The low level was defined as 30% of the maximum speed what resulted in 420 rpm.

Classifier size: The opening of the classifier installed was 80 mm which was chosen as the high value. In order to investigate the effect of the classifier a second one with a smaller opening of 60 mm was constructed in house which was the DoE low value. As no third classifier was available or constructed the classifier with the opening of 60 mm was used for the center point experiments.

Feed rate: As low value the minimum relative screw speed of 1% was chosen what corresponds to a feed rate of 1 kg/h. The high level was restricted by the amount of material available for the experiment and was set for 3 kg/h. The exact feed rate was determined by calibration (chapter 4.1.3, page 30). Even as it was not possible to run the experiments with the exact low and high levels, the ratio between high and low level was three and the ratio between center point and low level was two.

Model substance: In the DoE the model substance was regarded as constant factor. However to investigate material influence two complete DoE were performed for two different model substances adipic acid and ibuprofen (chapter 3.6, page 23).

Feed solid content: The solid content was set constant after first preliminary experiments. The concentration depends on the material used with the goal to have a thick pasty feed. However as will be explained later (chapter 4.1.2, page 28), the feed concentration varied during the experiment due to segregation at the beginning and drying over time. The actual feed concentration was estimated by sampling feed over time. So actually the feed solid content was uncontrollable but constant within boundaries.

Inlet air temperature: For adipic acid the inlet air temperature was set constant at 80°C as required by the aims of the work. For ibuprofen, having a lower melting point, the inlet air temperature was set at 70°C.

The resulting worksheet for adipic acid is shown in table 3-5. For ibuprofen the worksheet is similar but with lower inlet air as stated above. The run order is given by Modde with the goal to avoid systematic failures.

Table 3-5: DoE worksheet for adipic acid.

Exp No	Exp Name	Run Order	Controlled factor				Constant factor		
			Air throughput [kg/h]	Classifier opening [mm]	Agitator speed [rpm]	Feed rate [kg/h]	Inlet air temperature [°C]	Model substance	Feed solid content [wt%]
1	SFD 62 / DOE 01	19	200	60	420	1.19	80	Adipic acid	71
2	SFD 12 / DOE 02	1	400	60	420	1.19	80	Adipic acid	71
3	SFD 15 / DOE 03	4	200	80	420	1.19	80	Adipic acid	71
4	SFD 56 / DOE 04	13	400	80	420	1.19	80	Adipic acid	71
5	SFD 13 / DOE 05	2	200	60	1400	1.19	80	Adipic acid	71
6	SFD 60 / DOE 06	17	400	60	1400	1.19	80	Adipic acid	71
7	SFD 59 / DOE 07	16	200	80	1400	1.19	80	Adipic acid	71
8	SFD 14 / DOE 08	3	400	80	1400	1.19	80	Adipic acid	71
9	SFD 23 / DOE 09	6	200	60	420	5.34	80	Adipic acid	71
10	SFD 52 / DOE 10	10	400	60	420	5.34	80	Adipic acid	71
11	SFD 57 / DOE 11	14	200	80	420	5.34	80	Adipic acid	71
12	SFD 21 / DOE 12	5	400	80	420	5.34	80	Adipic acid	71
13	SFD 53 / DOE 13	11	200	60	1400	5.34	80	Adipic acid	71
14	SFD 24 / DOE 14	7	400	60	1400	5.34	80	Adipic acid	71
15	SFD 25 / DOE 15	8	200	80	1400	5.34	80	Adipic acid	71
16	SFD 58 / DOE 16	15	400	80	1400	5.34	80	Adipic acid	71
17	SFD 54 / DOE 17	12	300	60	910	3.26	80	Adipic acid	71
18	SFD 61 / DOE 18	18	300	60	910	3.26	80	Adipic acid	71
19	SFD 51 / DOE 19	9	300	60	910	3.26	80	Adipic acid	71

Responses of the DoE

Residual moisture: As stated in the aims the residual moisture is the crucial value for the product quality. The residual moisture was measured on-line by near-infrared spectroscopy (chapter 3.4.2, page 19) and off-line by Karl Fischer titration

(chapter 3.5.1, page 20). The results from Karl Fischer titration were used for the evaluation of the DoE.

Particle size distribution: Depending on the process a narrow or broad particle size distribution can be of advantage. However in both cases it is of interest if the particle size distribution is affected by the drying process and if it can be controlled. Measurement methods are explained in chapter 3.5.2, page 21.

Production rate: Even as dry particles are produced this guarantees no stable stationary process. Measuring the production rate gives a fast first impression if the process setting lead to a stationary process (chapter 3.5.5, page 22).

3.2.3. Additional Investigation of the Drying Energy

After investigation of the main factors of the drying process a set off smaller experiments was designed to further investigate the influence of the drying energy. For this DoE, lactose was used as hydrophilic model substance. The factors for this DoE were the air throughput, varied again from 200 kg/h to 400 kg/h with the center point at 300 kg/h and the inlet air temperature, varied from 60°C to 80°C with the center point at 70°C. The responses were the same as for the main DoE.

Table 3-6: Doe worksheet "influence of the drying energy".

Exp No	Exp Name	Run Order	Controlled factor		Constant factor				
			Inlet air temperature [°C]	Air throughput [kg/h]	Model substance	Classifier opening [mm]	Agitator speed [rpm]	Feed rate [kg/h]	Feed solid content [wt%]
1	SFD 75 / DOE TL01	1	60	200	Lactose	80	910	3	70
2	SFD 80 / DOE TL02	6	80	200	Lactose	80	910	3	70
3	SFD 76 / DOE TL03	2	60	400	Lactose	80	910	3	70
4	SFD 79 / DOE TL04	5	80	400	Lactose	80	910	3	70
5	SFD 77 / DOE TL05	3	70	300	Lactose	80	910	3	70
6	SFD 78 / DOE TL06	4	70	300	Lactose	80	910	3	70
7	SFD 81 / DOE TL07	7	70	300	Lactose	80	910	3	70

3.2.4. Lab work

The task of the laboratory work now is to fill the response list with data according to the worksheet. This is the first part of this thesis and will be explained in chapter 4, page 26.

3.2.5. Analyses

In the analyses the responses are correlated to the factors. Insignificant factors are excluded and a statistical predictive model can be generated. The analyses will be explained exemplarily for the DoE adipic acid (chapter 5 page 33).

3.3. Additional Experiments

In addition to the DoE investigation further experiments were conducted. Process settings which weren't covered by the DoE are qualitatively investigated as well as additional products were dried at similar conditions as during the DoE study.

Performed experiments for qualitative investigation are drying of pump-able feed (chapter 4.1.1 page 26), drying above critical temperature of the material and the influence of surfactants (chapter 5.4 page 55).

Products dried with the SFD after DoE investigation and the additional qualitative experiments are benzoic acid, salicylic acid, acetylsalicylic acid and flour.

3.4. On-Line Measurement

3.4.1. Temperature and Pressure

As shown in figure 3-2 the inlet and outlet temperature of the gas as well as the pressure drop over the cyclone were measured in-line and the data was processed by the dryer unit control. The temperature is measured by a PT100 probe. The pressure drop over the cyclone is measured by a differential pressure transmitter. Automatic data logging for later evaluation was not possible. Therefore these data as well as the pressure drop over the drying chamber which was only displayed on a manometer had to be documented by hand for every experiment.

In addition to this data, further process data displayed on the control panel and environment data (temperature and relative humidity) were documented on paper for later evaluation. The documentation is exemplarily shown in the appendix, chapter 10.2, page 113. The documentation language was German.

3.4.2. Residual Moisture

Residual moisture was measured online via near-infrared spectroscopy (NIR). NIR is a fast and nondestructive technique for real-time measurement. The NIR probe used is from Sentronic GmbH (Germany). The NIR probe was positioned in a flange between the cyclone and the product container (figure 3-3, left).

At the position of the flange the product particles are separated from the air stream. This ensured a high concentration of particles crossing the probe lens. Monochromatic light from an external source is emitted by the NIR probe (figure 3-3, right). Particles passing by the

probe reflect the light and the spectrum is recorded for post processing. The absorption bands in NIR are typically broad and in the range of 780 nm to 2526 nm [15]. The characteristic absorption bands for water are roughly at 1400 nm and 1900 nm.

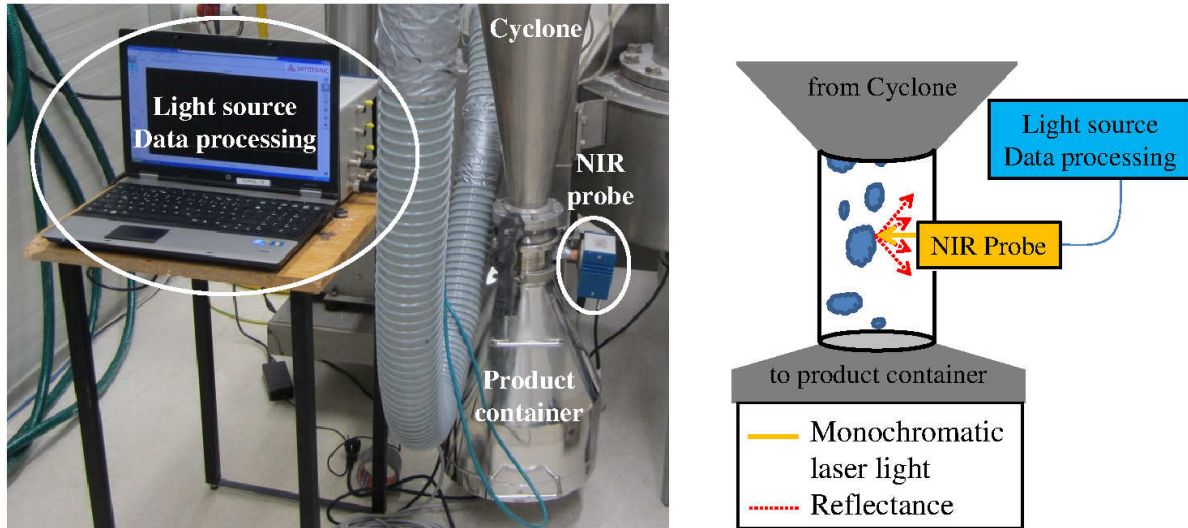


Figure 3-3: NIR measurement principles and NIR probe position.

Generally speaking, NIR is a well described measurement method to detect moisture and is already used by the pharmaceutical industry and accepted by regulatory agencies. Further advantages are that, not only water content of the dried particle can be measured but also residues of organic solvent, with limitations [16]. As particles are not only dried from watery solutions other residues might need to be detected. Another advantage is that with NIR it is possible to differentiate between bound water and surface water [17].

In this work only the on-line measurement is done in parallel to the drying experiments to generate data. The evaluation and post-processing of the spectrum are not part of this thesis.

3.5. Off-Line Measurement

3.5.1. Residual Moisture

For evaluation of the DoE analyses and the validation of the NIR data the residual moisture for every DoE experiment was measured by Karl-Fischer titration, a standard method to determine small amounts of water [18]. The titration was performed by the RCPE laboratory staff using the measurement device Titro Line KF from SCHOTT. For the titration the titration media (Combi Titrat) was calibrated thrice. The measurement then was performed twice and the excess of iodide is determined potentiometricly. The mass of water contained

by a certain mass of sample can be calculated and then from that, the residual moisture content.

The sample for Karl-Fischer Titration was taken right after drying from the whole batch and the container (150 mL) was sealed with Parafilm, a plastic paraffin film, to avoid water exchange with the environment.

3.5.2. Particle Size Distribution (PSD)

The particle size distribution PSD measurement was performed by the RCPE laboratory staff. Depending on the range of particle size the PSD was either measured by laser diffractometer HELOS/KR (Sympatec, Germany) for small particles or by image analyzer QICPIC (Sympatec, Germany) for bigger particles.

The laser diffractometer was equipped with the dry dispersing unit HELOS. Dispersion pressure was 2.5 bar with an injection opening of 4 mm. Measurement ranges were 4.5 μm to 875 μm for particles with $x_{\text{max}} > 80 \mu\text{m}$ and 0.45 μm to 87,5 μm for particles with $x_{\text{max}} < 80 \mu\text{m}$. Each measurement was performed thrice.

The image analyzer QICPIC was equipped with the dispersing unit Rodos. Dispersion pressure was 1.5 bar with an injector opening of 4 mm. Measurement range was 20 μm to 2000 μm . The resulting particle diameter is the diameter of the circle of same area (EQPC).

The result of the PSD measurement is the particle size density distribution (q_3) and the cumulative particle size distribution (Q_3). From them it is possible to calculate typical values like the median diameter x_{50} or the material damage to compare the results.

$$\text{material damage} = \frac{x_{50, \text{product}}}{x_{50, \text{feed}}} \quad (3-1)$$

Also the 2 parameters of the RRSB distribution (Rosin, Rammler, Sperling, Bennett) were calculated by use of least squares sum fit. The parameters of the RRSB distribution are the location parameter x' giving the range of particle size and the spread of distribution n .

$$Q_3(x) = 1 - \exp\left(-\left(\frac{x}{x'}\right)^n\right) \quad (3-2)$$

3.5.3. Particle Surface Area

The particle surface area measurement was performed by the RCPE laboratory staff using TRISTAR measurement unit.

The sample was degased for 12 h at 0.1 mbar and room temperature. A N₂-isotherm was measured with 70 sample points between the relative pressure of 0.01 and 0.99. The BET specific surface area was calculated with 8 sample points between the relative pressure of 0.05 and 0.20. BET surface area is then used to determine the particle specific surface area.

3.5.4. Scanning Electron Microscope (SEM) images

Using ESEM Tescan 500 PA with EDX high magnitude images of the product could be taken to analyze the shape and get an optical impression of the particle size.

Carbon tape was used to fix the sample on the probe. The sample was spattered with gold/palladium. Electron intensity was chosen to match the sample melting point and heat capacity and was either 20.00 kV or 10.00 kV. Images were taken at different magnification levels.

3.5.5. Production Rate

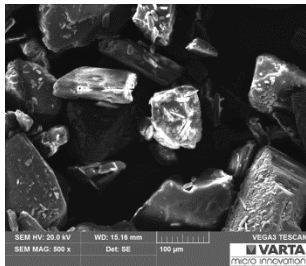
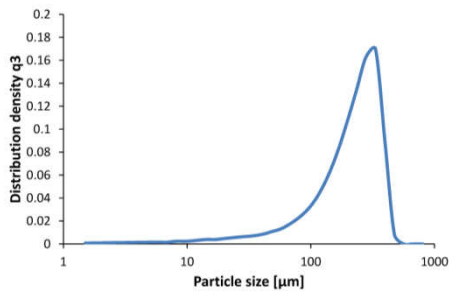
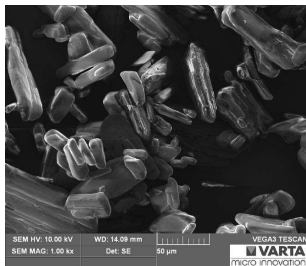
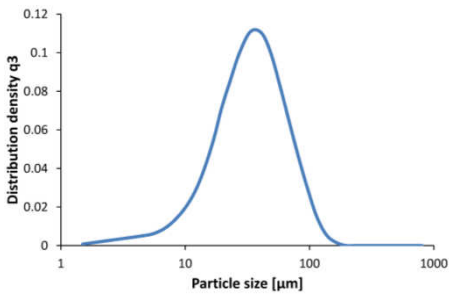
As soon as steady state conditions were reached the product container was emptied and time was recorded. Later the produced powder was weighed and the mean output over the production time calculated.

$$production\ rate = \frac{material\ in\ the\ product\ container}{production\ time} \quad (3-3)$$

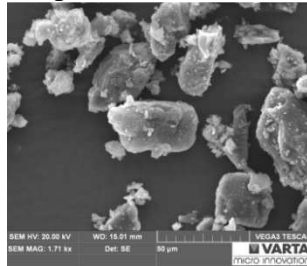
3.6. Materials

Several organic materials have been examined that serve as model substance for pharmaceutical substances. The model substances comprise a large variation in physical properties, are easily available and easy to deal with, which means their bio-activity should be low. Materials used for the DoE experiments were adipic acid, ibuprofen and lactose (Granulac 230). Material used for additional experiments were benzoic acid, salicylic acid, acetylsalicylic acid and flour. These model materials and their physical properties are listed in table 3-7. The materials were suspended in water, water/iso-propanol or water with sodium pyrophosphate tetrabasic. The slurry composition for the experiments is listed in table 4-1.

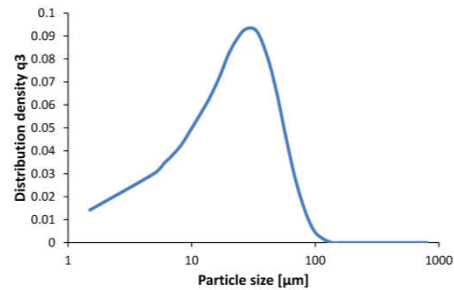
Table 3-7: Properties of the materials used for the DoE study.

Material Producer	Powder and particle characterization	Particle size and distribution	Physical properties
Adipic acid Merck (Germany)	Easy flowing particles. Shape: Cubes.	$x_{10} = 76.16 \pm 2.66 \mu\text{m}$ $x_{50} = 233.29 \pm 1.96 \mu\text{m}$ $x_{90} = 363.15 \pm 1.04 \mu\text{m}$	Melting point 151°C Hydrophobic
	 Magnitude 500		
Ibuprofen BASF (Germany)	Ibuprofen25. Bad flowing powder. Tends to form agglomerates and exposes adhesive behavior. Shape: Voluminous needles.	$x_{10} = 13.35 \pm 0.15 \mu\text{m}$ $x_{50} = 34.13 \pm 0.30 \mu\text{m}$ $x_{90} = 73.44 \pm 0.60 \mu\text{m}$	Melting point 77°C Hydrophobic
	 Magnitude 1000		

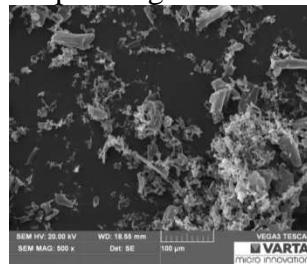
Lactose MEGGLE (Germany)	Granulac 230.	$x_{10} = 3.19 \pm 0.09 \mu\text{m}$	Melting point 233°C Hydrophilic
	Monohydrate crystals.	$x_{50} = 19.23 \pm 0.25 \mu\text{m}$	
	Flow able powder.	$x_{90} = 50.12 \pm 0.35 \mu\text{m}$	
	Tends to form agglomerates. Shape: Cubes.		



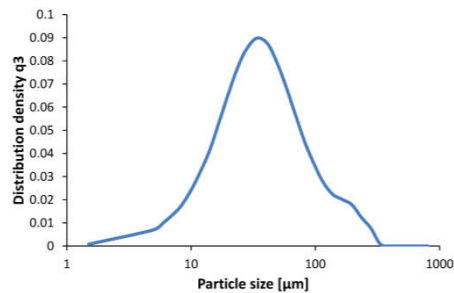
Magnitude 500



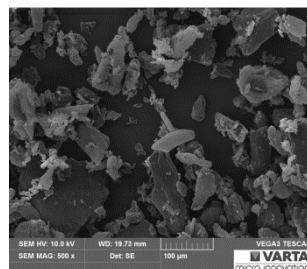
Benzoic acid Merck (Germany)	Milled particles. Flow able with dust formation.	$x_{10} = 46.60 \pm 0.59 \mu\text{m}$	Melting point 122°C Hydrophobic
	Shape: Irregular.	$x_{50} = 110.43 \pm 1.83 \mu\text{m}$	
		$x_{90} = 291.20 \pm 1.91 \mu\text{m}$	



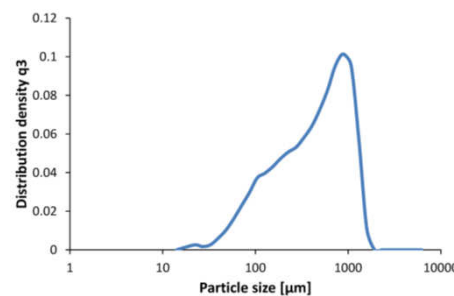
Magnitude 500



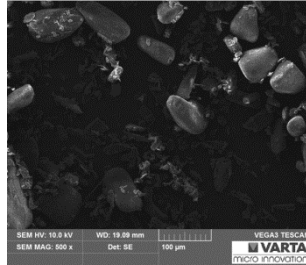
Salicylic acid Alfa Aesar (Germany)	Flow able powder.	$x_{10} = 99.04 \pm 3.28 \mu\text{m}$	Melting point 159°C Hydrophobic
	Shape: Cylindrical.	$x_{50} = 467.24 \pm 23.08 \mu\text{m}$	
		$x_{90} = 1111.66 \pm 39.74 \mu\text{m}$	



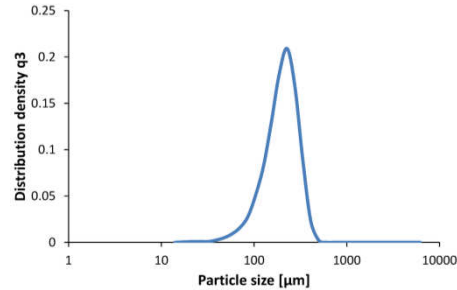
Magnitude 500



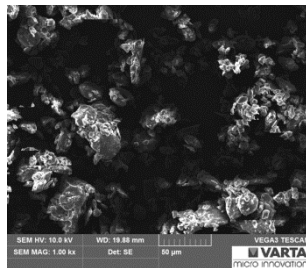
Acetyl salicylic acid GL-Pharma (Austria)	Rhodine 3080. Flow able with dust formation.	$x_{10} = 109.17 \pm 0.44 \mu\text{m}$	Melting point 135°C Hydrophobic
	Shape: Cubes.	$x_{50} = 204.18 \pm 0.46 \mu\text{m}$ $x_{90} = 315.07 \pm 0.59 \mu\text{m}$	



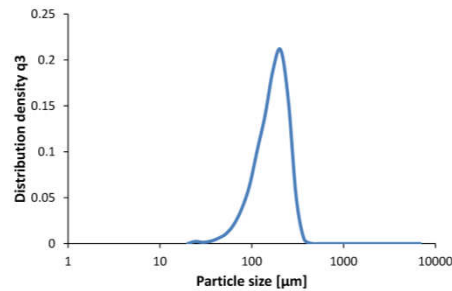
Magnitude 500



Flour Delikatessa (Austria)	Commercial flour “Clever® glatt”. Bad flow able powder forming avalanches.	$x_{10} = 82.49 \pm 0.09 \mu\text{m}$	No actual melting point but flour will disintegrate. Denaturation of amino acids at 67°C Hydrophilic
		$x_{50} = 157.48 \pm 0.50 \mu\text{m}$ $x_{90} = 238.10 \pm 0.72 \mu\text{m}$	



Magnitude 1000



Iso-propanol: VWR (France), purity is for technical usage.

Sodium pyrophosphate tetrabasic: Aldrich chemistry (USA) with a purity of $\geq 95\%$.

4. Experimental Work

First preliminary experiments were conducted to determine the achievable feed rate.

Second the DoE experiments were conducted to qualitatively evaluate the drying behavior of the SFD 47.

Third the additional experiments were conducted. Building up on the knowledge gained from the DoE experiments, some further parameters were investigated.

All conducted experiments were documented and labeled by “SFD” followed by a two digit number. For example SFD 01 stands for the first experiment. Additional DoE experiments were labeled with “DOE” followed by a number stating their run order in the worksheet. All experiments conducted are listed in the appendix (chapter 10.3, page 113).

4.1. *Preliminary Experiments*

4.1.1. **Drying of Pump Able Liquid Suspensions**

As described by Anhydro/SPX the SFD is capable of drying liquid suspensions [9]. For that the feed has to be introduced by a pump preferably using an atomizer to generate a spray of small particles which can be dried in the hot air stream. Additional literature states that drying of liquid suspensions is possible in a pneumatic dryer by recirculation, meaning that a powder bed is established in the dryer acting as dry carrier particles for the wet feed [19].

For the SFD the powder bed is established by agitation. However no atomizer was available. In an early conducted experiment the liquid suspension therefore was only pumped into the SFD by a small pipe to check if drying is possible without the use of an atomizer. As shown in figure 4-1 the set-up consisted of a stirred feed vat and the peristaltic pump IP65 (ISMATEC, Germany). The feed pipe was kept as short as possible to avoid particle settling. The feed was introduced just above the agitator. The pipe was inserted into the process chamber approximately one fourth the height of the cylinder diameter. The feed slurry was continuously stirred. As a model substance, a 45.5wt% adipic acid in iso-propanol/water (5wt% iso-propanol) mixture was prepared.

The principal idea of the set-up was that droplets of the pump-able feed fall directly on the agitator where they break into smaller droplets which are faster to dry.

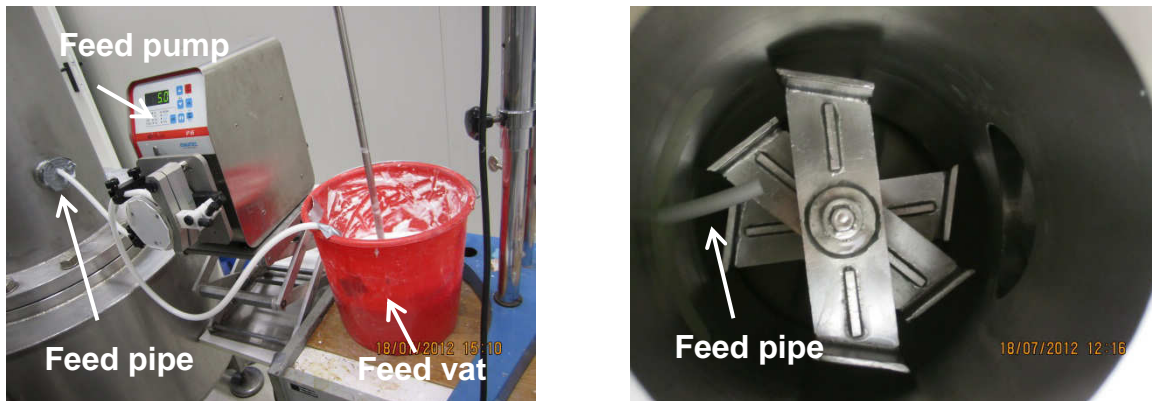


Figure 4-1: Process set-up for drying of liquid suspension feed, experiment SFD 18.

However when running the experiment droplets were caught by the circulating air and thrown onto the wall. Reduction of the air throughput led to minimal improvements. The droplets formed a material layer on the wall (figure 4-2, left). The layer was dried on the surface by overflowing hot air. When thick enough, material was scrapped from the layer (figure 4-2, right). Even with an established bed, droplets settled on the material layer making it bigger and increasing the amount of material scrapped off and dried.

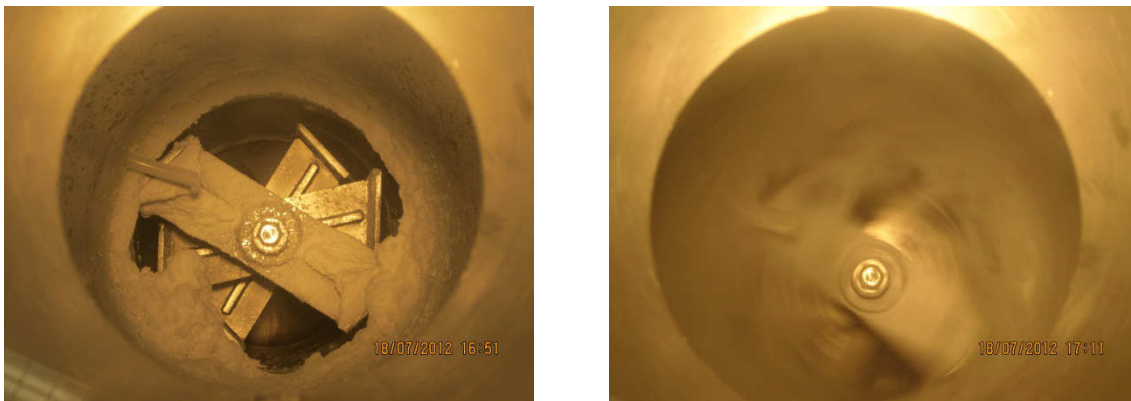


Figure 4-2: In-process pictures of experiment SFD 18.

Controlled drying of the adipic acid slurry was not possible with the present equipment. Particle residues on the wall continued to grow over time.

In addition a second experiment pumping liquid lactose feed into the SFD was conducted. The results were similar to these from the above experiment with adipic acid.

In conclusion it can be said that drying of pumpable (with solid content of 45.5wt%) feed is not possible with the present equipment. Therefore, experiments for this feasibility study can only be conducted with pastes and slurries as feed.

4.1.2. Feed composition

The solid content of the feed was determined empirically. In a given and noted amount of continuous phase, later called fluid, solid material was mixed in until a thick and pasty slurry was produced. The solubility of the material in the fluid was taken from the literature. The solid concentration of the suspension then can be calculated with equation (4-1).

$$\text{solid concentration} = \frac{\text{mass of solid material} - \text{mass of dissolved material}}{\text{mass of solid material} + \text{mass of fluid}} \quad (4-1)$$

The continuous phase was prepared according to the RCPE internal report “model substances” [20]. Differing from the instructions in the internal report, changes of tensile concentration were made for ibuprofen DoE experiments. Slurries used in this feasibility study and their solid concentration are listed in table 4-1.

Upon filling the feed into the feed vat fluid segregated from the slurry and entered the dryer immediately. Even as the feed in the feed vat was stirred by the feed vat agitator particle settled reducing the interparticle space. As a result the actual feed concentration was reduced. The feed concentration as fed into the dryer was measured for the DoE experiments and is listed in table 4-1. The concentration changed for the hydrophobic feed materials (adipic acid, ibuprofen, benzoic acid, salicylic acid and acetyl salicylic acid). For hydrophilic feed materials (lactose and flour) there was no segregation and thus no change of concentration. Both formed dough like feed.

In addition the feed concentration in the feed vat changed over time as it was dried. As only a small amount of feed material was prepared for the feasibility study enough air was present in the feed vat above the slurry to result in drying out of the feed. Sealing of the feed vat didn't change the effect.

Table 4-1: Feed concentration. Slurries for the DoE experiments are highlighted grey.

Material	Solid concentration [wt%]		Fluid / Solubility
	as produced	as fed	Description of the slurry
Adipic acid	71	77	Water/Iso-propanol 5wt% / 27 g/L Easily disperseable. Slurry consisted of discrete particles with surrounding fluid
Ibuprofen25	40	47	Water / 0.2 g/L First stirred at low and then at high speed to prevent foaming. Slurry consisted of wet particle agglomerates dispersed in cont. phase.
Granulac230	70	70	Water / 216 g/L Easily disperseable in cont. phase. Slurry had homogenous dough like consistency.
Ibuprofen25	53	-	Water/Surfactant 0.8wt% / 0.2 g/L Slurry consisted of homogenously distributed small agglomerates.
Ibuprofen25	53	-	Water/Surfactant 0.4wt% / 0.2 g/L Slurry consisted of homogenously distributed small agglomerates.
Benzoic acid	67	-	Water/Iso-propanol 16wt% / 50 g/L Slurry had similar consistency as adipic acid slurry.
Salicylic acid	69	-	Water/Iso-propanol 16wt% / 49 g/L Slurry had similar consistency as adipic acid slurry.
Acetyl salicylic acid	62	-	Water / 3 g/L Slurry consisted of fine particle homogenously distributed within the slurry.
Flour	54	54	Water / Insoluble Slurry looked like typical dough behaving sticky and of high viscosity.

The weight percentage wt% of isopropanol is based on the mass of the total fluid. The weight percentage wt% of surfactant is based on the mass of water.

4.1.3. Feed Rate Calibration

As the mass feed rate was of interest, the feed rate had to be calibrated first. For that the feed vat was disconnected from the drying chamber and slurry was screwed fed into a pot for a measured amount of time. The mass of slurry in the pot was weighed and the mass feed rate could be calculated. For calibration this procedure has to be repeated for different screw speeds.

$$\text{mass feed rate} = \frac{\text{mass of material in the pot}}{\text{runtime of the screw}} \quad (4-2)$$

The mass feed rate for adipic acid and ibuprofen can be calculated from the relative screw speed as following:

$$\text{mass feed rate (adipic acid)} = 2.0762 * \text{rel. screw speed} - 0.8891 \quad (4-3)$$

$$\text{mass feed rate (ibuprofen)} = 1.5354 * \text{rel. screw speed} - 0.7337 \quad (4-4)$$

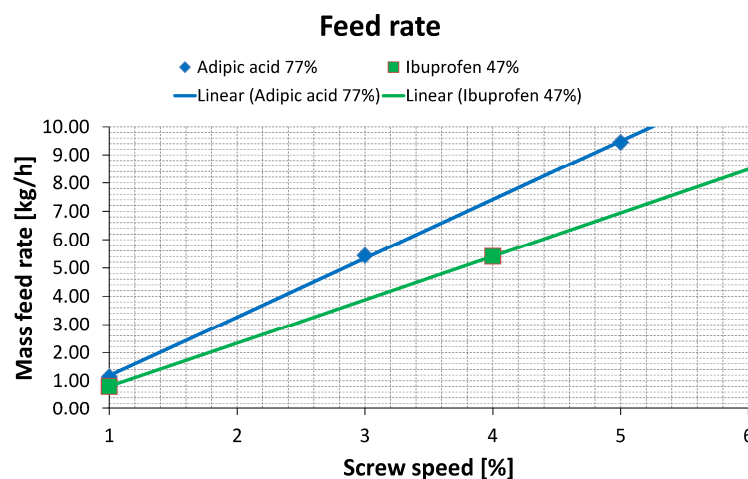


Figure 4-3: Feed rate calibration for adipic acid and ibuprofen.

For Granulac230 only the mass feed rate for the relative screw speed of 2% was determined as 3 kg/h.

It is to note, that the feed screw was oversized for the small feed rates and the actual feeding was discontinuous. Care was taken to consistently calibrate the feed rate, but the variability made the task difficult. In addition as the solid concentration of the feed changed over time also the feed rate changed during the experiment. It was difficult to control this effect.

As the determination of the feed rate is rather vague the feed rate was not determined for the additional experiments. At these experiments no focus was laid on the influence of the feed rate on the product quality. As the materials showed similar behavior as adipic acid or ibuprofen those calibration data were used.

4.2. Laboratory Work

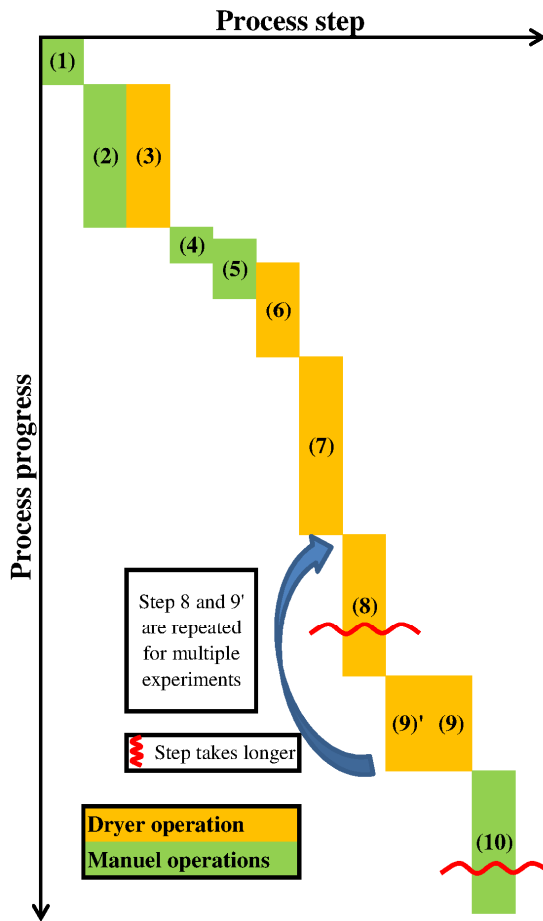


Figure 4-4: Process steps.

The drying experiment was divided into several process steps which are repeated for every work day. The process steps were standardized to reduce variations in the results due to different experimental conditions.

(1) SFD set-up

The SFD was checked before starting with the first experiment in a series. The connection to the RCPE exhaust system and the cleanness of the dryer were checked. Also the classifier used for the following experiments was installed.

(2) Slurry preparation

The slurry for the following experiments was prepared according to chapter 4.1.2, page 28. As the DoE experiments were performed in series to save time, slurry for several experiments was prepared at once.

(3) SFD warm-up I

During slurry preparation the SFD was started without any feed load to heat up the SFD and check its function.

(4) Filling of the feed vat

The feed was filled into the feed vat and the feed vat agitator was started.

(5) Fluid segregation

The continuous phase segregated from the slurry and is transferred into the drying chamber.

(6) SFD warm-up II

The segregated fluid was most times removed by evaporation. Only if the amount of fluid was high enough to threaten flooding of the air inlet the fluid was removed via the drain. After removal of the fluid, the SFD had to be brought up to temperature again.

(7) SFD start-up

During start-up the agitated fluidized bed has to be established. The step is crucial to ensure later steady-state production. Normally start-up is performed at a lower feed rate and a lower agitator speed. The intent is to keep material residues, which preferably build-up during start-up, to a minimum. After a circulating powder bed is established the dryer settings are switched to the settings for the following experiment.

(8) Production

After establishing a steady-state process the product container was emptied and the production was started. During production the process behavior was continuously checked and pictures were taken as well as records of process settings. At the end of production the product in the product container was collected for measurements.

(9)‘ Switch settings

If further experiments were performed with the same feed the process settings were switched according to DoE requirements. Process point (8) was repeated to re-establish steady-state. Point (8) and (9)‘ were repeated as long as enough feed was available.

(9) Emptying

After the last experiment the remaining feed was removed and the dryer was emptied by blowing out the particles at high velocity. The chamber agitator was turned off.

(10) Cleaning

All components of the dryer had to be cleaned. For that the drain was opened. When drying water insoluble products which tend to form floating agglomerates (like ibuprofen), the SFD had to be cleaned first with organic solvents. The feed screw can be cleaned by extruding crushed ice. The last cleaning step was always with water.

5. Experimental Results, Statistical Analysis and Discussion

5.1. Results for Adipic Acid

5.1.1. Process description

During start-up the agitator distributed the pasty feed on the dryer wall at the height of the feed entrance. The higher the feed rate, the more material was conveyed into the process chamber and bigger material rings could be observed. Because of the current agitator concept, some material remained on the wall during the whole process. Slowly, a particle bed at the bottom of the drying chamber was built up. As explained in the theoretical description of the drying process (chapter 2.1, page 9) further feed then is dried probably. In consequence fed material led to a dry particle stream. In figure 5-1 the start-up of the adipic acid process can be seen. In the left picture fresh feed is sputtered and smeared on the dryer wall. In the right picture already a particle bed is generated and material residues on the wall can be seen.

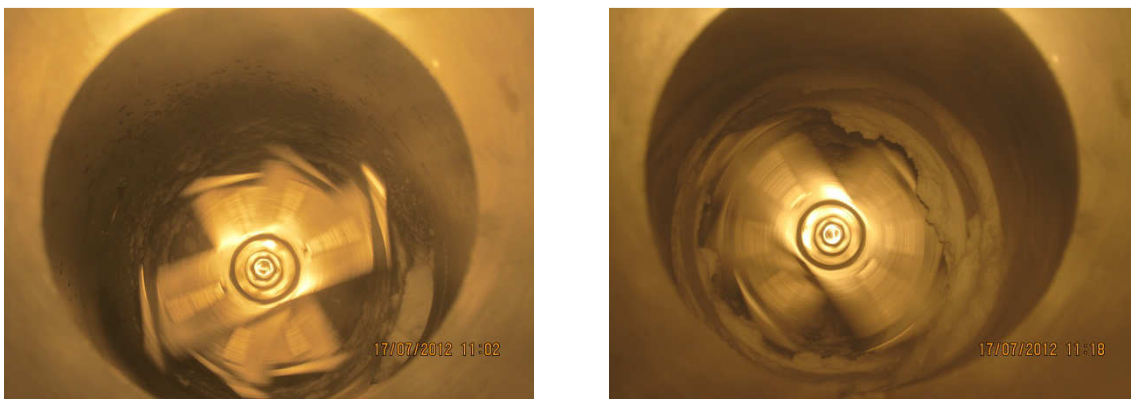


Figure 5-1: Start-up phase of adipic acid experiment SFD 15 / DOE 03.

Over time most of the initial material layer dried and broke off the wall. For some DoE cases dry particles settled and adhered on the wall of the drying chamber between the agitator and the classifier (the part which can be seen as a cylindrical pipe). For some cases (SFD 13, SFD 24 and SFD 59) the layer remained during the whole process. Two examples are shown in figure 5-2. The left figure shows SFD 13 and the right figure shows SFD 24 right after the end of the drying process. In both cases the particle could be blown off at high air-throughput and without the classifier. In this case the air flow along the wall is not hindered and moves upwards in a helical way along the pipe surface.



Figure 5-2: Adipic acid DoE experiment with dry particles adhering on the dryer wall.

Depending on the classifier size particle movement changed. Exemplarily the two types of flow pattern are shown in figure 5-3. At high air-throughput (figure 5-3, left) the particles generally tended to move upwards in a helical path along the wall. Strands of particles were moving upwards and fell back into the drying chamber, when reaching areas with lower air velocity near the classifier. For smaller air throughput (figure 5-3, right) the particles moved upwards more centrally but still in a helical way.

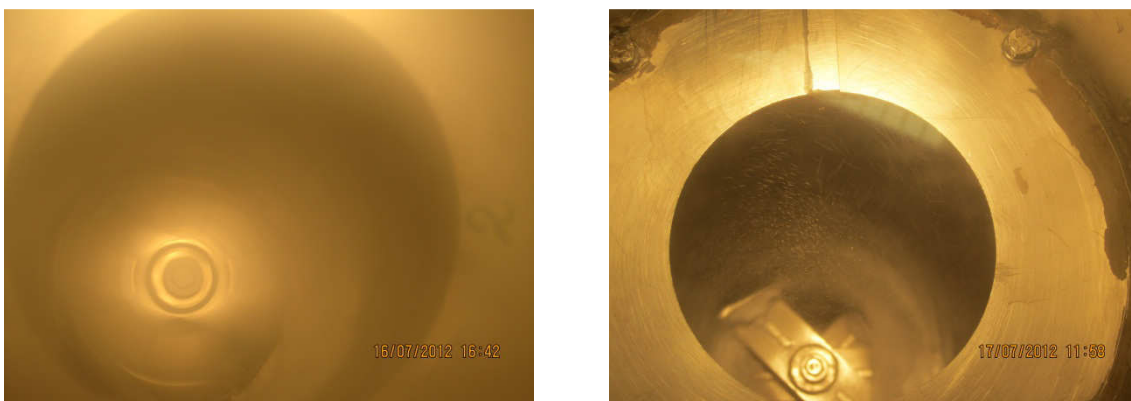


Figure 5-3: Different particle movement according to the air throughput.

5.1.2. Measured Results

Results for all adipic acid DoE cases are listed in the appendix (chapter 10.4.1, page 116). Exemplarily the results for high and low factor DoE experiments are compared to the feed here. Generally the residual moisture of all adipic acid DoE cases was equal or smaller than 0.10wt% what is within exactable limits. However the results for residual moisture have to be taken with care as the limit of detection was 0.01wt% and the standard deviation was on the same order as the results.

Material breakage was observed for all settings but the intensity varied with the setting. As consequence the median diameter and the shape of distribution changed as will be shown below.

Table 5-1: Settings and results for exemplary adipic acid experiments.

Exp. Name	Feed rate [kg/h]	Air throughput [kg/h]	Agitator speed [rpm]	Residual moisture [wt%]	x_{50} [μm]	BET surface [m^2/g]
Feed	-	-	-	-	223.29 ± 0.29	0.6139 ± 0.0019
SFD 14	1.19	400	1400	0.06 ± 0.01	23.18 ± 0.74	0.4775 ± 0.0012
SFD 15	1.19	200	420	0.10 ± 0.00	114.24 ± 0.84	0.6422 ± 0.0012

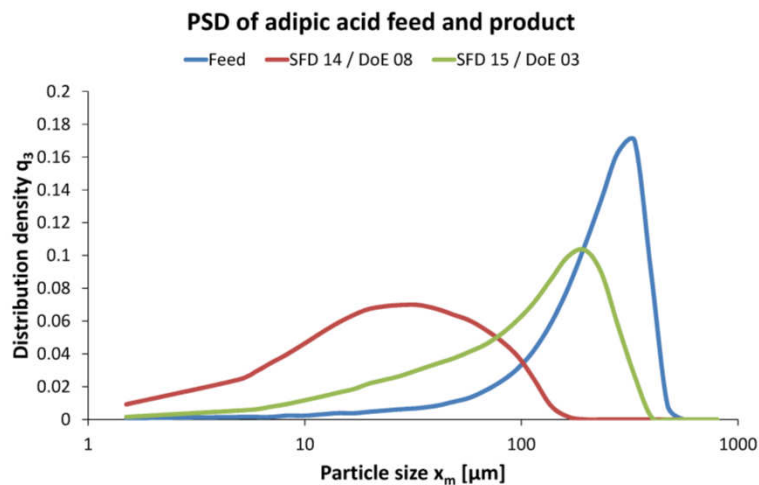


Figure 5-4: PSD distribution of adipic acid feed and products SFD 14 and SFD 15.

Starting from particles with a median size of around $220 \mu\text{m}$ the particle size was reduced. The degree of reduction seems to correlate with the agitator speed. The original shape of the PSD plotted as a logarithmical distribution showed a negative skew. For the product, especially for high values, the shape changed to a logarithmic normal distribution.

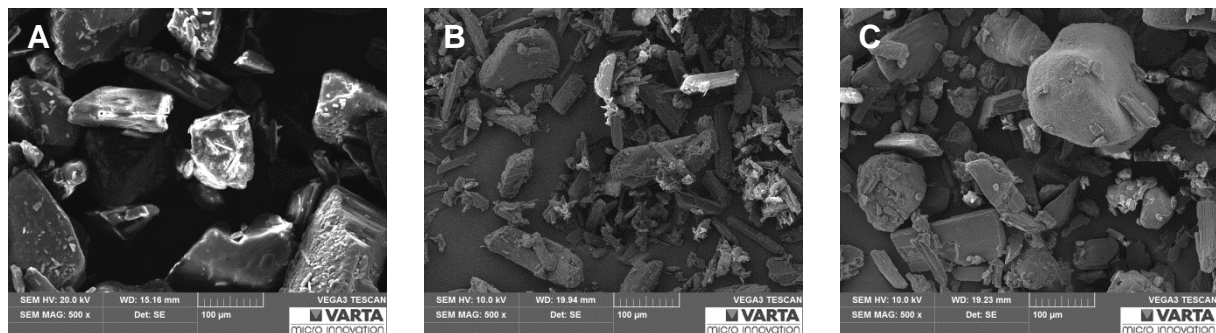


Figure 5-5: SEM images of adipic acid at a magnification level of 500. (A) feed, (B) SFD 14 and (C) SFD 15.

SEM images (figure 5-5) contribute to the results gained from the PSD analyses. Especially for the high factor case SFD 14, but also for SFD 15, it can be seen that the particles obtained from the drying process are fractured. For adipic acid the SFD clearly also acted as a mill. Bigger fragments showed a cylindrical to irregular shape and are loaded with smaller fragments of the original particle.

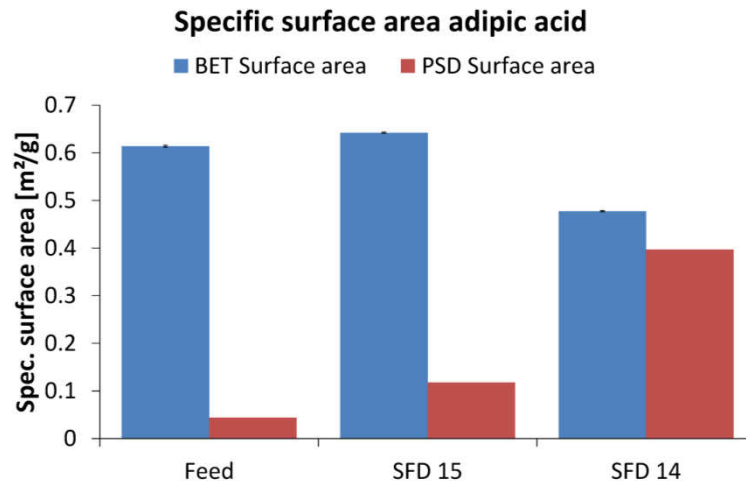


Figure 5-6: Specific surface area of adipic acid feed and experiments SFD 14 and SFD 15.

Figure 5-6 shows the specific surface area of the feed material and products from experiments SFD 14 and SFD 15. In addition specific surface area is calculated from PSD measurement. There particle pores are ignored and the calculated surface area shows naturally the same trend as the PSD.

Normally smaller particles gained here at higher agitator speed have a higher specific surface area. Surprisingly, the trend was reversed for the high value case (SFD 14) whilst the results for the low value case (SFD 15) are consistent with the results from PSD and SEM analyses. For smaller particle size, which was verified by SEM, the resulting specific surface area decreased. This effect has also been reported for milling of carbon nanotubes [21] or mechanical activation of boehmite [22]. For carbon nanotubes, first an increase of specific surface area was observed due to breakage of the nanotubes. Further grinding then flattened the end of the tubes and even closed the tubes to exclude them from the measureable surface area. Thermal decomposed boehmite with a large number of slit shaped pores was treated in a ball mill. As result the BET surface area decreased whilst the particle size decreased. An aggregation of small particles and destruction/alteration of pore structure was proposed.

Adopting these results from literature on the results of adipic acid it can be proposed that original adipic acid is with micro pores which were not seen at SEM images. At low

mechanical energy input the specific surface area increases due to break down of the original particles and generation of fresh external surfaces. For higher mechanical energy input, micro pores were destroyed or sealed, resulting in a decrease of the BET surface area.

5.1.3. DoE Analyses

The resulting responses from the experiments were put into the worksheet. Together with the factors Modde [14] then was able to compute the statistical dependence of responses and propose a statistical model. However the suggested results had to be proven and several changes to the model calculation were possible.

For every response a model performance indicator was calculated as well as a coefficient plot showing the impact and statistical significance of the factors or mix of factors on the response. Depending on the distribution of the results 3 different statistical models could be chosen to describe the effect shown in figure 5-7.

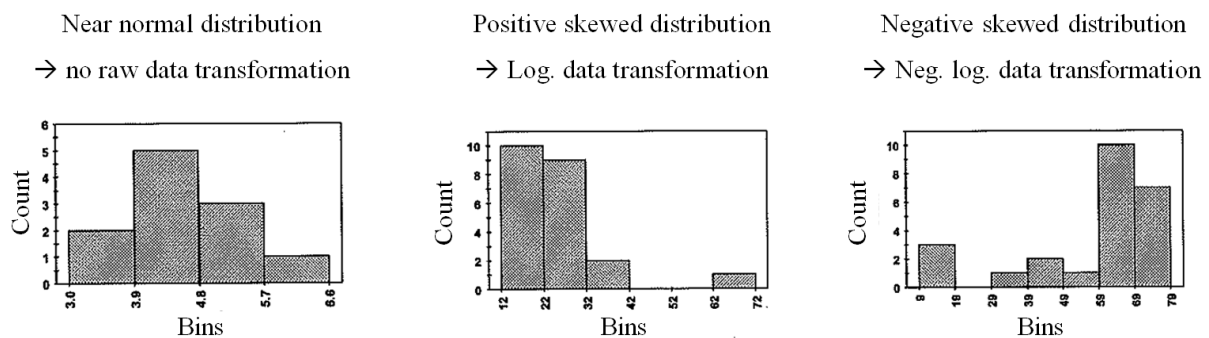


Figure 5-7: DoE raw data evaluation with Modde. Histogram plot [14].

Depending on the chosen model for the raw data evaluation and the factors having an influence on the response (figure 5-9 and figure 5-10) a **model performance indicator** was generated. The model performance indicator plot will be explained with the results of the adipic acid example in figure 5-8.

On the x-axis of the performance indicator plot all responses evaluated are shown. On the y-axis the magnitude of the effect is shown. In general the higher the value (or the closer to 1.0) the better is the statistical parameter.

Regression analysis (or R^2 as shown by the green bar) measures how well current runs can be reproduced. R^2 is an indicator showing how well the chosen model fits to the experimental data.

Q^2 (dark blue bar) is an indicator for how well the chosen model can predict new experiments. By that Q^2 is an indicator showing how useful the model will be. Q^2 values higher than 0.5

present a good predictive model and values higher than 0.9 present an excellent predictive model. However R^2 should not exceed Q^2 by more than 0.2 to 0.3. Practically this means that the blue bar should be as close to as high as the green bar.

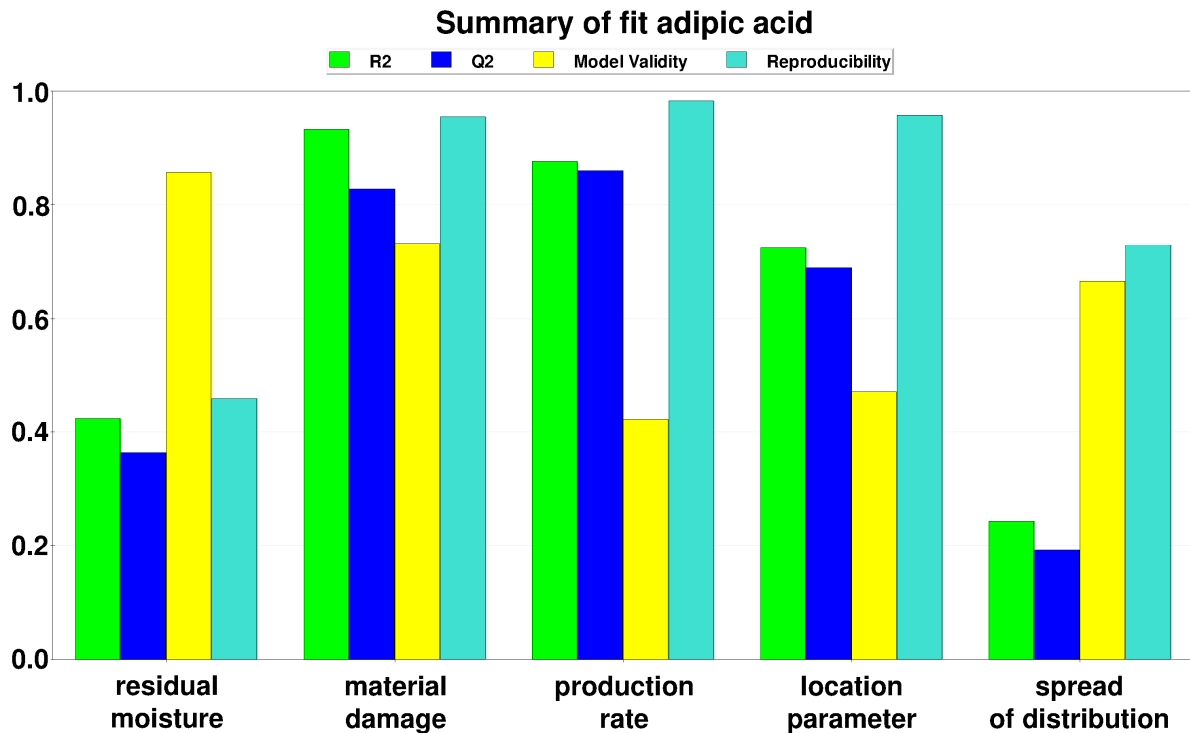


Figure 5-8: Model performance indicator for adipic acid for optimized model.

Model validity (yellow bar) is based on the F-test and compares the model error to the pure error from the measurement data. Model validity lower than 0.25 indicates significant lack of fit. Model validity higher than 0.25 indicates a good model. If model validity would reach 1.0 it is a perfect model.

Reproducibility (cyan bar) is the variation of the responses under the same conditions (repeated experiments = center point DoE cases) compared to the total variation of the response. If the reproducibility is below 0.5 one has a large pure error and poor control of the experimental procedure.

If poor values in the performance indication plot are observed, factors used or the statistical model can be varied in an effort to improve the fit. In this work factors showing to be statistically insignificant in the coefficient plot have been removed. Insignificant factors are shown as having “no influence” in the following result figure.

Raw coefficient plot material damage / adipic acid

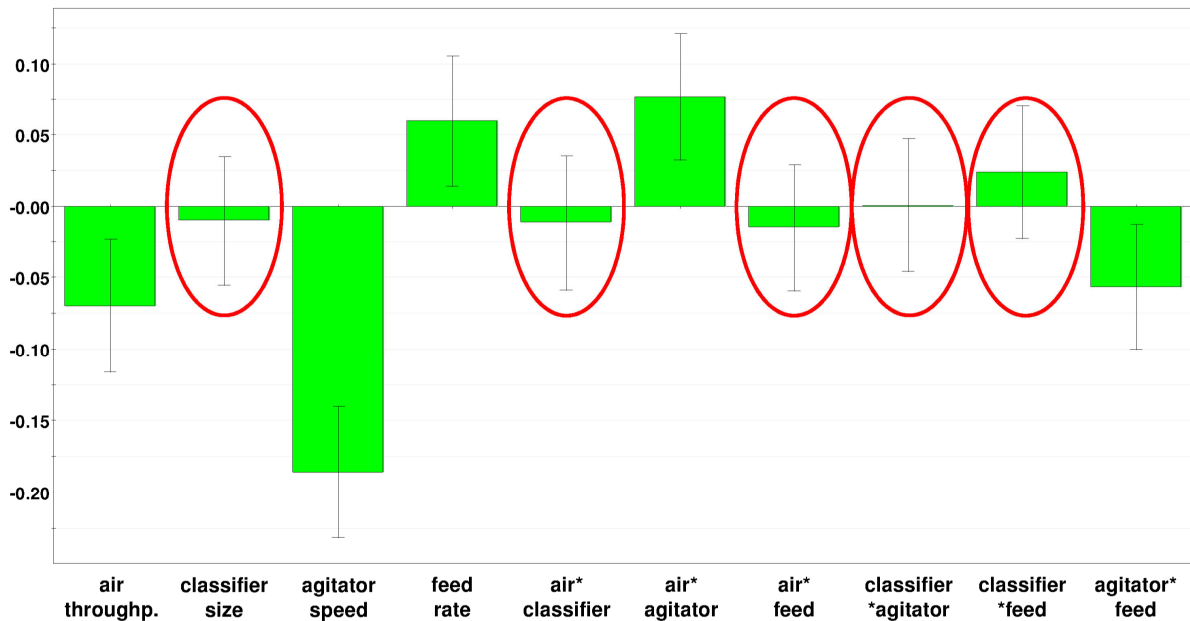


Figure 5-9: Raw coefficient plot for the material damage of adipic acid.

Coefficient plot material damage / adipic acid

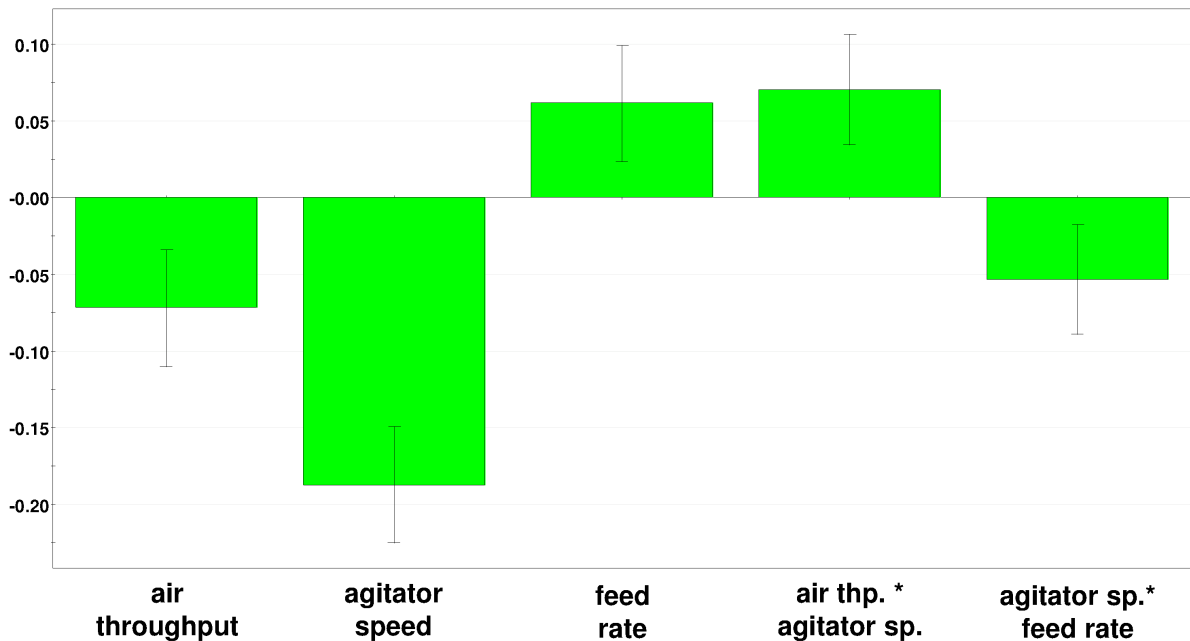


Figure 5-10: Coefficient plot after preparation showing only statistically significant factors.

Figure 5-9 shows the raw **coefficient plot** for material damage of adipic acid. The green bar presents the error of the pure data whilst the error bar presents the error of the model. If the error of the model is higher than the error of the pure data the factor is statistically insignificant for the response. Eliminating these factors, leaving only factors being

statistically significant, increases the quality of the model, which can be seen in the model performance indicator plot. Poor factors or factor combinations are marked in figure 5-9.

For material damage of adipic acid no statistical dependence on the classifier size could be found. The factor and its combination with other factors were removed resulting in the coefficient plot shown in figure 5-10. In addition the factor combination of the air throughput and the feed rate showed no statistical impact on the material damage and was removed as well. The air throughput and the feed rate alone however showed to have a statistical impact.

Summing up results from model quality shown in the model performance indicator (figure 5-8) and the coefficient plot for the material damage (figure 5-10) it can be seen that the air throughput, the agitator speed, the feed rate and the factor combination of air throughput and agitator speed as well as agitator speed and feed rate have a statistical influence. The model shows high values for R^2 and Q^2 and the model validity is above 0.25 indicating a good model for the prediction of the material damage.

All responses are evaluated similar and their coefficient plots as well as the model performance indicator are listed in the appendix (chapter 10.6.1 page 119). The results are summed up in figure 5-11.

Responses \ Factors	Residual moisture	Production rate	Material damage	Location parameter	Spread of distribution
Air throughput	NO	NO	YES	NO	YES
Classifier opening	NO	NO	NO	NO	NO
Agitator speed	NO	YES	YES	YES	NO
Feed rate	NO	YES	YES	NO	NO

Figure 5-11: Summary of statistically dependence of DoE responses on factors for adipic acid.

Residual moisture (figure 10-2) showed a dependence on the agitator speed in the coefficient plot. However the variance R^2 and the reproducibility showed low values in the summary of fit. For that no statistical model could be found describing the dependence of the residual

moisture on the agitator speed. As stated in the results section, the standard deviation of measured samples was on the same order as the results and for that measurement insecurities have an impact on the quality of the statistical model.

For the **material damage** (figure 10-3) dependence on the air throughput, agitator speed and feed rate could be found. The variance R^2 and Q^2 are both high and the model validity was above 0.25. As can be seen there is further a combined effect of the air throughput and the agitator speed and the feed rate and the agitator speed.

The rotating agitator seems to be capable of breaking down feed particles. This effect agrees with observed properties of the product powder which was smaller and less flow-able. The higher the rotation speed of the agitator the smaller the product particles become. For the air throughput the origin of the effect is not clear from the beginning. On the one hand higher air throughput means higher air velocity. With higher air velocity larger particle become air borne and so bigger particles can leave the agitated bed before being broken down. On the other hand it was observed that for higher air throughput the rotational speed of the air was higher and particles moved upwards along the drying chamber wall. There at the classifier the particles experience a higher velocity gradient as if rising in the middle of the drying chamber. A third effect could be that for higher air throughput also the air velocity in the agitated bed rises and accordingly the velocity of the particles in the bed. Kinetic energy of the particles was higher what led to higher probability of attrition. To identify the origin of the effect additional investigations have to be performed. However results of the statistical analyses show that the particle size reduces for higher air throughput.

As PSD measurement was performed after particle separation with a cyclone the air throughput has also an influence on the PSD when changing the flow conditions in the cyclone.

The origin of the effect of the feed rate also has to be investigated. Results of the statistical analyses show that for higher feed rates the relative amount of broken particles is reduced.

Interesting is, that the **location parameter** and the **spread of distribution** (figure 10-4) which together describe the PSD of the product didn't show any correlation on the feed rate. However the location parameter showed statistical dependence on the agitator speed and the spread of distribution showed statistical dependence on the air throughput.

The **production rate** (figure 10-4) depended on the feed rate and the agitator speed. As expected the feed rate had a major influence on the production rate. The influence of the

agitator speed can be explained by taking into consideration the higher attrition rate at higher rotation speeds. The problem being that a large fraction of the fine particles was expelled with the exhaust air in the cyclone.

For responses for which a statistical model could be found, it is possible and of interest to create a statistical predictive model. It has to be noted that with this model it is possible to predict the product properties but only for the current settings which are the SFD 47 and adipic acid slurry with given concentration. Taking the DoE results of adipic acid into account it is of interest to generate a model predicting the material damage and the median particle size of the product. The predictive model results are shown in figure 5-12. The color indicates the degree of material breakage with red showing the highest degree. Contour lines divide the areas of similar material breakage.

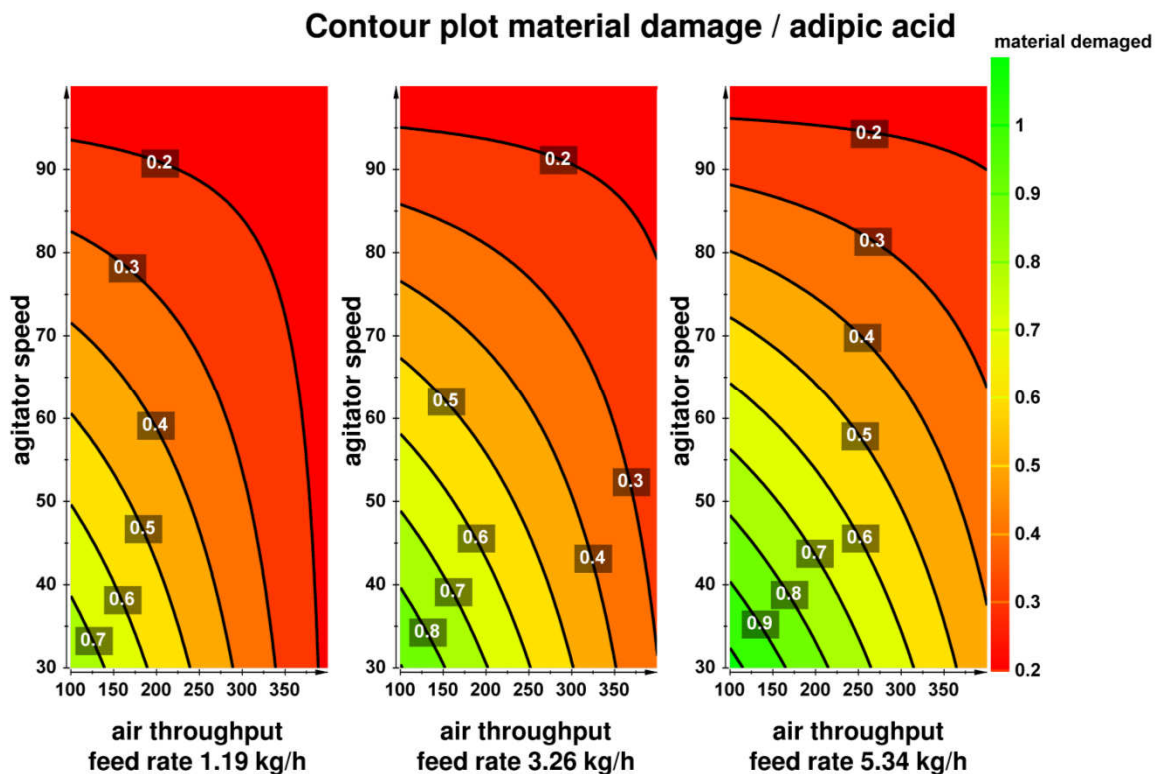


Figure 5-12: Predictive model for the material damage of adipic acid. The agitator speed is in % of maximum revolution which is 1400 rpm. The air throughput and feed rate are in kg/h.

The dependence of the material on the air throughput, agitator speed and feed rate is shown. With this model drying operations can be planned and the SFD settings can be adjusted to target certain levels of material breakage. However when working with such predictive models and setting up a design space it also has to be taken into account if the desired process settings would work, or in other words, if drying is possible. For high feed rate, low air

throughput and low agitator speed, which results in minimum material breakage, flooding of the SFD is expected.

The results of the statistical model correlate with observations taken during the experiment. The influence of the air throughput weakens as the feed rate increases. The influence of the agitator speed remains unchanged.

5.1.4. Result Summary of Adipic Acid

The **residual moisture** of adipic acid product was well below 2wt% for all experiments. The standard deviation of the results was on the same order as the results. The statistical evaluation showed a dependence on the agitator speed, but no statistical model could be generated.

Material breakage occurred for all cases and the degree depends on several process settings. For this effect a predictive model could be developed showing the magnitude of dependence on the process settings. For high rotational speed and air throughput, which results in a high level of material breakage, it was found that the internal structure of the particle changed. Pores were either blocked or deformed resulting in lower specific surface area.

Drying adipic acid in the SFD 47 led to material residues which were built up on the drying chamber wall during the start-up phase. It was later not possible, if by the agitator blade or the self-cleaning effect that all the material was removed. In addition material adherence of dried powder was possible, especially for low air throughput.

5.2. Results for Ibuprofen

5.2.1. Process description

In general the small classifier (60 mm) led to difficulties observing the drying process as dry particles adhered onto the view glass and blocked the view into the drying chamber. Therefore most process insight was gained from experiments using the wide aperture opening (80 mm).

Drying Ibuprofen with a small air throughput of 200 kg/h proved to be difficult. At the small feed rate as for the experiment SFD 40 / DOE IP07 (figure 5-13, left) slurry was scraped off at the feed inlet with only a small amount of feed remaining on the dryer wall. Dried particles on the contrary, adhered on the dryer wall from the classifier downwards. For high feed rates as for experiment SFD 43 / DOE IP15 (figure 5-13, right) drying was not possible. Feed accumulated in the lower dryer section threatening to flood the lower dryer chamber. In addition dried particles adhered on the wall.

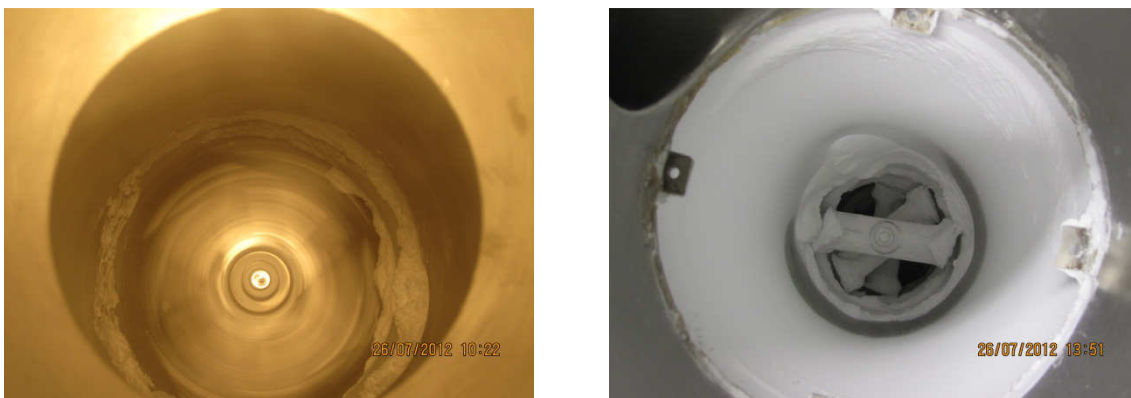


Figure 5-13: Non-ideal experiments SFD40 / DOEIP07 and SFD43 / DOEIP15. Material residues built up at feed entrance and on dryer wall.

However by increasing the air throughput to 400 kg/h the particle layer on the wall could be blown off. At an air throughput of 400 kg/h drying was possible for low and high feed rates. The feed was taken off at the entrance producing little slurry residuals on the wall. Dried particles left the process without adhering to the wall. For the high feed rate the process seemed to work in phases. In the first phase a feed strand was pressed into the drying chamber. As soon as the strand was heavy enough, the feed strand broke off and was dried as a whole. This resulted in a burst of dried particles. Meanwhile a new feed strand was pushed forward into the drying chamber and the process was repeated.

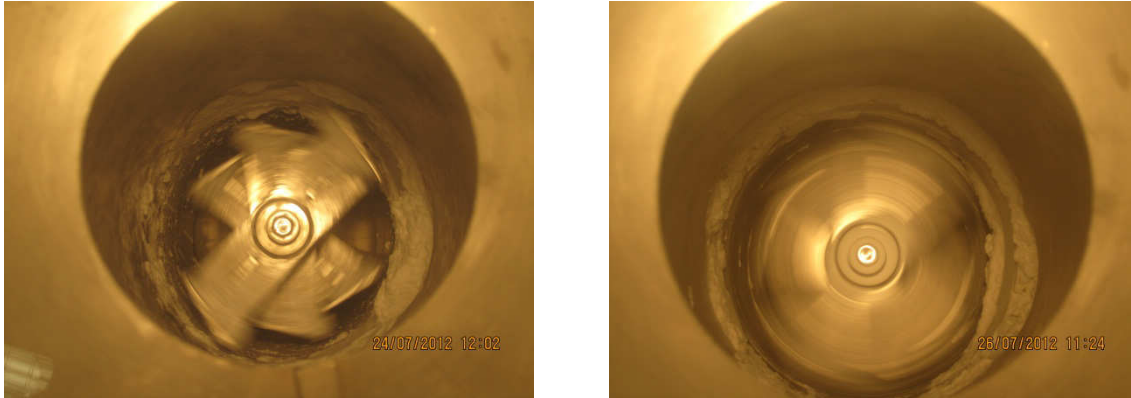


Figure 5-14: Ideal experiments SFD28 / DOEIP04 and SFD42 / DOEIP16.

Figure 5-14 shows two processes with an air throughput of 400 kg/h, SFD 28 / DOE IP04 at low feed rate and SFD 42 / DOE IP16 had high feeding rate. For both cases drying was possible without any problems.

5.2.2. Measured Results

Results for all ibuprofen DoE cases are listed in the appendix (chapter 10.4.2, page 117). As an example, the results for high and low factor DoE experiments are compared to the feed.

Table 5-2: Settings and results for exemplary ibuprofen experiments.

Exp. Name	Feed rate [kg/h]	Air throughput [kg/h]	Agitator speed [rpm]	Residual moisture [wt%]	x_{50} [μm]	BET surface [m^2/g]
Feed	-	-	-	-	34.13 ± 0.30	0.5172 ± 0.0128
SFD 27	0.98	200	420	0.05 ± 0.01	30.32 ± 0.23	0.5139 ± 0.0137
SFD 39	0.98	400	1400	0.02 ± 0.00	20.15 ± 0.29	0.7724 ± 0.0178

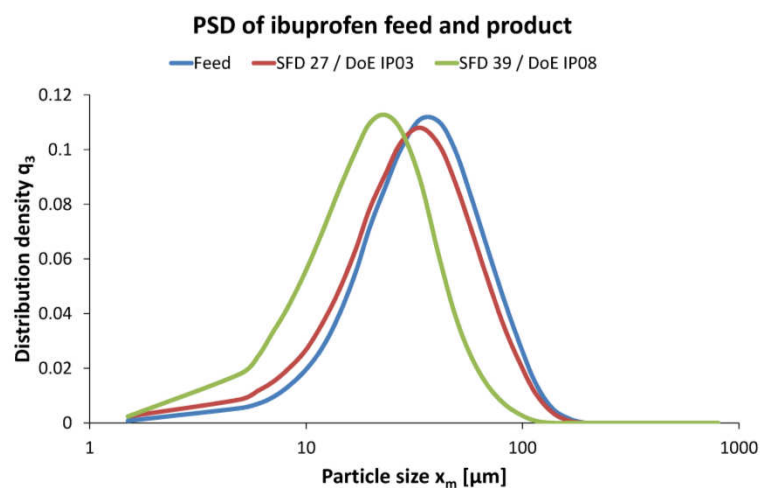


Figure 5-15: PSD distribution of ibuprofen feed and products SFD 27 and SFD 39.

The residual moisture of adipic acid was equal or smaller than 0.15wt% what is within exactable limits. Again the standard deviation of the measurement was on the same order as the results. Material breakage could be discovered for all settings but the intensity varied with the setting. The particle size was reduced slightly whilst the shape of the PSD remained logarithmically distributed. The degree of reduction could correlate to the agitator speed.

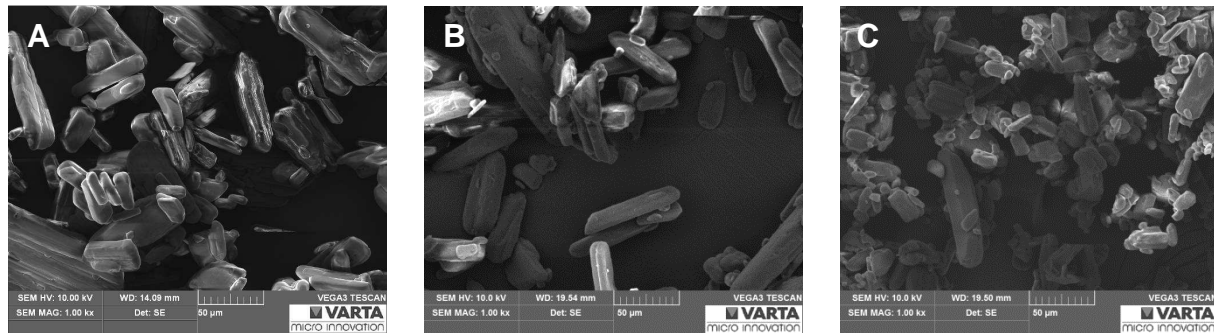


Figure 5-16: SEM images of ibuprofen at a magnification level of 500. (A) Feed, (B) SFD 14 and (C) SFD 15.

SEM images contribute to the results gained from the PSD. Needle shaped particles are broken down into smaller pieces. Especially for experiment SFD 39 (figure 5-16 C) small breakages cover bigger needle shaped particles. For experiment SFD 27 (Figure 5-16 B) the result looks similar to the feed particles. It is assumed that only small fragments were formed as a result of attrition. The particles themselves were not broken.

The degree of material breakage is lower than for adipic acid. Ibuprofen particles are initially smaller than adipic acid particles. Having the same impact speed when they bump against the dryer wall the impact force is smaller due to their lower weight. Also the likelihood of impact with other particles or the agitator is smaller for small particles than for big particles. In addition smaller particles are removed faster from the dryer as smaller particles weigh less than bigger particles. With reduced residence time in the dryer the chance of being broken and/or the milling degree decreases. Also, ibuprofen was dried close to its melting point. At this temperature deformation is possible at high impact velocity, which reduces the energy remaining for particle breakage. However the mentioned effects are only first assumptions which have to be verified by further investigation.

The BET measured specific surface area is near the double of the specific surface area calculated from the PSD. The calculated surface area from PSD is calculated for spherical particles which have the lowest specific surface area. The particles are needle shaped,

resulting in a higher specific surface area than spheres. For low values of air throughput and agitator speed, less increase in specific surface area is observed.

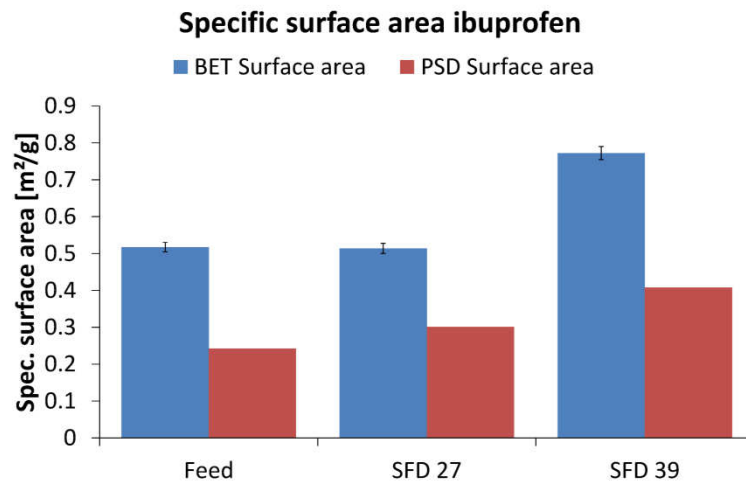


Figure 5-17: Specific surface area of ibuprofen feed and experiments SFD 27 and SFD 39.

This contributes to the results of PSD and SEM analyses that only a few particles were damaged during the process. At higher values an increase of the specific surface is measured, suggesting material breakage occurs. There is no evidence, however, that the pore structure is changed due to the milling processes.

5.2.3. DoE Analyses

Ibuprofen responses were evaluated similarly as for adipic acid and the graphical results can be found in the appendix (chapter 10.6.2 page 121). The results are summed up in figure 5-18.

Responses \ Factors	Residual moisture	Production rate	Material damage	Location parameter	Spread of distribution
Air throughput	NO	NO	YES	YES	YES
Classifier opening	NO	NO	NO	YES	YES
Agitator speed	NO	NO	NO	NO	NO
Feed rate	NO	YES	NO	NO	NO

Figure 5-18: Summary of statistical dependence of DoE responses on factors for ibuprofen.

Residual moisture (figure 10-6) showed low variance R^2 and Q^2 . No statistical model could be found to describe the correlation of the residual moisture and the factors. Again the standard deviation of measured residual moisture was on the order of the results.

Material damage (figure 10-6) shows a statistical dependence on the air throughput. However model validity of 0.2 indicates significant lack of fit of the model. This means that a statistical dependence of the material damage on the air throughput could be seen but no model could be found describing the effect. As shown in the experimental results section, ibuprofen at low air throughput tended to build up a layer of dried particles on the walls of the drying chamber. A theoretical explanation could be that ibuprofen particles experienced some breakage but to a less extent as for low air throughput. In addition for low air throughput smaller particles tend to adhere on the dryer wall as the ratio of surface forces to body forces is higher for smaller particles. The effect has to be investigated further to be justified.

The **location parameter** and the **spread of distribution** (figure 10-7) both depend on the air throughput. In addition the size of the classifier has an effect on these factors. However the effect is close to statistical insignificance and therefore the effect of the classifier size on these responses requires further investigation to be justified.

The **production rate** (Figure 10-6) has a statistically significant dependence on the feed rate. No further factors influence the production rate. As for adipic acid, the dependence of the production rate on the feed rate is obvious and expected.

5.2.4. Result Summary of Ibuprofen

The residual moisture of ibuprofen products showed no dependence on the process settings and was for all cases below the limit of 2wt%.

Material breakage was less severe and occurred mostly for high air throughput and agitator speed. At low values the particles were not broken down, only debris were chipped off. No change of internal pore structure, if present, could be noted.

However drying at low air throughput seems hard and results in a high degree of material residues on the wall. Without dryer adaption it is not advised to dry ibuprofen at low air throughput. Further suggestion is to dry ibuprofen at low feed rate and medium to high air throughput.

5.3. Results for Drying Energy (Lactose)

5.3.1. Process description

Drying of lactose differed from the previous experiments with adipic acid and ibuprofen. Already the slurry showed different behavior as being a homogeneous paste. Shown in figure 5-19 slurry fed into the dryer first was smeared and spattered on the wall. As soon as a thicker material layer was built up dry particles could be produced. Also the material layer was dried by the over-flowing air leading to a harder, cracked surface.

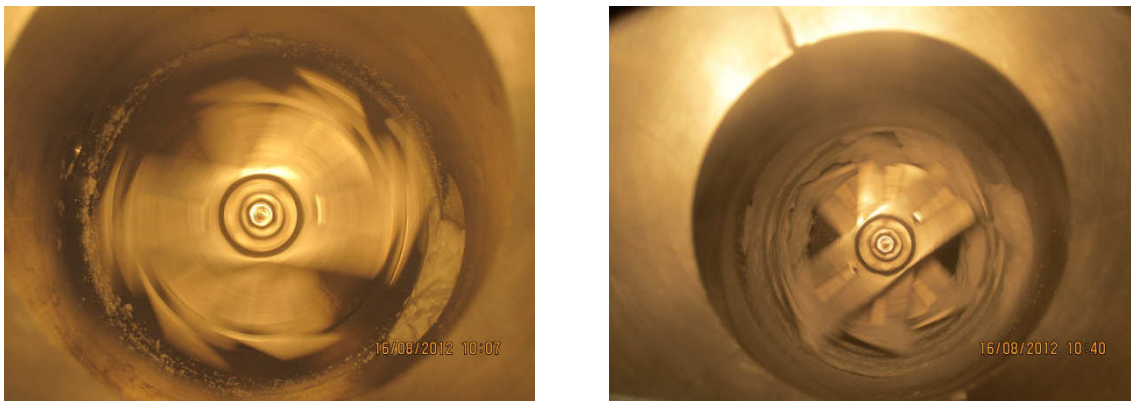


Figure 5-19: Start-up with slurry of 70% Lactose. Feed entering the dryer covers the wall.

Most of the initial deposited material was removed by the agitator and/or the SFD's self-cleaning process. The self-cleaning effect could be observed to take place in two steps. First the built up material dried during the drying process and crumbled. Then the dried fragments were removed by the air-particle stream. However in between the agitator blades rings of material residues remained throughout the whole experiment. These rings were bigger than the material residues observed in previous experiments. Also the structure was different as lactose residues formed a hard cake adhering to the wall. Circulating particles stuck to the surface of the Lactose feed and covered it preventing any further adhesion to the process chamber walls.

Drying of Lactose slurry was possible for all cases. In case of low inlet temperatures of 60°C, as for experiment SFD 76 / DOE TL03 (figure 5-20, left), most of the feed circulated at the height of the agitator. For higher temperatures of 80°C, like for experiment SFD 80 / DOE TL02 (figure 5-20, right), particles seemed to be blown out faster resulting in a high optical particle concentration in the upper part of the dryer.

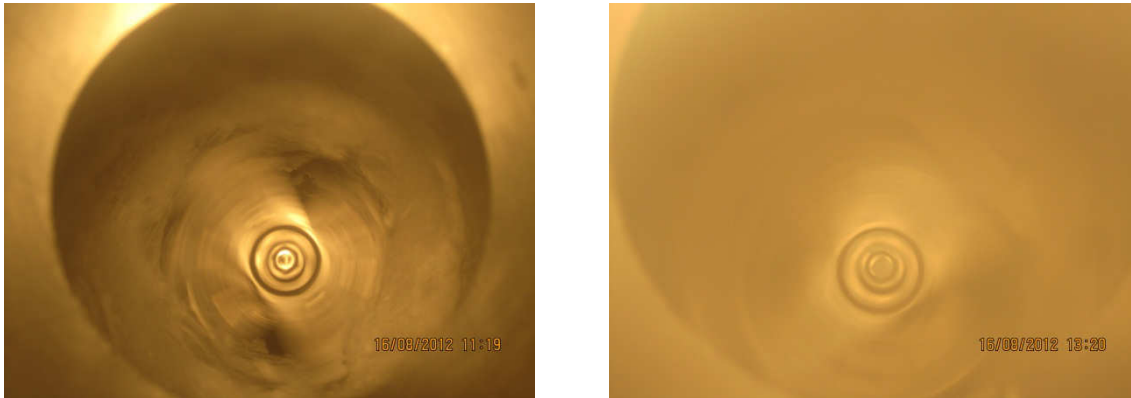


Figure 5-20: Optical lactose particle concentration and distribution in dependence of the drying air temperature.

5.3.2. Measured Results

Results for all lactose DoE cases are listed in the appendix (chapter 10.4.3, page 118). The results for high and low factor DoE experiments are compared to the feed in the table below.

Table 5-3: Settings and results for exemplary lactose experiments.

Exp. Name	Air throughput [kg/h]	Inlet air temperature [°C]	Residual moisture [wt%]	x ₅₀ [µm]	BET surface [m ² /g]
Feed	-	-	-	19.23 ±0.25	1.0414 ±0.0036
SFD 75	200	60	3.86 ±0.12	26.19 ±0.08	0.5041 ±0.0046
SFD 79	400	80	4.14 ±0.11	63.23 ±1.02	0.4546 ±0.0055

Generally presented the residual moisture of lactose was higher than the limit of 2wt%. An increase of particle size was measured that could indicate agglomeration.

Measuring the residual moisture with Karl-Fischer titration the total amount of water, this means adhering surface water and crystal bound water is measured. The relative amount of crystal water in lactose monohydrate (feed material) is calculated to 5wt%.

Lactose monohydrate (C₁₂H₂₂O₁₁·H₂O, MM = 360.31 g/mole) contains one mole of lactose and one mole of water (MM = 18.02 g/mole). MM is the molar mass. The molar ratio of water to lactose monohydrate is 1. That means for one mole lactose monohydrate which is 360.31 g there are 18.02 g of bound water.

$$x(\text{water}) = \frac{m_{\text{water}}}{m_{\text{Lactose monohydrate}}} * 100\% = \frac{18.02 \text{ g}}{360.31 \text{ g}} * 100\% = 5\text{wt}\% \quad (5-1)$$

From literature it is known that crystal bound water in α -lactose monohydrate decomposes at temperatures higher than 95°C [23]. In solution lactose exists in equilibrium of β -lactose and α -lactose. Both forms are precipitated during drying. Especially at high temperature there is a high amount of β -lactose. β -lactose is then present in an amorphous matrix with no hydrate water but is hygroscopic, especially at a high moisture level [24].

For that it can be argued, that the measured residual moisture actually originates from crystal water of α -lactose monohydrate. The particles themselves are then free of surface moisture and therefore dried successfully.

For dried lactose this means that the measured water contained derives from the intact α -lactose mono hydrate crystals. Due to precipitating β -lactose binding to the original particles the water content is slightly below its theoretical value. The decrease in residual moisture therefore states the amount of β -lactose. The ratio of precipitated β -lactose to α -lactose depends on the precipitation condition and therefore could be used for statements about the drying process. The particles can be seen as free of adhering surface water.

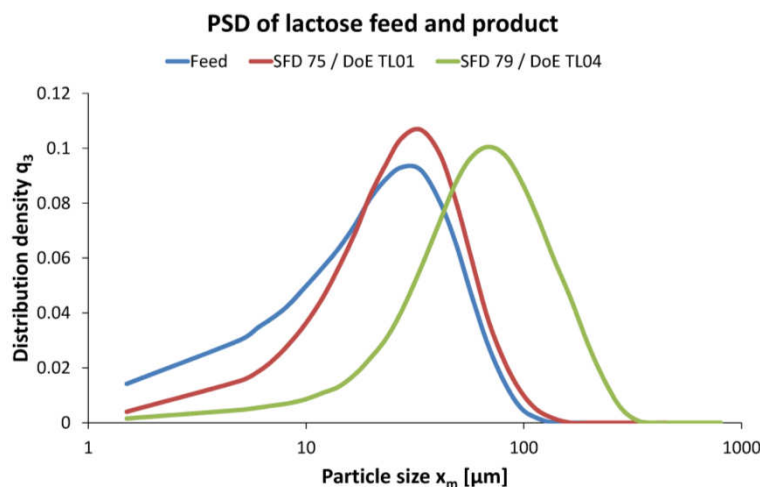


Figure 5-21: PSD distribution of lactose feed and product SFD 75 and SFD 79.

The particle size of lactose increases depends on the process settings. On a first look it seems that for higher drying energy bigger particles are produced. Lactose dissolved in the fluid crystallizes and initiates or enhances agglomeration. For higher energy input more but smaller lactose particles are produced acting as a link between the bigger particles. The results are bigger agglomerates.

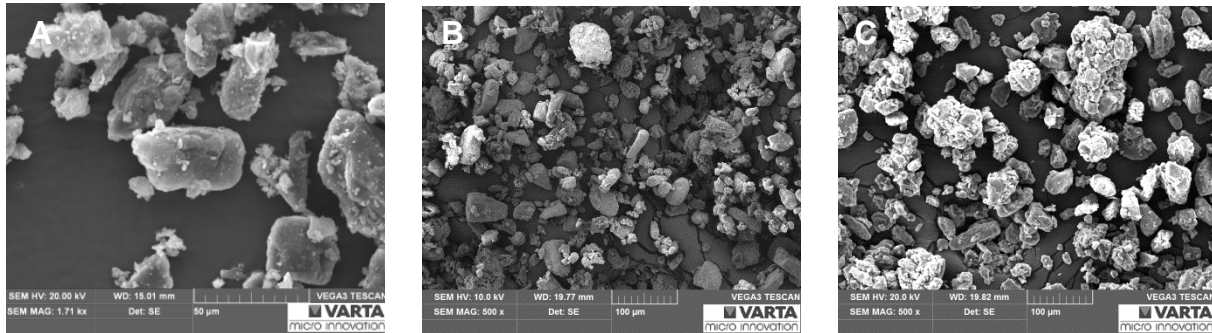


Figure 5-22: SEM images of lactose at magnification level of 500. (A) feed, (B) SFD 75 and (C) SFD 79.

SEM images (figure 5-22) show that the product (SFD 14 and SFD 15) consists of smaller agglomerated particles and bigger particles covered with smaller particles. The shape of the agglomerates is spherical. Comparing the SEM images from the feed to the products it seems that lactose particles are first broken down and later agglomerated to spherical particles.

The results show that the amount of fine particles changes for high and low drying energy. The small particles cover bigger particles reducing there number and the specific surface area. For higher drying energy agglomerates are produced increasing the particle size.

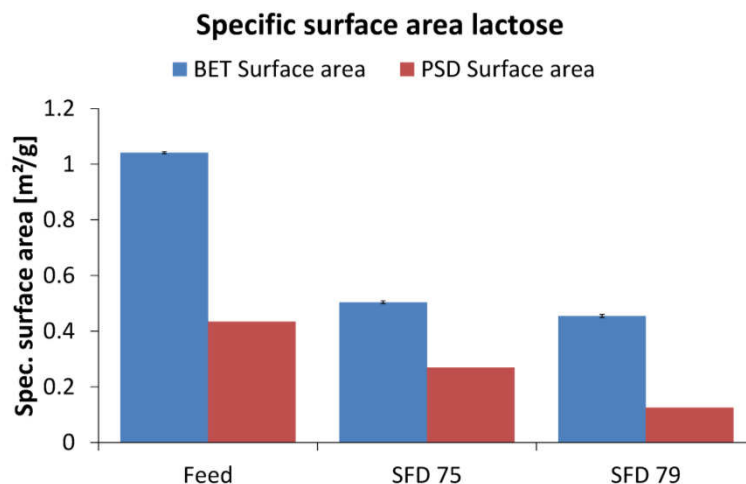


Figure 5-23: Specific surface area of lactose feed and experiments SFD 75 and SFD 79.

The results from the BET analyses show a drastic drop of specific surface area for both cases. During the agglomeration it could be possible that pores in the lactose crystal are closed and irregular surface structure is smoothed. The difference between the low and high value case is smaller than results from the PSD analyses would suggest. It could be possible that between the particles linked together by small crystallized particles voids are entrapped. These voids can increase the inner surface whilst the external surface becomes smaller due to growth of the agglomerates.

5.3.3. DoE Analyses

The responses for lactose were evaluated similar as for adipic acid and the graphical results can be found in the appendix (chapter 10.6.3 page 122). The results are summed up in the following figure.

Responses Factors	Residual moisture	Production rate	Material damage	Location parameter	Spread of distribution
Air throughput	NO	NO	YES	YES	NO
Air inlet temperature	NO	NO	YES	YES	NO

Figure 5-24: Summary of statistically dependence of DoE responses on factors for DoE drying energy (lactose).

Residual moisture (figure 10-9) showed a statistical dependence on the air throughput. The variance is low, but within acceptable limits to generate a statistical model. However, as discussed above, the change in residual moisture levels does not derive from the dried lactose particle but from the precipitated lactose. The air throughput has compared to the inlet temperature in the varied range the most influence on the drying energy. Changing the air throughput the precipitation process is changed resulting in a different ratio between α -lactose and β -lactose. This is what then was measured by Karl-Fischer titration. For the actual residual moisture of lactose particle no model was found as the stated effect above was stronger.

Material damage (figure 10-9) shows statistical dependence on the air temperature and the air throughput. With increasing temperature and air throughput the resulting particle size also increases. Each of these factors increases the thermal energy input needed for drying. With higher drying energy the probability of nucleation increases whilst the final particle size decreases. Depending on the particle size of the precipitants their effect on agglomeration changes resulting in a changed PSD. Further, small free precipitated particles cannot be removed by the cyclone as reflected in the measured PSD.

In addition the **location parameter** (figure 10-10) increases in a statistically significant fashion with an increase in inlet air temperature and air throughput. The **spread of**

distribution (figure 10-10) shows no statistically effect on these two factors. The results agree with the results from the experimental study presented above.

Production rate (figure 10-10) depends on the air throughput. Effects are the size of produced agglomerates and the separating behavior of the cyclone which changes with the air throughput.

5.3.4. Result Summary of DoE Heat Influence (Lactose)

After literature research it can be stated that drying of lactose was successful and the particle's surface moisture was below the acceptable limit.

Drying lactose as a model for material being solvable in the fluid showed that precipitating particles might lead to agglomeration behavior. For that the SFD not only acts as drier but can be used for agglomeration as well. More information about agglomerating in agitated fluidized beds can be found in the literature [25].

Drying of lactose with the SFD proved to be no problem. The amount of initial residues during start-up depended on the air throughput but later during steady state most of the initial residues could be removed by the agitator rotor and the self-cleaning effect.

5.4. Additional Experiments

In this chapter the results of the additional performed experiments are presented in compressed form. The result data are listed in the appendix (chapter 10.5, page 118).

5.4.1. Influence of Surfactants

With the used mixing equipment it was possible to produce ibuprofen slurry without the addition of any surfactant. However in preliminary experiments performed at site of the SFD supplier Anhydro/SPX, ibuprofen slurry with surfactant sodium pyrophosphate tetra basic was dried [26]. Furthermore addition of surfactant might be necessary for the precedent filtration process and will be found in the slurry for drying. Generally speaking surfactants reduce the surface tension of the water and improve the wetting behavior of the slurry material. For that surfactants will adhere on the feed particles. Therefore the used surfactant can also be seen as an impurity in the continuous phase which is not removed in precedent washing steps.

DoE cases listed in table 5-4 are repeated with ibuprofen slurry containing 0.8wt% surfactant based on the mass of water.

Table 5-4: SFD process settings for drying of ibuprofen/surfactant.

Exp No	Exp Name		Controlled factor				Constant factor		
			Air throughput [kg/h]	Classifier opening [mm]	Agitator speed [rpm]	Feed rate [kg/h]	Inlet air temp. [°C]	Model substance	Feed solid content [wt%]
1	SFD 46	DOE IP04	400	80	420	0.98	70	ibu/Surfactant	40
2	SFD 47	DOE IP07	200	80	1400	0.98	70	ibu/Surfactant	40
3	SFD 48	DOE IP11	400	80	1400	3.00	70	ibu/Surfactant	40

The Ibuprofen particles were suspended more homogenously and formed smaller agglomerates. Figure 5-25, left shows the feed after preparation. Still, fluid was segregated after the slurry was filled into the feed vat. Also drying of the slurry in the feed vat over time was observed as for the ibuprofen slurry without surfactant. Feed after drying in the feed vat is shown in figure 5-25, right.

For experiments SFD 46 and SFD 47 drying was possible. However a large amount of feed stuck to the process chamber wall as can be seen in figure 5-26. Subsequently already circulating material adhered to the crust formed by sticky feed material leading to increased material build up. After further drying, bigger agglomerates were circulating in the agitated part of the dryer. Above the classifier a residual layer on the wall built up. Even the final dried product exhibited adhesive behavior.



Figure 5-25: Ibuprofen suspension 40wt% with surfactant.

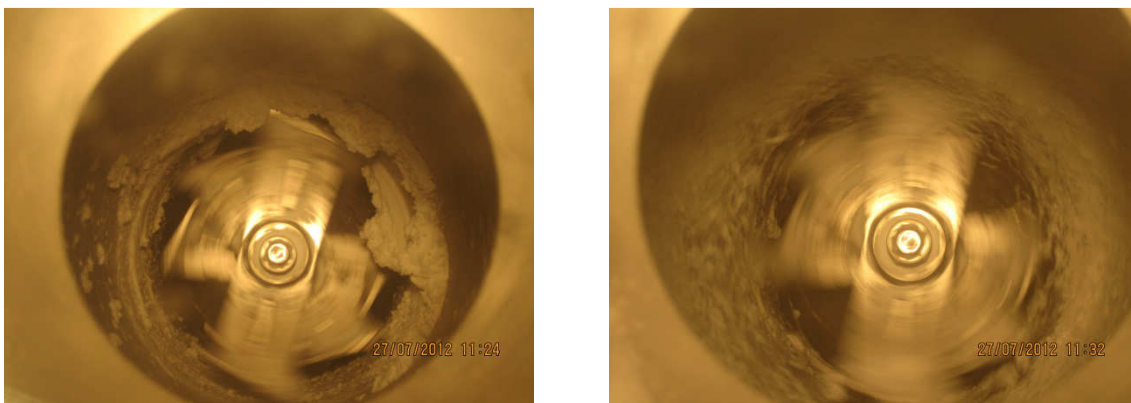


Figure 5-26: SFD 46 in-process images. Residues built up on the wall and lumps of particles are stirred by the agitator.

For SFD 48 drying was not possible. At a high feed rate of 3 kg/h, even with high air throughput and agitator speed drying was not possible and the SFD was flooded (figure 5-27).

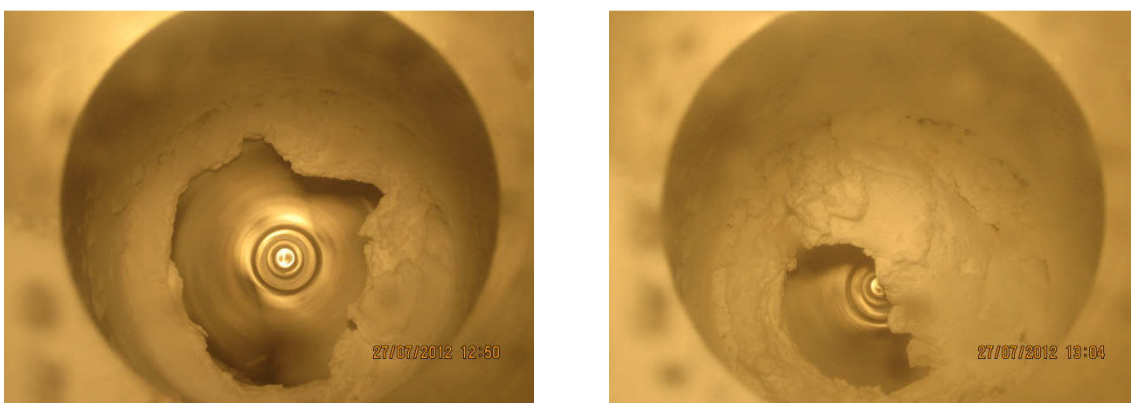


Figure 5-27: Aborted experiment SFD 48. The dryer tended to flood.

Due to the surfactant it seemed, that ibuprofen got stickier at given concentrations and process settings. Differential Scanning Calorimetry (DSC) analyses performed in RCPE analytic laboratories showed that surfactant sodium pyrophosphate tetra basic reduces the melting point of Ibuprofen from 77°C for the raw Ibuprofen to approximately 66°C.

In our test setup the air inlet temperature was 70°C and the outlet temperature was around 63°C. However material in the lower section of the dryer will experience temperatures around 70°C. Melting itself was not observed in these experiments. But close to the melting point the material might already get softer and stickier on the surface. This might lead to the observed effect that ibuprofen tends to stick on the wall and form big agglomerates instead of being pulverized and carried out.

For the experiment SFD 46 and SFD 47 the measured residual moisture were 0.070wt% and 0.050wt%. The results are in the same order of magnitude as the drying results for ibuprofen without surfactant obtained during the DoE study.

Summing up it can be said that surfactants can alter the material behavior and influence the drying process. In the case of ibuprofen it was observed that it was harder for the agitator to break down feed lumps which then more adhered to the wall. The feed appeared stickier than for ibuprofen without surfactant.

5.4.2. Drying above the melting point

As pharmaceutical products are often temperature sensitive, drying has to be performed on very low temperature levels. Any possibility to raise acceptable drying temperature facilitates the drying process leading to faster drying kinetics and lower residual moisture contents. For example it is known that in co-current spray drying, the inlet temperature of the drying air can be much higher than the material melting point, as the evaporating fluid reduces the temperature exposure of the sprayed droplet. It was evaluated whether similar effects could be utilized during spin flash drying.

For the experiment SFD 06, ibuprofen slurry with a content of 0.4wt% of surfactant was used.

Table 5-5: Process settings for drying over the melting point.

Exp Name	Air throughput [kg/h]	Classifier opening [mm]	Agitator speed [rpm]	Feed rate [kg/h]	Inlet air temp. [°C]	Model substance	Feed solid content [wt%]
SFD 06	400	80	840	1.60	varied	Ibu/Surfactant	50

The process was started with a drying-air inlet temperature of 60°C as shown in figure 5-28, left. At these settings the slurry could be dried successfully and only a little material stuck to the wall. For the experiment the temperature then was steadily increased whilst observing the process. At an inlet temperature of 75°C it was seen that dried particles started to adhere to the wall. At an inlet temperature of 80°C Ibuprofen started to melt on the wall in the lower region of the dryer, which can be seen in figure 5-28, right.

It can be noted that deposited material has no protective fluid layer which could cool the material by further evaporation. Also dried particles which could not follow the air stream, for example because of increased adhesiveness, will be exposed to the drying air temperature directly. For that it can be concluded that for drying with the SFD the temperature has to be kept under the critical material temperature such as melting point or temperature of degradation.

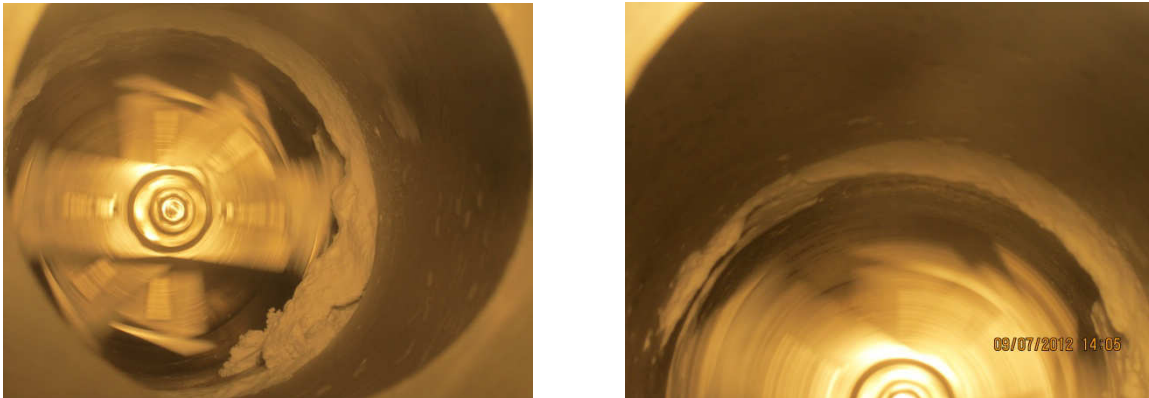


Figure 5-28: Experiment SFD 06, drying of heat sensitive materials at different temperatures.

Left: under critical; right: critical.

5.4.3. Drying of Benzoic acid

The solid concentration of the slurry was 67wt%. The slurry had a crystalline structure similar to adipic acid but segregated less from the fluid when filled into the feed vat.

Table 5-6: Process settings for drying Benzoic acid.

Exp Name		Air throughput [kg/h]	Classifier opening [mm]	Agitator speed [rpm]	Feed rate [%]	Inlet air temp. [°C]	Model substance	Feed solid content [wt%]
SFD 67	start-up	300	80	1400	2.00	80	Benzoic acid	67
	steady-state	400	80	1400	2.00	80	Benzoic acid	67

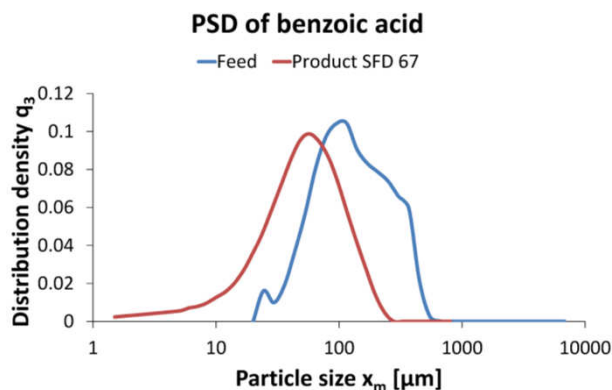
As observed for experiments with adipic acid a material layer built up around the agitator during start-up (figure 5-29, left). Later during drying the material broke off and only a little residue remained (figure 5-29, right). During steady-state, agglomerates and coarse particles were circulating around the agitator in the lower part of the dryer. Finer particles moved upwards along the dryer in strands. The same effect could be observed during drying of adipic acid with high air throughputs.



Figure 5-29: Left: Start-up phase. Material stuck to the wall. Right: Process end, little material residues are found.

The obtained residual moisture was 0.030wt% (KF titration).

The PSD of the product shifted to smaller particle sizes after drying. The PSD of the benzoic acid feed originates from milling the feed in smaller batches and then mixing the batches together. Due to further milling effects in the SFD the product shows a smoother distribution but still with a shift to smaller particles.



	Feed	Product
x_{50} [μm]	110.43 ± 1.83	35.62 ± 11.11
x' [μm]	151.51	49.80
n [-]	1.6126	1.3925

Figure 5-30: PSD of benzoic acid feed and product.



Figure 5-31: SEM image of benzoic acid at a magnitude of 500. (A) feed and (B) SFD 67.

Both, the feed and the product show particles of cubic and cylindrical shape in the SEM images (figure 5-31). For the product, a higher amount of small particles can be seen resulting from fragments produced during drying.

Drying of benzoic acid proved to be no problem. The drying behavior was similar to adipic acid. Similar to adipic acid, benzoic acid showed little residual moisture. Material breakage was observed.

5.4.4. Drying of Salicylic Acid

The solid concentration of the slurry was 69wt%. The slurry had a crystalline structure similar to adipic acid. When filling the slurry into the feed vat, fluid segregated into the drying chamber.

Table 5-7: Process settings for drying salicylic acid.

Exp Name		Air throughput [kg/h]	Classifier opening [mm]	Agitator speed [rpm]	Feed rate [%]	Inlet air temp. [°C]	Model substance	Feed solid content [wt%]
SFD 69	start-up	200	80	1400	2.00	80	Salicylic acid	69
	steady-state	400	80	420	4.00	80	Salicylic acid	69

During the start-up phase feed trickled into the dryer as a thin suspension for a time of approximately 20 minutes which was longer than for similar materials (benzoic acid and adipic acid). The feed splashed on the dryer wall, building residues (figure 5-32).

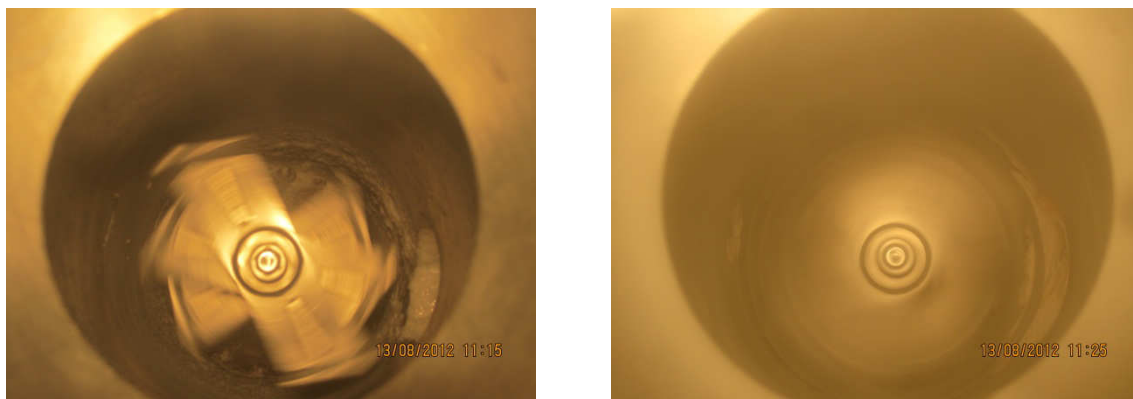


Figure 5-32: Experiment SFD 69 during start-up. Thin feed suspension is smeared around the agitator.

Due to the low water content of the feed in the steady-state phase and due to the dry particle stream around the agitator little new feed adhered onto the wall. The layer built up during start-up could be removed during steady-state drying. No bigger agglomerates could be seen circulating in the lower dryer area. It has to be noted that the drying chamber was highly

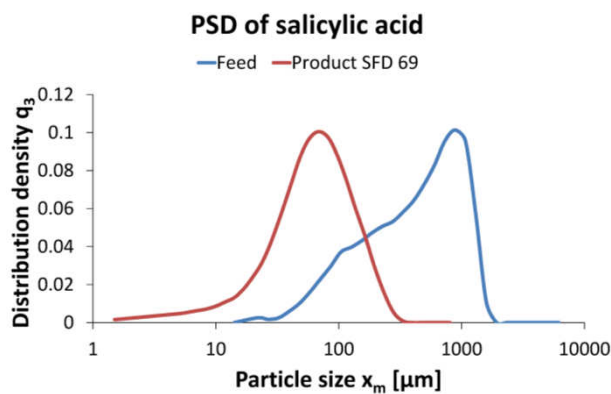
loaded with particles, blocking the view into the process chamber. After drying, it was observed that the dryer wall was covered with particles (figure 5-33, left) which, however, could be blown off when operating the dryer at high air throughput without fresh feed (figure 5-33, right).



Figure 5-33: Salicylic acid particles covering dryer wall (left). Particles being blown off (right).

The obtained residual moisture was 0.030wt% (KF titration).

Salicylic acid experienced dramatic material breakage with a reduction of median diameter from 467 μm to 85 μm . It also should be mentioned, that salicylic acid feed material showed the biggest initial particle size (table 3-7).



	Feed	Product
x_{50} [μm]	467.24 \pm 23.08	84.62 \pm 7.57
x' [μm]	602.47	119.14
n [-]	1.2450	0.8006

Figure 5-34: PSD of salicylic acid feed and product.

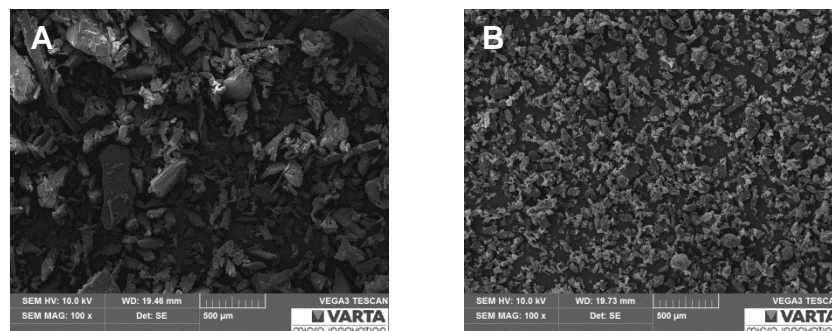


Figure 5-35: SEM image of salicylic acid at a magnitude of 100. (A) feed and (B) SFD 69.

In the SEM analysis (figure 5-35) the material breakage is easy to see. The product is composed of smaller particles showing a more homogeneous distribution than the feed. Feed particles and product particles both are of cubic shape.

Salicylic acid was easy to dry. The obtained residual moisture was within acceptable limits. Material breakage occurred and with the given settings a thin layer of dried particles adhered to the dryer walls at the end of the process.

5.4.5. Drying of Acetyl Salicylic Acid

The solid concentration of the slurry was 62wt%. The slurry consisted of fine particle agglomerates which were homogeneously distributed within the slurry. The slurry could build no structures. Plenty of water segregated from the feed slurry when filled into the feed vat.

Table 5-8: Process settings for production of acetyl salicylic acid.

Exp Name		Air throughput [kg/h]	Classifier opening [mm]	Agitator speed [rpm]	Feed rate [%]	Inlet air temp. [°C]	Model substance	Feed solid content [wt%]
SFD 83	steady-state	200	80	1400	2.00	80	Acetyl salicylic acid	69

During start-up the slurry glided from the feed inlet downwards in a helical way. At the height of the feed inlet a layer of crystals could be observed on the wall.

During steady-state the slurry was pulverized and dried immediately after entering the dryer. During the process a layer of particles adhered first on the wall of the dryer (figure 5-36, left) and then on the sight glass. Only little material build-up occurred in the lower drying chamber and the agitator. It was also observed that a particle layer covered the inner walls of the cyclone (figure 5-36, right).

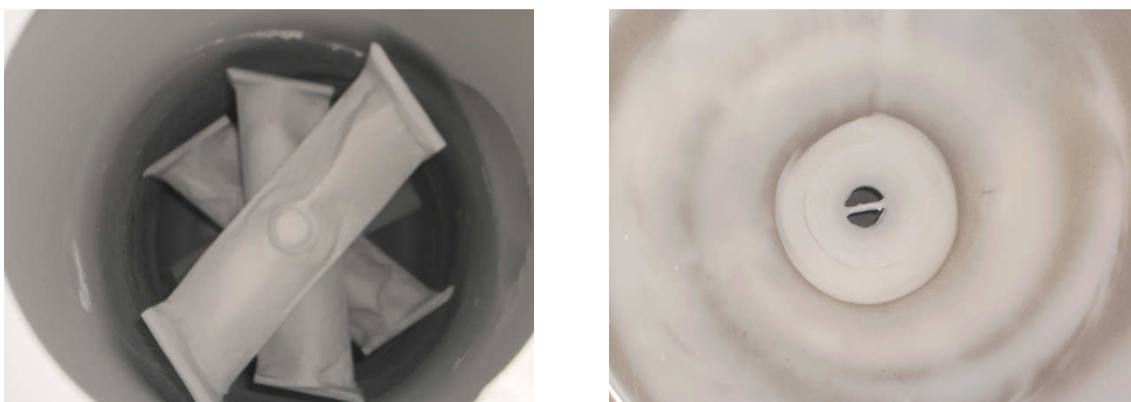
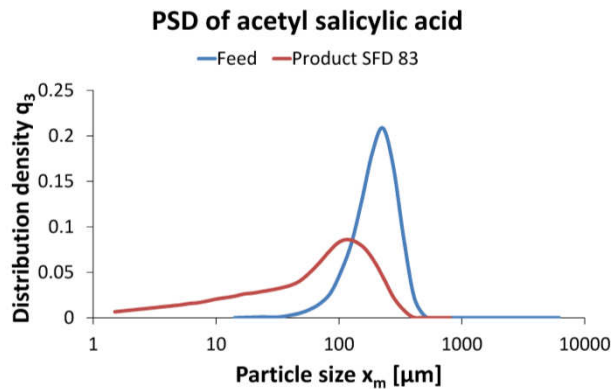


Figure 5-36: Experiment SFD 83. Both the dryer wall (left) and the cyclone wall (right) were covered with adhering particles.

The residual moisture was 0.060wt% (KF titration).

From PSD analyses it can be seen that the spread of the distribution increased largely during the drying operation. Also material breakage occurred but with less intensity than observed for salicylic acid.



	Feed	Product
x_{50} [μm]	204.18 ± 0.46	73.66 ± 2.91
x' [μm]	232.07	94.23
n [-]	2.9637	0.9363

Figure 5-37: PSD of acetyl salicylic acid feed and product.

The acetyl salicylic acid feed consisted of cylindrical shaped crystals of more or less similar size as can be seen in figure 5-38. The crystal surface looked scaled and the crystals themselves showed some orientation. The disc-shaped particles are remains of the original cylindrical particles. The cubic and needle shaped smaller crystals are fragments of the original particles.

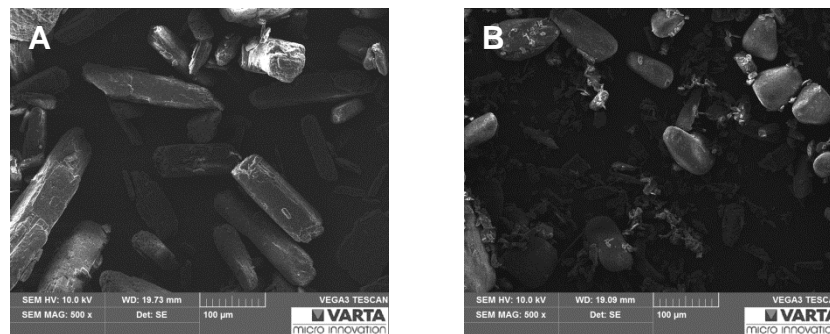


Figure 5-38: SEM image of acetyl salicylic acid at a magnitude of 500. (A) Feed and (B) SFD 83.

Acetyl salicylic acid was easy to dry. The feed was pulverized and dried quickly. However, whilst drying significant material breakage occurred. This led to an abrupt change in PSD. The produced particles tended to adhere on surfaces forming a particle layer.

5.4.6. Drying of Flour

Common plain flour with a protein content of around 11% was used. Flour is a hydrophilic material with poor solubility in cold water. The particle shape is cubic with a scaled surface.

The solid concentration of the slurry was 54wt%. The slurry looked like typical dough: sticky and of high viscosity.

Table 5-9: process setting for drying flour.

Exp Name		Air throughput [kg/h]	Classifier opening [mm]	Agitator speed [rpm]	Feed rate [%]	Inlet air temp. [°C]	Model substance	Feed solid content [wt%]
SFD 68	steady-state	400	80	1400	N.A.	70	Flour	54

During start-up the sticky dough adhered to the walls as well as to the agitator. Dough chunks were moved and stirred by the agitator. Due to the static pressure difference between the feed vat and the drying cylinder the dough was sucked into the process chamber. Therefore feed rate control was not possible. Some dough had to be removed by hand during the start-up phase as the lower drying chamber was completely filled.



Figure 5-39: Start-up phase for flour slurry. The lower dryer chamber is filled by dough.

As soon as the first dry particles were produced they started to cover the surface of the fed dough. As a result the fed in dough was less adhesive. The feed was then drawn into the drying chamber forming a dough strand that reached towards the center of the cylinder. This strand wobbled in the air and was cut by the agitator into bigger chunks. Figure 5-40, left shows the strand of dough wobbling in the circulating air.

However, remaining material built up during start-up and the non-stationary behavior of the feed rate led to blockage of the agitator. In some cases the agitator could restart by itself. In other cases it had to be restarted manually. At the end of the process it was observed that material had remained in the lower part of the dryer during the whole process time. The

material had the consistency of hard bread and was stuck to the wall as can be seen in figure 5-40, right. Such residues were also discovered in the drying air inlet.



Figure 5-40: Experiment SFD 68 during drying (left) and at the end (right).

The obtained residual moisture was 5.12wt% (KF titration). The water content might be a mixture of surface adhering water, by hydroxyl group bound water or entrapped water. It could not be distinguished how much these effects contribute to the total amount of residual moisture.

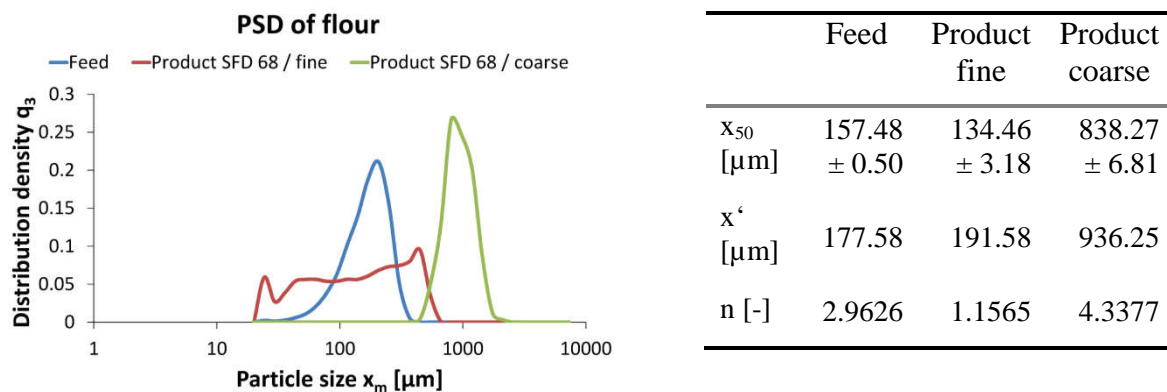


Figure 5-41: PSD of flour feed and product.

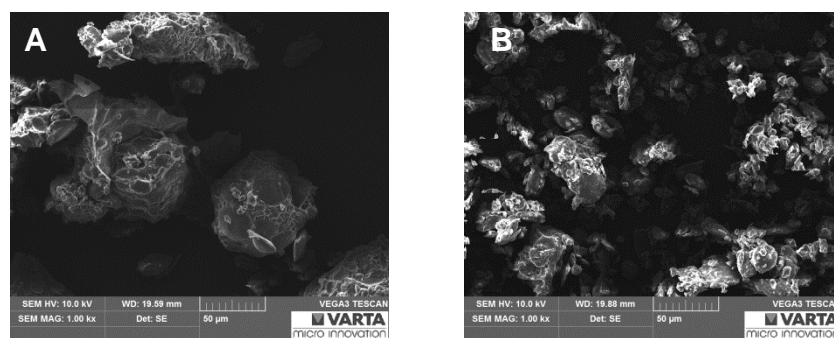


Figure 5-42: SEM images of flour at a magnitude of 1000. (A) Feed and (B) SFD 68, fine product.

Two different types of powder were obtained as product. The main part of the product consisted of a white powder similar to the original flour. The smaller part consisted of larger

yellow colored spheres. The particles were separated into a fine product and into a coarse product containing only the spheres.

For the fine powder fraction SEM (figure 5-42) images were taken and compared to the feed powder. The analyzed powder bulk consisted of cubic agglomerates of fine particles which looked smaller than the initial feed particles. Both particles show a kind of scaled surface.

Even though powder was produced, the achievable residual moisture content was above the acceptable limit of 2wt%. The process was irregular and the chamber filled up with material.

5.4.7. Summary of additional experiments

The additional experiments were performed to increase process understanding without undergoing the extensive experiment set-up of a full DOE.

The effect of surfactants in the slurry was investigated by example of an ibuprofen / sodium pyrophosphate tetrabasic (surfactant) mixture. It is known that the addition of surfactant decreases the melting temperature of the model system. Our tests were performed slightly over the melting point. The addition of surfactant led to an increased adhesiveness of the partially dried and the dried product. By that, big agglomerates were formed which couldn't be reduced by the agitator and threatened to flood the dryer.

An additional test setup was launched to investigate the effect of drying over the melting point of ibuprofen/surfactant mixture. Only minimal overheating was possible. At elevated drying temperatures effects like increased adhesiveness or melting occurred. As a result it is advised to only dry at temperatures lower than critical material temperature.

Milling behavior was exposed for drying of acetyl salicylic acid, salicylic acid and benzoic acid. As all 3 substances are similar to adipic acid this observed effect strengthens the conclusion that for crystalline products milling can be encountered. The degree of material breakage depended on the initial particle size. High values of material breakage were experienced for the larger feed particles of salicylic acid.

Flour, also a hydrophilic material like lactose, could not be dried sufficiently. In contrast to lactose the flour dough was sticky, easily clinging to any surface. This behavior led to significant material build-up in the dryer. In addition the dough was highly cohesive and it was hard to disintegrate the feed into smaller particles which could then be dried. The resulting residual moisture was around 5wt% and exceeded the limit of 2wt%. Summing up, highly cohesive and adhesive feeds like the flour dough cannot be dried with the SFD.

5.5. Discussion and Conclusion of the Experimental Study

Conducting experiments and using statistical methods for the evaluation provides a first answer of whether the SFD 47 is feasible for use in the pharmaceutical industry or not.

The most important product property is the residual moisture which has to be smaller than 2wt%. Materials investigated were either hydrophobic or hydrophilic. Even as the tendency to bind water is higher for hydrophilic materials, drying of lactose was possible in the investigated range of settings. Measurement of residual moisture above the limit for lactose could be found to originate from the bound crystal water. The surface of the resulting lactose particle can be regarded free of adsorbed water. For hydrophobic materials which were the main part of investigated materials the product residual moisture was well below the limit. It can be concluded that drying in the SFD 47 at temperatures of 80°C or 70°C is possible and leads to a dry product. The level of residual moisture did not depend on the drying settings in the investigated range of settings. The provided drying energy and the residence time in the dryer have been large enough for all cases. Higher drying temperatures are not applicable using the SFD 47. The particles dried having no protective fluid layer to shield the material from the hot air stream. For heat sensitive materials higher temperatures can cause degradation or change in their bio physiological properties.

In the special case of flour, a sticky high viscous paste (flour dough), no drying settings leading to a successful and stable process have been found. As a result it seems that the SFD is not capable of drying highly cohesive and adhesive feeds.

As typical for pneumatic dryers, particles suffered from attrition leading to fragments or even particle breakage. Large particles will be milled in the SFD. The degree of material breakage depends also on the particle size and increases with it. Further it seems to depend on the agitator speed and the air throughput. Both factors contribute to the speed of the particle in the agitated bed, which defines the force on the particle when bumping into each other or against the wall. Additionally the residence time of particles might depend on the air throughput. But here the relationship is not as easy, as the flow pattern of the particles in the dryer seems to change with the air throughput.

For the DoE study of adipic acid, a statistically significant relation between the material damage and the factors air throughput, agitator speed and feed rate could be found. With the

resulting data a statistical model could be developed predicting the material damage. For small particles as used in the DoE study of ibuprofen little material damage was experienced.

In addition to the change of size, also a change of pore structure was found for adipic acid. The effect is possibly caused by blockage of the pores by debris or simply destruction of the pores due to the mechanical treatment. Subsequently the specific surface area reduces, which can be disadvantageous for later processes which depend on the surface area (for example dissolution). Not investigated is the effect of attrition on stress sensitive materials like proteins. Such materials could take harm during the drying process. Process settings are adjustable, leading to lower stress but without further investigation it is not advised to dry such materials with the SFD 47.

In order to guarantee unchanged particle size of the product only small particles can be dried in the SFD 47.

For drying materials which largely dissolve in the fluid, agglomeration was observed during the drying operation. The number and size of precipitated particles depends on the drying energy available. For high drying energy (high temperature and high air throughput) smaller particles are produced. A large number of small particles means a large number of particles linking the original particles suspended in the fluid together. The result is larger agglomerates.

Even as the SFD 47 is advertised to be designed for small scale production it seems to still be over-sized for the investigated cases. The feed screw had to be operated at screw velocities lower than advised. The drying results for ibuprofen show that drying at slightly higher feed rates is problematic and can lead to flooding. For applications in the pharmaceutical industry the feed system should be adapted to allow smaller feed rates.

In addition the agitator concept has to be revised. The current concept is unsatisfying concerning the amount of material residues. Being scratched of due to self-cleaning effect of the dryer these particles lead to uncontrolled particle residence time and was not always sufficient enough. Material remains on the dryer wall can be counted as production loss which should be kept at a minimum. The gap between the agitator blade and the wall should be reduced. As an alternative, the scrapper could be brought into contact with the wall by springs.

The solid/gas separation system has to be changed. Using a cyclone, a high amount of material is lost leading to reduced production. This is a direct decrease of sell-able products.

The classifier showed no statistically significant effect on any product response in the investigated range of factors. However it is obvious from a theoretical standpoint, that the size of the classifier influences the flow profile in the dryer and hence the degree of separation of the particles as well as the residence time.

With the current setting it was not possible to investigate the effect of the feed moisture on the drying process. Excess water ran out of the feed slurry and into the dryer. To avoid segregating water from running into the dryer in industrial processes a drain in the feed vat could help. Excess water can be removed via this drain not influencing the drying process. Drying of pump-able feeds with higher water contents was not possible. However, drying of such feed was performed without the equipment advised by Anhydro/SPX. The experiments should be conducted with the proper equipment before conclusions of the possibility of drying pump-able feed are drawn.

6. Theoretical Description of the SFD 47

In the first part of this work principles of pneumatic drying and the principles of the spin-flash dryer were explained. In an experimental work the SFD 47 was investigated and for results of interest (responses) statistical models were developed. Even as these models might describe the SFD on hand they are not capable of predicting drying results for dryers with varying parameters such as SFD geometry or process settings outside of the investigated parameters.

In this chapter first attempts are made to describe the SFD by use of known mathematical correlations for drying operations and particle movement. Focus is given to the residual moisture level and the material breakage. For that, first experimental temperature and residual moisture values are compared. Later, the dependence of theoretical residual moisture level and drying time on the feed condition is calculated. Closing the particle movement through the dryer is discussed.

6.1. *Drying of Particles*

When modeling a dryer one has to balance the complexity of the system and the purpose of the model. For example, with an easy balance equation it is possible to calculate the outlet temperature of the drying air or the residual moisture of the product. However no information about drying kinetics which determine the residence time of the particle in the dryer is given. In literature [19] drying models are categorized into 4 levels depending on the amount of information needed.

Heat and mass balances: These balances only give the property of the resulting product or allow the calculation of drying air needed. They don't give any information about the dryer size, residence time or drying performance

Scoping: Approximate calculations use simple data and calculation simplifications to give information about dryer size and throughputs. First order drying or heat transfer controlled drying is assumed.

Scaling: The calculations use information gained by pilot-plant experiments and allow a scale-up of the dryer.

Detailed: Rigorous calculation of the dryer. It is possible to describe and track the temperature and moisture of the particles in the dryer. For these calculations, complex equations are used which require many parameters.

6.2. Balance Area

Modeling a system, first the system size and its input and output mass and energy flows have to be determined. For the drying calculation the SFD 47 can be abstracted as followed.

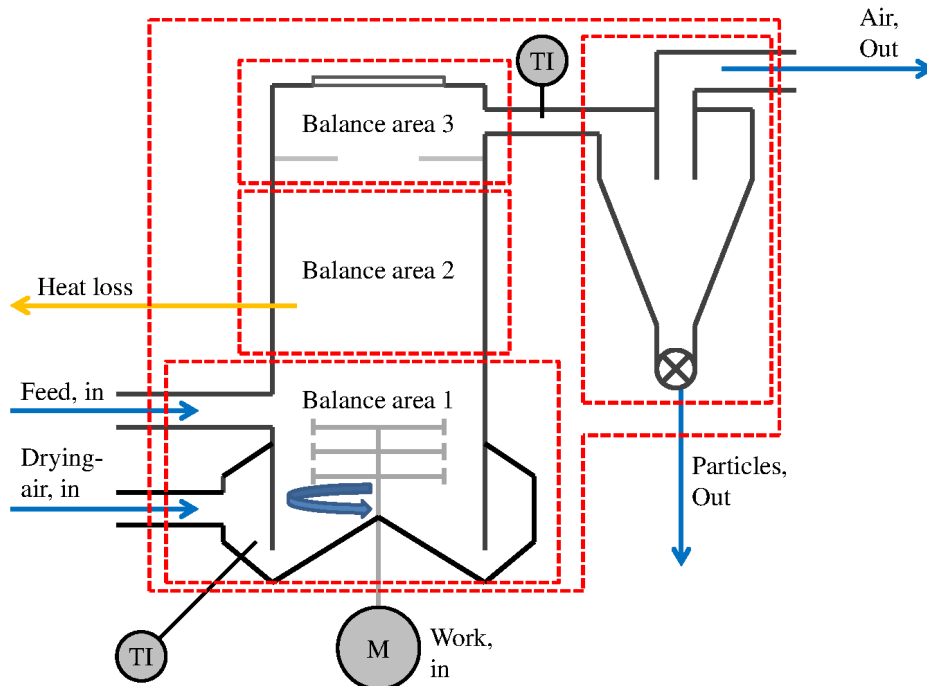


Figure 6-1: Balance areas of the SFD 47.

For the **all-over balance area** the wet feed and the drying air enter the SFD. Dried particles eventually loaded with residual moisture and the drying air eventually loaded with particles not removed by the cyclone leave the SFD.

In **balance area 1** the actual particle drying takes place in an agitated fluidized bed. No heat loss is assumed for this area and the drying air enters at set temperature. Mechanical energy is introduced by the agitator.

In **balance area 2** the particles are already assumed dry. However the system loses energy through the walls of the drying chamber.

In **balance area 3** no effect for the drying calculation is assumed. At balance area 3 the outlet temperature is measured.

In **balance area 4** additional heat loss occurs especially as the cyclone is not insulated. With the geometry known, the amount of energy loss could be calculated. For this work no information about the geometry was available. The residual moisture was measured after the cyclone.

6.3. Mass and Energy Balances

In stationary drying, a bed of particles is circulating in the agitated part of the SFD. Wet feed entering the dryer is disintegrated, dried and leaves the dryer as explained in chapter 2.1, page 9. For that the SFD can be abstracted as shown in figure 6-2. The solid feed is heated up by the hot inlet air stream and moisture from the feed evaporates. By that the air temperature drops. The evaporated water transfers from the solid stream to the air stream. Theoretical drying principles are well explained in various standard literatures [27], [19], [28] and [29].

For that the mass and energy balance can be solved and the following questions can be answered:

- 1) Correlation of outlet temperature and residual moisture
- 2) Theoretical drying capacity

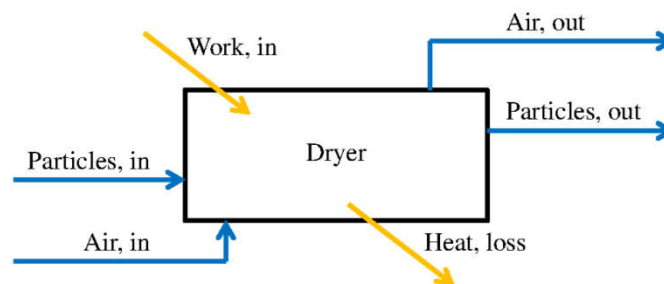


Figure 6-2: Overall mass and energy balance in drying operations.

6.3.1. Mass balance

The mass balance is given by the equation for the solid stream and for the gas stream. Here S [kg/s] is the dry solid mass flow rate and G [kg/s] the dry gas mass flow rate. The water content for both is given as water content on a dry basis. X [kg water / kg solid] is the liquid water content on a dry basis and Y [kg water / kg gas] the vapor content on a dry basis. W [kg/s] is the mass flux of evaporating water.

$$S * (1 + X_{in}) = S * (1 + X_{out}) + W \quad (6-1)$$

$$G * (1 + Y_{in}) + W = G * (1 + Y_{out}) \quad (6-2)$$

$$W = S * (X_{in} - X_{out}) = G * (Y_{out} - Y_{in}) \quad (6-3)$$

S can be calculated from the feed composition using the feed rate F_{feed} [kg/s] and the solid content on a wet basis w_{solid} [-]. The liquid water content on a dry basis X_{in} for the inlet stream can also be calculated from these values.

$$S = F_{feed} * w_{solid} \quad (6-4)$$

$$X_{in} = \frac{F_{feed} * (1 - w_{solid})}{S} = \frac{1}{w_{solid}} - 1 \quad (6-5)$$

X_{out} can be calculated with known evaporation rate W :

$$X_{out} = X_{in} - \frac{W}{S} \quad (6-6)$$

Knowing X_{out} the residual moisture of the product can be calculated:

$$RM = \frac{X_{out}}{1 + X_{out}} \quad (6-7)$$

As stated in chapter 3.1 (page 11) the air flow is measured by the pressure drop over the cyclone. By that, not the dry gas mass flow rate, G , but the total air throughput F_{air} [kg/s] is measured.

$$G = \frac{F_{air}}{(1 + Y_{out})} \quad (6-8)$$

The data known for the inlet air is its relative humidity φ at room temperature and the room temperature T_{room} [°C]. With T_{room} the saturated partial water vapor pressure P^S_{water} [Pa] can be calculated using the Antoine equation (6-10). With this data Y_{in} can be calculated.

$$Y_{in} = \frac{MM_{water}}{MM_{air}} * \frac{\varphi * P^S}{P - \varphi * P^S} \quad (6-9)$$

$$\log(P^S) = A - \frac{B}{T + C} \quad (6-10)$$

$$\varphi = \frac{p_{i,water}}{P^S_{water}} \quad (6-11)$$

The Antoine coefficients A , B and C for water are listed in the table below. The pressure P^S is given in [kPa] and the Temperature T in [K]. Pressure P in equation (6-9) is the total pressure.

Table 6-1: Antoine parameters for water [30].

Temperature T [°C]	Temperature T [K]	A	B	C
30.17	303.32	7.19622	1730.63	-39.724
70.10	343.25	7.19951	1730.63	-39.724

MM is the molar mass of the components. The molar mass is 18 kg/kmol for water (MM_{water}) and 28.9 kg/kmol for air (MM_{air}).

As can be seen from equation (6-11) the relative humidity φ is the ratio of the partial pressure of water vapor p_i to the vapor pressure of pure water at given temperature P^S . By that φ also indicates how close the moisture content in air is to the saturation point $\varphi = 1$.

$\phi < 1$: under-saturated condition. The air could take up more water vapor

$\phi = 1$: Air is saturated with water vapor.

$\phi > 1$: Over-saturated condition. Water vapor condenses and fog or liquid layers are emerging.

For the drying operation this means, that only cases leading to $\phi < 1$ are processable. Taking in mind the difference of pressure as the driving force for evaporation the resulting relative humidity of the exhaust gas ϕ_{out} should be well below 1.

Y_{out} is then calculated from Y_{in} and W .

$$Y_{out} = Y_{in} + \frac{W}{G} = Y_{in} + \frac{W \cdot (1 + Y_{out})}{F_{air}} \quad (6-12)$$

Equation (6-12) can be transformed to

$$Y_{out} = Y_{in} \cdot \frac{F_{air}}{F_{air} - W} + \frac{W}{F_{air} - W} \quad (6-13)$$

With equation (6-13), equation (6-8) for the air stream G can be formulated as followed:

$$G = \frac{F_{air} - W}{(1 + Y_{in})} \quad (6-14)$$

Compared to G , the mass of evaporated water W is small. Also the inlet water vapor load is on the order of 10^{-2} . Therefore only little error is encountered setting $G = F_{air}$. For DoE adipic acid, the error was calculated to be $\frac{F_{air}}{G} - 1 \approx 1\%$.

6.3.2. Energy balance

For the energy balance, mechanical energy input $P_{agitator}$ and loss of heat energy E have to be taken in account, in addition to the energy flow due material flow.

$$S \cdot h_{X+1,in} + G \cdot h_{Y+1,in} + P_{agitator} = S \cdot h_{X+1,out} + G \cdot h_{Y+1,out} + E \quad (6-15)$$

h_{X+1} and h_{Y+1} [J/kg] are the specific enthalpy of the dry solid mass flow rate S and the dry gas mass flow rate G . The energy of the solid particle stream is divided into the heat energy of the particles and the heat energy of the water which is loaded onto the particles. The temperature of both, the particles and the water, is assumed to be the same.

As for the mass balance, the water is seen as loaded onto the particles. Therefore the specific enthalpy is also formulated on a dry basis.

$$\begin{aligned}
 h_{X+1} &= h_{particles} + X * h_{water} = & (6-16) \\
 & c_{p,p} * (T - T_0) + X * c_{p,w} * (T - T_0)
 \end{aligned}$$

T_0 is the reference temperature. Usually in drying or when operating with water, the reference temperature is $T_0 = 0^\circ\text{C}$ or 273.15 K . c_p [J/(kg*K)] is the specific heat capacity at constant pressure. $c_{p,p}$ is the sensible heat of the particles and $c_{p,w}$ is the sensible heat of liquid water.

As for the particle stream, for the gas stream the water is seen loaded onto the gas stream and therefore the enthalpy is formulated on a dry basis.

$$\begin{aligned}
 h_{Y+1} &= h_{air} + Y * h_{water\ vapor} = & (6-17) \\
 & c_{p,air} * (T - T_0) + Y * (h_{vl} + c_{p,v} * (T - T_0))
 \end{aligned}$$

h_{vl} [J/kg] is the latent heat of vaporization

Energy introduced by the agitator $P_{agitator}$

The maximum power of the agitator which can be introduced is stated as 1100 kW by its producer, SEW [13].

Anyway, as could be seen by the current uptake of the agitator during drying, the energy consumption of the motor is well below maximum. In addition most of the energy will be used to disintegrate the entering slurry and to increase the kinetic energy of the gas stream. It is assumed that only a little mechanical energy dissipates into heat energy. Therefore it is assumed that the heat energy input derived from the agitator is small and negligible.

Loss of Heat H_{loss}

As no value could be provided by the producer Anhydro (SPX) the loss of heat has to be estimated. From the technical drawing [13] the dimensions of the dryer and the material used for insulation are known and shown in figure 6-3. The length of the dryer exposed to the environment and considered for loss of heat energy is $L = 692\text{ mm}$. The radii are listed in table 6-2. From these data the wall thickness and the insulation thickness can be calculated. The dryer wall is made of stainless steel. The insulation is Vermiculite. The conductivity values for the materials are taken from literature [31] and are listed in the table below.

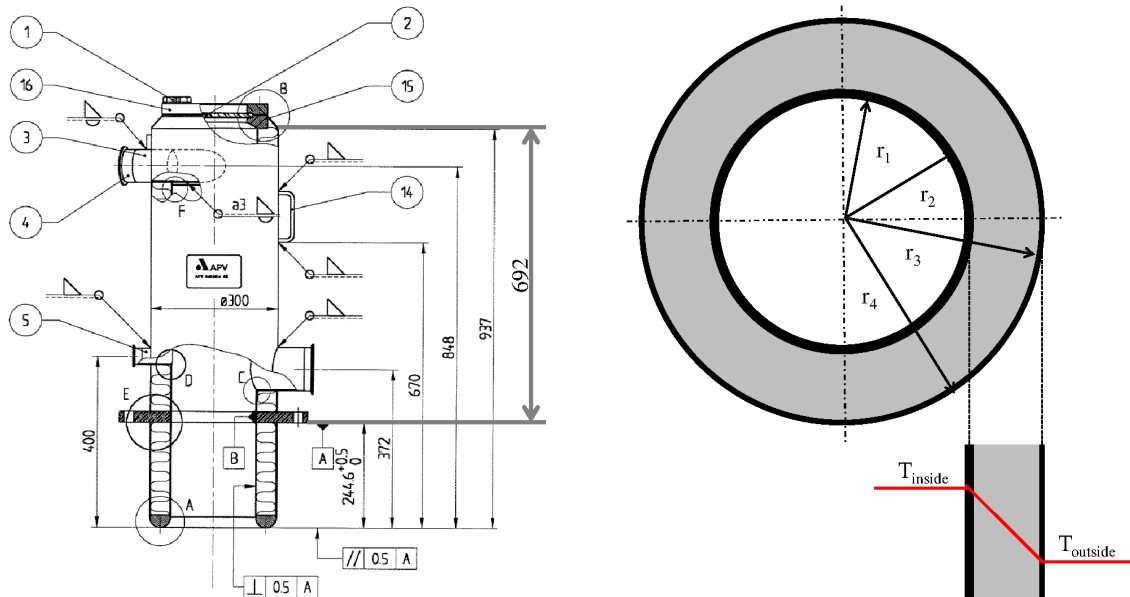


Figure 6-3: Technical drawing of the SFD and its dimensions.

Table 6-2: Physical and geometrical data of wall material and insulation.

Heat conductivity [W/(m*K)]		Dimensions [m]	
Steel λ_1	16.00	r_1	0.1000
Insulation λ_2	0.07	r_2	0.1020
		r_3	0.1495
		r_4	0.1500
		L	0.6870

As the main heat conductive residence comes from the insulation only a negligible error is made when ignoring the convection on the inner and outer surfaces. The air temperature above the drying zone varies depending on the drying conditions. The temperature is assumed to be not higher than 75°C.

The mean temperature ΔT_m is calculated as arithmetical mean value.

$$\dot{Q} = k * A * \Delta T_m \quad (6-18)$$

$$\dot{Q} = \frac{2 * \pi * L * (T_{inside} - T_{outside})}{\frac{1}{\lambda_1} * \ln\left(\frac{r_2}{r_1}\right) + \frac{1}{\lambda_2} * \ln\left(\frac{r_3}{r_2}\right) + \frac{1}{\lambda_1} * \ln\left(\frac{r_4}{r_3}\right)} \quad (6-19)$$

The resulting loss of heat is then not more than 40 W (= 144 kJ/h). For comparison to the power of the agitator and the loss of heat, the enthalpy flux H [J/s] of the inlet air from the air can be calculated roughly as:

$$H_{air,in} = F_{air} * c_{p,air} * (T_{air,in} - T_0) \quad (6-20)$$

The smallest value for the inlet heat flux is then for 200 kg/h of air throughput at an inlet temperature of 70°C equaling 3889 W (14000 kJ/h).

Comparing the loss of heat to the minimum inlet heat flux of the air $\frac{E}{H_{Air,in}} = \frac{40 W}{3889 W} \approx 1\%$ it can be seen that the loss of heat is small compared to the heat flux over the entire unit.

6.3.3. Application of the Material and Energy Balances

With these balance equations the measured exhaust air temperature and residual moisture can be compared. Knowing the temperature drop of the air and the lost heat energy the amount of evaporated water can be calculated. With knowledge of the initial water content X_{in} the resulting water content X_{out} and hence the residual moisture RM can be calculated and compared to the measured data. For that, equation (6-15) is rearranged and equations (6-16), (6-17) and (6-12) are integrated leading to an equation for X_{out} .

$$X_{out} = \frac{L * h_{X+1,in} + h_{Y+1,in} - \frac{E}{G} * T_{out} * (L * A_T * c_{p,p} + c_{p,air}) - (L * X_{in} + Y_{in}) * (h_{vl,w} + c_{p,v} * T_{out})}{(L * c_{p,w} * A_T * T_{out} - L * (h_{vl} + c_{p,v} * T_{out}))} \quad (6-21)$$

X_{out} is calculated and with equation (6-7) the RM of the product can be expressed. In equation (6-21) L is the ratio of the dry particle stream S to the dry air stream G , $L = \frac{S}{G}$. A_T is the ratio of the particle outlet temperature to the temperature of the exhaust gas, $A_T = \frac{T_{out,particle}}{T_{out,air}}$. The actual outlet temperature of the particles depends on the conductivity of the particles as well as on their size, the flow behavior and the residence time. The temperature distribution within the particle depends on its size and conductivity. For small particle diameters the temperature distribution can be assumed homogenous. The residence time of the particle is assumed to be longer than the time needed for drying and thus A_T is stated equal 1.

Using physical property data (table 10-1) from literature the theoretical RM content of the product powder was calculated for adipic acid DoE cases. The total pressure P is 990 mbar for all cases.

As can be seen in table 6-3 and for all results in table 10-8 (appendix) the resulting water content X_{out} drops below zero in several cases. This would mean that more water evaporated than was actual present in the feed.

Table 6-3: Liquid water content on dry basis X_{out} for dried particles of adipic acid.

Case	T_{room} [°C]	ϕ [%]	F_{Air} [kg/h]	F_{Feed} [kg/h]	w_{Solid} [wt%]	T_{in} [°C]	T_{out} [°C]	X_{out} [-]
SFD15/DOE03	25.5	37.4	200	1.19	77	79.8	73.1	-0.221
SFD14/DOE08	25.5	37.4	400	1.19	90	80.1	76.4	-0.401
SFD57/DOE11	27.1	44.5	200	5.34	84	80.1	68.3	0.019
SFD58/DOE16	27.1	44.0	311	5.34	90	79.2	73.3	-0.008
SFD51/DOE19	24.9	52.6	300	3.26	77	79.8	70.7	-0.096

Reasons for the results can be that:

- more heat energy is lost during the drying process, which leads to a higher temperature drop.
- the measurement inaccuracies of inlet and outlet air temperature are too high. As only a little water is evaporated compared to the air stream, small inaccuracies in air temperature would cause a significant error on calculated water load.
- fluctuations of the actual feed led to periodic changes of the air temperature which could not be observed by the measurement accuracy.

Rearranging equation (6-21) the outlet air temperature can be calculated using the experimentally determined residual moisture. The calculated temperature can be compared to the measured data showing the deviation of theoretical data to measurement data.

$$T_{out,air} = \frac{h_{Y+1,in} + L * h_{X+1,in} - \frac{E}{G} - Y_{out} * h_{vl}}{c_{p,air} + Y_{out} * c_{p,vapour} + L * A_T * c_{p,particles} + L * A_T * X_{out} * c_{p,water}} \quad (6-22)$$

The term $L * A_T * X_{out} * c_{p,water}$ is on the order of 10^{-5} and can be ignored for practical analyses. To calculate T_{out} , measured data for the residual moisture of adipic acid DoE cases were used. The exact values from the calculation can be found in the table 10-9. The results are presented in figure 6-4.

For a low feed rate, high divergence between the measured and calculated temperature is observed. For these cases only a little water evaporates and errors could have a bigger effect. Also for a low feed rate discontinuous feeding was observed. Periodically the water load is higher, which would lead to a lower outlet temperature. But also there would be times where the water load is lower, which would show an even higher outlet temperature. In the results, only the lower temperatures for the low feed rate can be seen.

For a high feed rate, the difference is smaller. For those cases the feeding was more continuous. This would clearly speak for an influence of the feed rate on the divergence between measured and calculated data. However the exact cause and mechanism of the effect can yet not be explained.

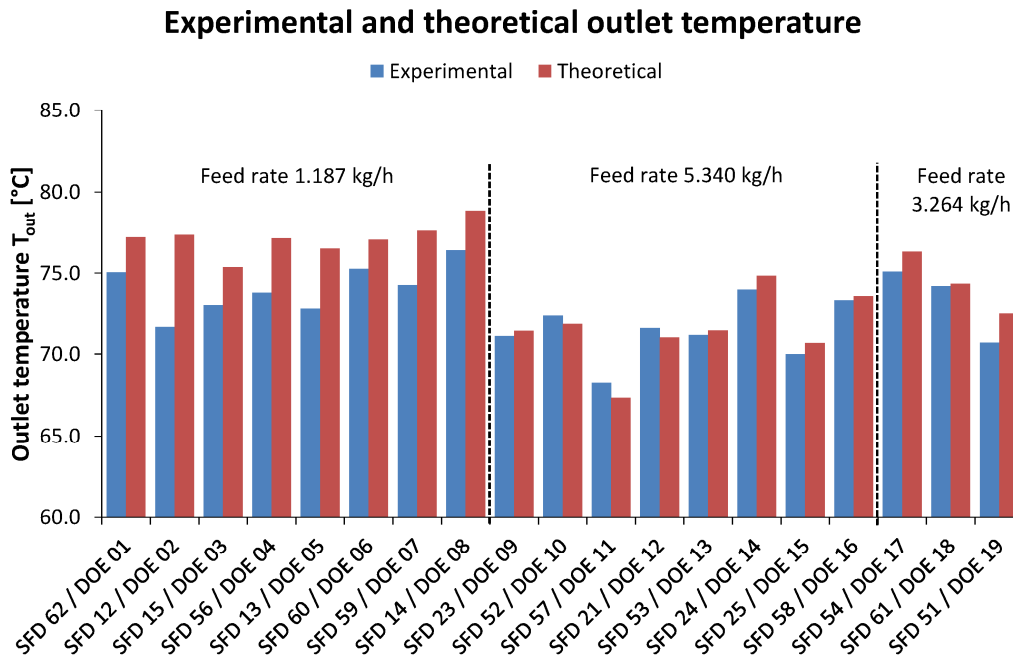


Figure 6-4: Comparison of the experimental and theoretical outlet temperature for adipic acid.

From the results it can be concluded that the two dependent values, outlet air temperature and residual moisture, cannot be compared due to inaccuracies in the measurement and the non-ideal process behavior causing fluctuations in the actual feed load.

6.3.4. Sorption Isotherm

As mentioned in the previous chapter the resulting residual moisture and the outlet air temperature are related to each other by the mass and energy balance equations. In addition the residual moisture is also related to the relative humidity expressed by the sorption isotherm. The relative humidity itself is a function of the air temperature and the water load as shown in equations (6-9) to (6-11).

The sorption isotherm presents the equilibrium distribution between water bound or adhering on the particle, the residual moisture, and the relative water content of the drying air, the relative humidity [29]. The sorption isotherm is specific for every material. Shown in figure 6-5, left are the adsorption isotherms for (a) potatoes, (b) copper beech wood, (c) sulfate paper, (d) 6-polyamide and (e) soap. Generally porous and hygroscopic materials tend to strongly absorb water. Shown in figure 6-5 right is that the sorption isotherm also depends on the gas temperature. For the same relative humidity the amount of water load on potato decreases with an increase in temperature. For all materials it can be said that low relative humidity leads to low residual moisture which can be achieved by prior dewatering of the drying air and/or high drying temperature.

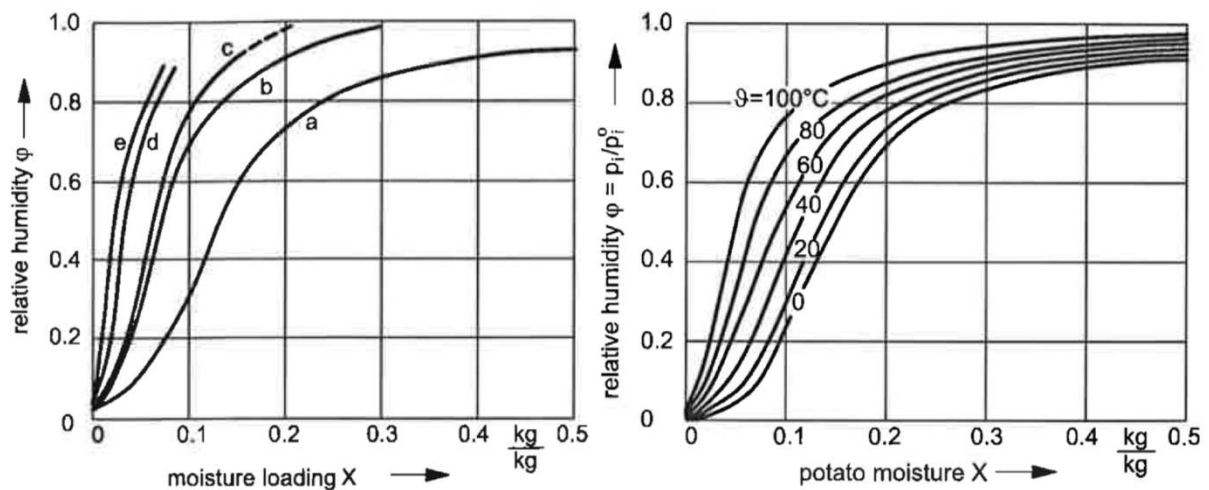


Figure 6-5: Sorption isotherm for various products and temperature [29].

Sorption isotherms are determined experimentally in the laboratory. With the resulting data the equations of Freundlich Langmuir, equation (6-23) as well as Brunauer, Emmet and Teller are suitable for mathematical description of the isotherms [29].

$$X = X_0 * \frac{K*RH*P^S}{1+K*RH*P^S} \quad (6-23)$$

The Freundlich Langmuir equation considers a monolayer of water molecules on the surface of the particle. Hereby is X_0 the number of available locations on the surface. X is Number of surface locations with water adhering. X is expressed as kg water per kg particle space, which equals the liquid water content on a dry basis. K is the ratio of the adsorption rate to the desorption rate. The lower K the better water can be removed from the particle surface.

For the test system adipic acid / water only one source of sorption isotherm data was accessible [32]. The data was read from the plot for adipic acid dried in a stream of hot air at 80°C.

The Freundlich Langmuir equation was fitted by use of least squares sum using MS Excel.

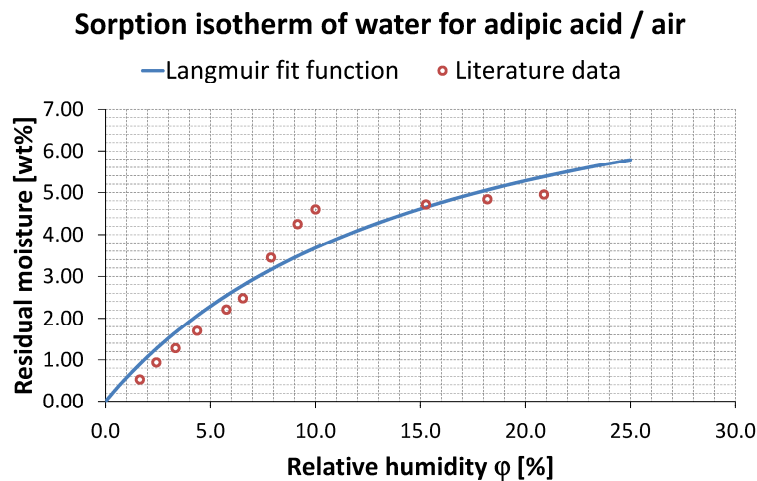
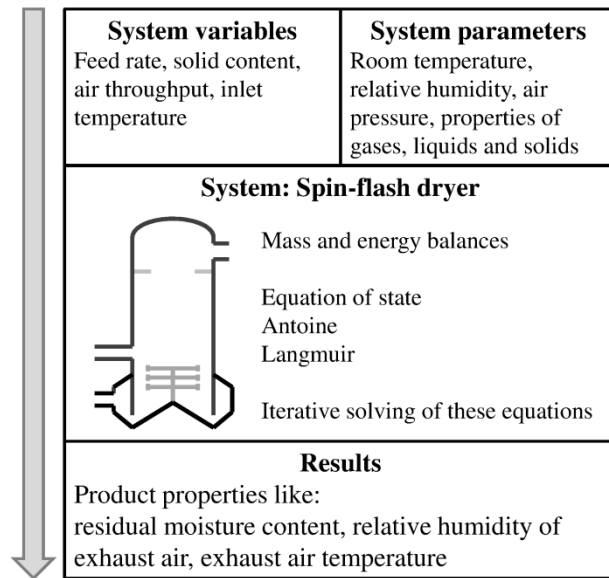


Figure 6-6: Freundlich Langmuir sorption isotherm for the system water / adipic acid. Data from literature [32].

For the system of adipic acid / water the coefficient for the Freundlich Langmuir equation is $K = 1.2431 \cdot 10^{-4} \text{ 1/Pa}$ and $X_0 = 1.0319 \cdot 10^{-4}$. The saturated partial water vapor pressure P^S is expressed in Pa.

6.3.5. Drying capacity

Using the mass and energy balances combined with the two presented equations of state, the Antoine equation (6-10) and the Freundlich Langmuir equation (6-23), the theoretical drying capacity of the SFD can be calculated (figure 6-7).



In this calculation the same simplifications as for the mass and energy balances are assumed. The feed is fully dispersed and dried in the lower part of the SFD. The residence time of the particles is long enough to ensure equilibrium conditions at the dryer exit. The solid temperature is the same as the temperature of the exhaust gas. The loss of heat is 150 kJ/h. System parameters are the room temperature, relative humidity and the air pressure.

Figure 6-7: Estimation of drying capacity. Calculating the equilibrium residual moisture load

Physical data for gases, liquids and solids are taken from literature (table 10-1).

System variables are the feed rate, solid content, air throughput and inlet air temperature. As for the DoE cases these variables can be changed.

Using mass and energy balances, the Antoine equation and the Freundlich Langmuir equation the residual moisture can be calculated iteratively. The loop exit condition was a change of residual moisture content of less than 10^{-5} . The equations were solved using MatLab. The calculation is shown in the appendix (chapter 10.8, page 126). Results are shown in figure 6-8 and figure 6-9.

In figure 6-8 the residual moisture is plotted above the feed rate and the feed solid concentration. The critical level of residual moisture which is 2% is drawn as a thick line. Feeding conditions leading to results below this critical value lead to acceptable product properties. The residual moisture is calculated for different air throughput at an inlet air temperature of 80°C. Figure 6-8, left is for 400 kg/h air throughput and figure 6-8, right for 200 kg/h air throughput. It can be seen that the number of feeding conditions leading to acceptable product properties is smaller for an air throughput of 200 kg/h.

In the figure it can be seen that for dry feed (solid content of 100%) water vapor originating from the drying air condenses on the particle surface leading to higher outlet moisture than inlet moisture. The effect is higher for lower air throughput as the temperature loss due loss of heat and heating of particle is more significant. The effect of feed moisture on the residual moisture of the product gains in importance with increasing feed rate. For low feed rate the evaporated mass of water is close to the order of water content from the drying air. The relative humidity of the drying air only changes a little and the residual moisture is at similar level.

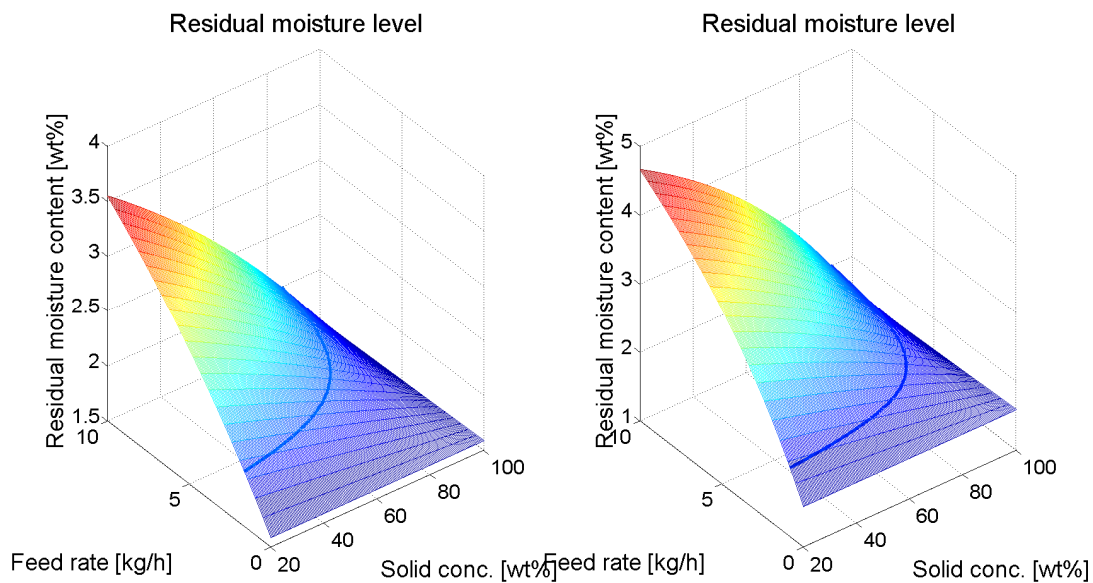


Figure 6-8: Results for equilibrium residual moisture using an iterative calculation. The thick line indicates the critical residual moisture level of 2wt%.

Contours can be drawn on top of the 3D plot. The influence of the factors air throughput, air inlet temperature and relative humidity of the inlet air are shown and discussed in figure 6-9. The line represents the critical residual moisture level of 2wt%. The upper left corner or the area above the critical moisture curve represents unacceptable residual moisture levels. The lower right corner or the area beneath the critical moisture line represents acceptable residual moisture levels.

Figure 6-9A compares different magnitudes of air throughput at the same inlet air temperature and water content. As already discussed the operational field increases with the air throughput. The shape changes a little but generally the curve is shifted to higher levels. For an air throughput of 100 kg/h only small feed rates < 1 kg/h or dry feed with a solid content > 90wt% can be dried.

Figure 6-9B also compares the air throughput but at a lower inlet air temperature. The shape of the curve is the same as for Figure 6-9A and the same area is covered. For that it can be concluded that the influence of the inlet air temperature is small in the range of 60°C to 80°C. It has to be noted that for both calculations, RM at 80°C and RM at 60°C, the same adsorption isotherm was used. The adsorption isotherm itself, however, would depend on the drying temperature [32]. Therefore errors are made when comparing both results. However from the investigation it can be said that the magnitude of influence is higher for the air throughput than for the inlet temperature of the drying air in the investigated range of settings.

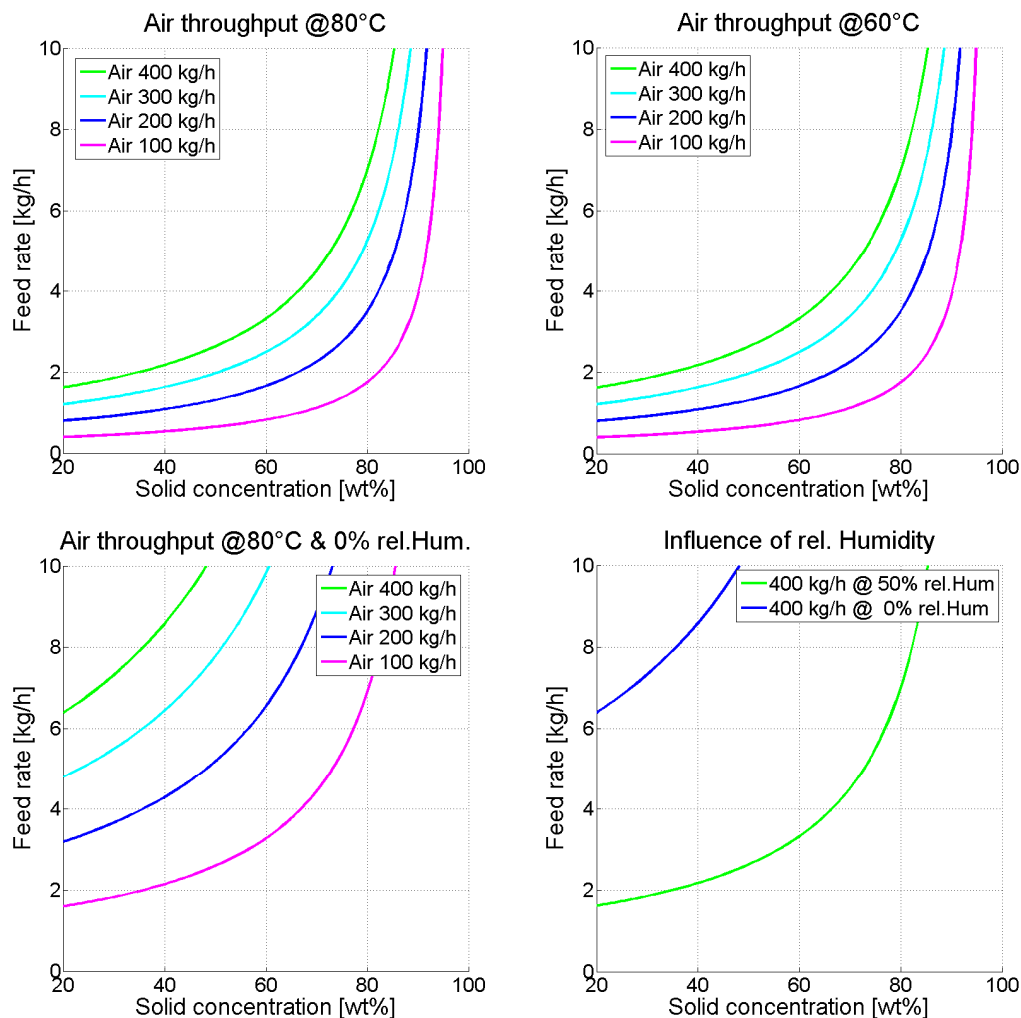


Figure 6-9: Contour plots for several drying conditions. A: Influence of the air throughput at 80°C; B: Influence of the air throughput at 60°C; C: Influence air throughput for dry air and D: Influence of initial air water load.

Figure 6-9C and D both show the influence of the initial water load of the drying air. For previous calculations air was used at a room temperature of 24°C and a relative humidity of 50% representing the conditions in summer when the drying experiments were performed. A

reduction of the water content has a dramatic effect on the operational field. The cause of the effect can best be explained on hand of the sorption isotherm shown in figure 6-6. The liquid water content on a dry basis of the solid particle increases sharply with an increase of the relative humidity. The rate of increase slows for higher relative moisture content of the air. For residual moisture levels of 2wt% and below the residual moisture is quite sensitive on small changes in the relative humidity of the air. Therefore removing the water from the drying air increases the operational field dramatically.

With knowledge about physical properties of other materials and material combinations the residual concentration can be calculated. For example the residual concentration of organic solvents can be calculated knowing their Antoine parameters and sorption isotherm. Another example is that drying operations under inert gas can be calculated showing the residual moisture level; for example for N₂ instead of air as drying gas.

From the results it can be seen that the performed adipic acid experiments were inside the good drying zone for high air throughput.

6.3.6. Summary of Mass and Energy Balances

With the mass and energy balances it was possible to calculate the product properties (particle or air) with limited physical data which are easily accessible.

The mass and energy balance would have the potential to predict the quality of either the drying air or, more interestingly, the particles, knowing the properties of the other. However the results of the DoE experiment did not correlate properly. As potential causes, variability in temperature measurement of the air and fluctuation in the actual feed rate had been discussed.

Adding equations of state it was possible to predict residual moisture levels for different feed conditions. Investigations of the operational space, which depends on the air throughput, air inlet temperature and the relative moisture of the inlet air were conducted. The air throughput and the water content of the inlet air had an influence on the resulting residual moisture level. While variation of the air throughput also has an influence on particle motion in the dryer, the water content of the air only has an influence on the residual moisture level of the product. Reducing the water content of the drying air can increase the performance of the SFD. The equations can also be used to calculate drying results for materials which are not easy to handle in the laboratory, such as toxic organic solvents.

It could be shown that mass and energy balances, combined with equation of state, are a useful tool for planning drying operations.

6.4. Drying Kinetics and Evaporation Rate

Especially when drying heat sensitive products which can easily degrade or lose their physiological activity (which APIs are susceptible to), it is of interest to understand how fast the wet solid is dried and how long it remains in the dryer. Prolonged residence time can be promoted by back mixing or adherence of the material to dryer parts. Also agglomeration can contribute to a long residence time.

The ideal drying operation would be fast drying in the agitated zone with immediate discharge when desired residual moisture content is reached.

With drying kinetics and mass transfer the moisture content of a particle in the SFD can be calculated over time. Stating desired residual moisture content the time until the value is achieved can be calculated. This would result in an ideal residence time without regard to particle movement and sedimentation in the dryer.

For drying goods several phases with distinct drying behavior are known in literature [19], [28] and [27]. The different phases are represented by drying curves (an example is shown in figure 6-10). Drying curves represent the change of the drying rate over the drying process. For that, the drying rate is noted as function of time or water load on a dry basis.

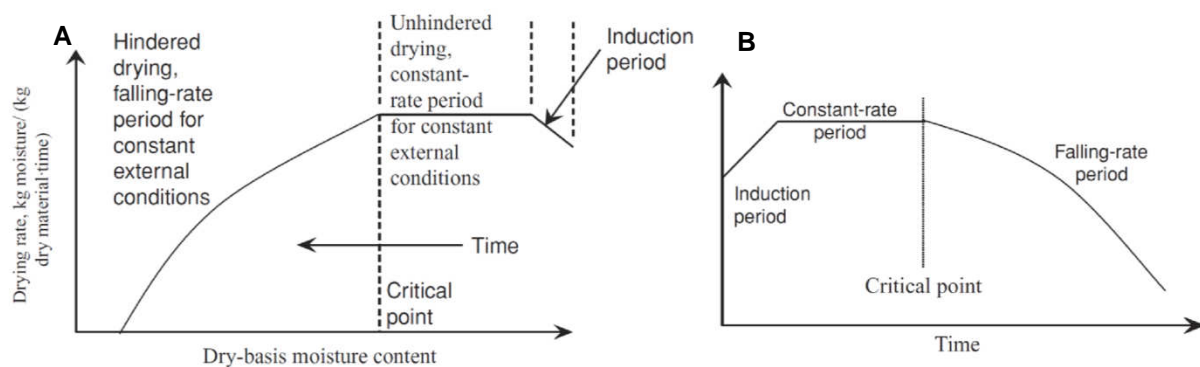


Figure 6-10: Typical drying curves [19]. A: Drying rate over the dry-basis moisture content. B: Drying rate over drying time.

Typical phases during drying operations are:

Introduction period: Material is heated up and the drying rate rises accordingly.

Constant-rate period: Energy absorbed leads to evaporation of surface moisture. The evaporation rate is only limited by the amount of heat energy provided or transferred to the material and is thereby governed by the heat transfer rate. The vapor pressure over the surface equals the vapor pressure of the pure fluid at the same temperature [33].

Critical point: At the critical point all surface moisture is evaporated. Only porous captured moisture, absorbed moisture and crystal water remains.

Falling-rate period: In the falling rate period the evaporation is governed by the mass transfer. Depending on the material nature the mass transfer can be the product of pore diffusion or material diffusion, if the material is capable of swelling.

The drying rate rapidly decreases in the falling-rate period. As the residence time in the SFD is stated as rather short [8] it can be assumed with reason that mainly surface drying occurs. The mass flux of evaporating water W [kg/s] equals the specific heat flux e [W/m²] over the particle surface A [m²] divided by latent heat of vaporization h_{vl} [J/kg] [19].

$$\text{Mass flux} = W = \frac{A \cdot e}{h_{vl}} = \frac{A \cdot \alpha \cdot (T_{air} - T_{drop})}{h_{vl}} \quad (6-24)$$

α is the heat-transfer coefficient [W/(m²*K)] , T_{air} the temperature of the drying air [°C] surrounding the particle and T_{drop} is the wet-bulb temperature [°C]. The wet-bulb temperature comes from the properties of the drying air. With the present properties, the relative humidity of the air would be adiabatic, increasing until reaching a maximum level of 100%. The temperature decreases according to equation (6-17) resulting in the wet-bulb temperature.

The mass flux in the SFD is determined by the heat-transfer coefficient and the free particle surface. Both will be derived and explained in the following chapters.

6.4.1. Heat-transfer coefficient

The heat-transfer coefficient depends on the flow regime and material properties and can be expressed by the Nusselt number Nu :

$$\frac{\alpha \cdot L}{\lambda} = Nu = C \cdot Re^m \cdot Pr^n \quad (6-25)$$

Equation (6-25) is valid for systems with forced convection as it occurs for the SFD. L is a characteristic length [m]. For example, particle diameter or particle length if cylindrical coordinates [34]. λ is the thermal conductivity of the material [W/(m*K)].

Re is the **Reynolds number** describing the relation of the kinetic forces to the viscous forces. Depending on the system (pipe flow, plate flow, particle flow) the Reynolds number is related to different system characteristic dimensions. For particles moving in a bubbling fluidized bed the Reynolds number Re_p is formulated as follows [35]:

$$Re_{p,t} = \frac{d_p \cdot u_t \cdot \rho_g}{\eta_g} \quad (6-26)$$

d_p is the particle diameter [m], ρ_g the gas density [kg/m³] and η_g the dynamic viscosity of the gas [Pa*s]. u_t is the terminal particle velocity [m/s] which is the free falling velocity of the particle in the surrounding gas resulting from force equilibrium between gravitational force, buoyancy force and drag force.

$$u_t = \left(\frac{4 * d_p * (\rho_p - \rho_g) * g}{3 * \rho_g * C_D} \right)^{1/2} \quad (6-27)$$

g is the acceleration due to gravity [m/s²] and $(\rho_p - \rho_g)$ expresses the density difference between particle and gas. C_D is the drag coefficient. It expresses the resistance force the particle experiences against the flow direction and its value depends on the flow velocity itself. To calculate the drag coefficient without iteration several equations are known. The following equations can be used to calculate the terminal velocity of spherical and non-spherical particles [35].

$$u_t^* = u_t * \left(\frac{\rho_g^2}{\eta * (\rho_p - \rho_g) * g} \right)^{1/3} \quad (6-28)$$

$$u_t^* = \left(\frac{18}{(d_p^*)^2} + \frac{2.335 - 1.744 * \phi_s}{(d_p^*)^{0.5}} \right)^{-1} \quad \text{for } 0.5 < \phi_s < 1 \quad (6-29)$$

$$d_p^* = d_p * \left(\frac{\rho_g * (\rho_p - \rho_g) * g}{\eta^2} \right)^{1/3} \quad (6-30)$$

$$\phi_s = \left(\frac{\text{surface of sphere}}{\text{surface of particle}} \right)_{\text{of same volume}} \quad (6-31)$$

Depending on the sphericity of the particle ϕ_s the dimensionless terminal velocity u_t^* can be calculated knowing the dimensionless particle diameter d_p^* . d_p^* can be calculated with PSD measurement data and the terminal velocity settling then can be calculated for each particle size fraction.

Pr is the **Prandtl number** describing the relation of the viscous diffusion rate to the thermal diffusion rate.

$$Pr = \frac{c_p * \eta}{\lambda} \quad (6-32)$$

It is noteworthy that the Prandtl number solely depends on material properties.

The coefficient C and the exponent m and n in equation (6-25) are system functions and depend on, for example, the flow regime. The coefficient and the exponent are often determined empirically for a system.

Calculation approach for Nusselt number

Fluidized beds are the most intensely investigated dispersed particle systems. For fluidized beds the particles are set in motion by an air stream. Depending on the air velocity, different regimes are experienced. For them a Nusselt correlation was determined which is broadly used and cited [35]:

$$Nu = 2 + 1.8 * Re_p^{1/2} * Pr^{1/3} \quad (6-33)$$

The Nusselt correlation proved to be valid for fluidized beds with $Re_p > 100$. For lower Re_p a simpler correlation was found to be in agreement with experimental data:

$$Nu_{bed} = 0.03 * Re_p^{1/3} \quad (6-34)$$

However in the case of the SFD particles are in motion after they enter the dryer (material residues on the wall are neglected in the theoretical calculation). Therefore the Nusselt correlation for fixed beds may not apply for modeling the SFD.

In a newer consideration the particle form was considered. The constant factor of 2, also referred to as limit value of the Nusselt number in equation (6-33) is true for spheres and spherical particles. For different particle shapes the constant factor varies [34]. Equation (6-25) is expanded by a factor describing the particle shape.

$$Nu_p = \frac{h * A}{\lambda} * \frac{L}{A} \quad (6-35)$$

$A [m^2]$ is the external particle surface and $L [m]$ a characteristic length. For different particle shape corrective terms are formulated and listed [34]. The correction is of use if the convective term of the Nusselt number in equation (6-33), which is the term containing Re and Pr is smaller than the limit values of the Nusselt number.

Limited literature was available for agitated fluidized beds. In one reference [12] the drying behavior in the agitated fluidized bed was analyzed by experiment. In the experiment wetted pharmaceutical particles were dried in an agitated bed. Particles carried out by the air were reintroduced into the bed and the moisture content was measured in-line via IR. The heat transfer coefficient was found to be independent of the air temperature, but depended on the agitator speed, the air velocity and the particle size. With the resulting data an empirical Nusselt number correlation was formulated:

$$Nu_p = (29.96 * d_p - 0.027) * \left(v_g * \exp(-0.1 * N) * \frac{\rho_g}{\eta_g} \right)^{0.475} \quad (6-36)$$

v_g is the air velocity [m/s] and N the agitator rotational speed [1/s]. The particle size d_p is in [μm]. Even as the correlation was developed considering varying process conditions and particle size only one apparatus was used. Using the correlation on agitated fluidized dryer with a different geometry might lead to discrepancies. For example a bigger rotor has a higher circumferential velocity leading to different flow profiles for particles of the same size.

6.4.2. Free Particle Surface for Evaporation

From the process description of the SFD (chapter 2.1, page 9) it is apparent that the feed can be visualized as agglomerates falling into the dryer. Passing the agitator blades the agglomerates are disintegrated into smaller agglomerates and particles. The free particle surface increases. Moisture on the surface of the agglomerates and the particles exposed to the drying air is evaporated. Moisture being captured between particles in the agglomerate remains until the agglomerate is disintegrated again into smaller agglomerates and/or primary particles where the moisture then is exposed to the drying air.

For the present study however the deagglomeration process could not be investigated and no statement about the grinding time can be made.

Influence of agitator speed

In an experimental evaluation using a fluidized bed operating with inert particles it could be found that there is an optimum value for the number of agitator rotor revolutions N_{opt} [10]. At N_{opt} the evaporation rate and the Nusselt number has an optimum. At a lower number of revolutions, no homogeneous powder bed was present and bubbling as well as channeling can occur. For a higher number of revolutions the particles are concentrated on the dryer wall due centrifugal forces. There the interaction between the particles is higher leading to a decrease of the effective free particle surface.

For the DoE cases it could be seen, that the particles moved along the wall, especially for the high agitator speed. No homogeneous particle bed was present during drying. Without further investigation, unfortunately, the assumed reduction of free particle surface cannot be estimated.

An example of SFD 21 is shown in (figure 6-11, left). At high air throughput, high feed rate and low agitator speed the particles sprayed through the drying chamber above the agitator and circulated on the wall. The second example is SFD 57 (figure 6-11, right). There particles were dried at low air throughput, high feed rate and low agitator speed. Particles circulated at the wall at the agitator height but rose more centrally when leaving the dryer.

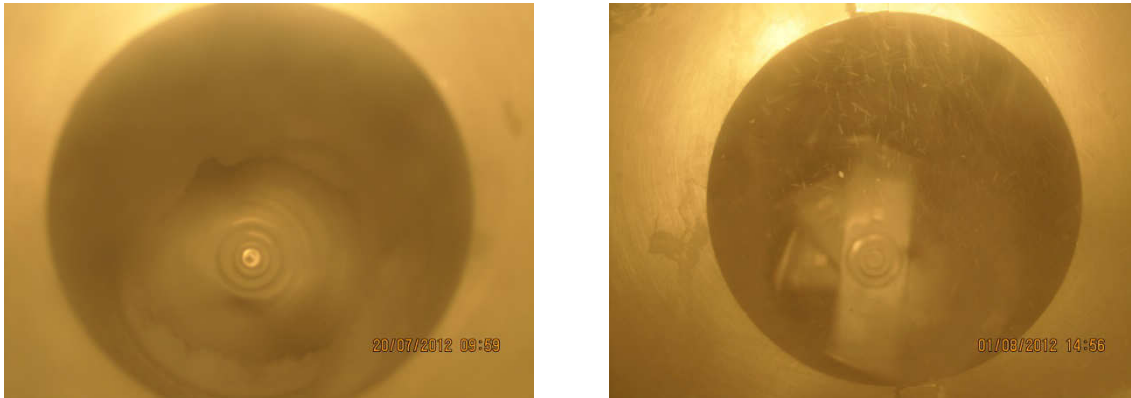


Figure 6-11: Drying of adipic acid at low agitator speed, high feed rate and different air throughput.

6.4.3. Calculation

Despite the variability and non-idealities the evaporation rate and the drying time for a mixture of spherical particles of different size but with homogeneously distributed water content will be calculated.

Following simplifications are made:

- Spherical particles with density of adipic acid.
- Particle size distribution taken from adipic acid feed.
- Homogeneous particle bed.
- No agglomerates. Particles are free moving and well distributed.
- Homogeneous moisture distribution between particle fractions.
- Active drying surface equals particle surface.
- No increase in air velocity from particle fluidization. Air velocity depends on air throughput and drying temperature.
- Air temperature and moisture load for drying air equals the conditions of the exhaust gas calculated by mass and energy balances (chapter 6.3.5, page 82).

For these simplifications the

- evaporation rate for each particle fraction and the mean evaporation rate using Nusselt number calculated with equation (6-34) and equation (6-36) and
- the drying time

can be calculated.

The air velocity needed for equation (6-36) is calculated using the outlet temperature and the environmental air pressure. In fluidized particle beds the particle concentration in the bed has to be accounted as the air velocity increases through a reduction in the pipe cross-section.

This influence is not accounted for as the concentration is not known. However as could be seen from process description in the results section (chapter part 5, page 33), particles tend to move at the dryer wall.

The air velocity is calculated using the ideal gas equation.

$$V_{air} = \frac{G/MM_{air} * R * T_{out,air}}{P} \quad (6-37)$$

$$v_g = \frac{4 * V_{air}}{D^2 * \pi} \quad (6-38)$$

R is the molar gas constant, which is 8.314 kJ/(kmol*K), D is the diameter of the dryer [m], V_{air} the dry gas volume flow rate and v_g is the vertical velocity of the drying air [m/s].

For the calculation MatLab is used. The code is shown in the appendix (chapter 10.9, page 127). The calculation process is shown below (figure 6-12).

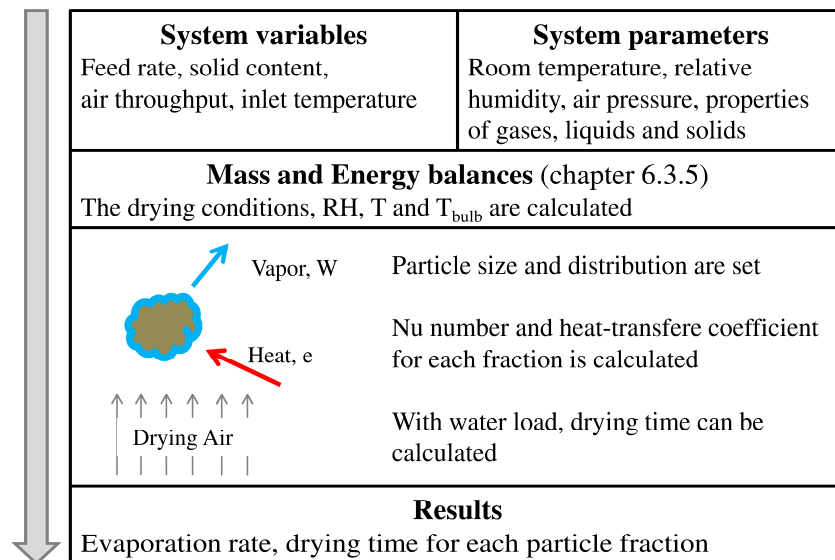


Figure 6-12: Calculation of drying time and evaporation rate.

Table 6-4: Evaporation rate using Ranz equation or Watano correlation for Nusselt number. Varying drying conditions.

F_{air} [kg/h]	F_{solid} [kg/h]	w_{solid} [wt%]	N	ϕ [%]	T_{in} [°C]	T_{bulb} [°C]	\bar{J}_{Ranz} [kg/(m ² *h)]	\bar{J}_{Watano} [kg/(m ² *h)]
400	3	70	1400	50	80	30.63	67	5.54*10 ⁶
200	1	70	420	50	80	30.57	70	8.97*10 ⁶
400	3	70	1400	0	80	25.51	75	6.15*10 ⁶
400	3	70	420	50	80	30.63	67	12.04*10 ⁶
400	1	70	1400	50	80	30.64	73	6.61*10 ⁶
Typical evaporation rate J for spin-flash dryer from literature [8]								
400	20	70	1400	50	200	45.60	187	16.37*10 ⁶
400	20	70	1400	50	300	52.68	337	30.96*10 ⁶
200	20	70	1400	50	300	52.49	270	17.48*10 ⁶

According to calculation routine presented in figure 6-12 the evaporation rate J [$\text{kg}/(\text{m}^2 \cdot \text{h})$] is calculated by the equation proposed by Ranz (equation (6-33)) and Watano (equation (6-36)). For every particle size the evaporation rate is calculated. With the particle size distribution density the evaporation rates for each fraction are summed up giving a global evaporation rate (equation (6-39)). The evaporation rates are compared to each other, as well as literature values in table 6-4.

$$\bar{J} = \sum_{i=1}^n J_i * q_{3,i} \quad (6-39)$$

n is the number of particle size fractions and q_3 is the particle size distribution density.

It can be seen, that the evaporation rate calculated by the empirical equation proposed by Watano is an order of 4 higher than typical evaporation rates for SFD listed in the literature.

Evaporation rates calculated by the equation proposed by Ranz are of the same order but a little lower than evaporation rates from literature. However, it has to be taken into account, that in this study a lower drying temperature as usually used when drying with a SFD is used. Increasing the drying temperature brings the calculated evaporation rate in the range of values listed in literature.

It can be concluded that the empirical Nusselt number correlation developed for a given design of an agitated fluidized bed dryer is not applicable in this case. The well-known and in fluidized bed operations broadly used equation proposed by Ranz leads to valid evaporation rates.

From the calculation result it can be seen that again the relative humidity of the inlet air has a significant influence. Compared to a relative air humidity of 50%, for dry air the drying rate increases by 12% at air inlet temperature of 70°C . This is due to a lower achievable bulb temperature. The difference between the air temperature and the bulb temperature on the solid surface represents the driving force for the heat flux and thus for the mass transfer. Accordingly the drying rate increases for a higher inlet temperature.

With knowledge about the evaporation rate for every particle fraction as well as its moisture load the drying time can be calculated. The mean drying time is the summation of the product of the drying time for each fraction multiplied by the fraction density.

$$\bar{t} = \sum_{i=1}^n \left(\frac{M_{p,i} * X}{J_i * A_i} \right) = \sum_{i=1}^n \left(\frac{d_{p,i} * \rho * X}{J_i} \right) \quad (6-40)$$

For the chosen particle size distribution of adipic acid (table 3-7), 754 μm is the biggest particle size. For that size the longest drying time will be accounted when the moisture is homogeneously distributed.

Table 6-5: Particle drying time in the SFD calculated for a simplified setting.

F_{air} [kg/h]	F_{solid} [kg/h]	W_{solid} [wt%]	φ [%]	\bar{t} [s]	$t_{754 \mu\text{m}}$ [s]
400	1	50	50	3.23	10.99
400	1	70	50	1.35	4.59
400	1	90	50	0.34	1.16
400	1	70	0	1.22	4.15

The calculated drying time is within several seconds. Even feed with 50% water dries immediately. In reality the drying time will be higher, as agglomerates first have to be disintegrated and particles then will interact with each other. However the result shows, in a qualitative way, that feed will be dried within seconds, as mentioned in the introduction (chapter 2, page 8).

6.4.1. Summary of Drying Kinetics and Evaporation Rate

The drying problem in the SFD could be formulated as surface drying. For that the mass transfer reduces to a heat-transfer problem (equation (6-24)). In literature two correlations for calculating the Nusselt number which expresses the heat transfer coefficient could be found. For the dryer settings used in the DoE analyses as well as dryer settings for common SFD drying operations the resulting Nusselt number had been compared to literature values. It could be shown that the empirical Nusselt correlation developed for the agitated fluidized bed dryer is not applicable for the SFD 47. However with the Nusselt equation from Ranz, which was formulated for fluidized beds, valid numbers of evaporation rate could be calculated.

Using this evaporation rate the drying time could be calculated for a simplified set of problems. The calculated drying time is within a few seconds. Lacking the time for agglomeration break up and ignoring particle/particle interactions, the results show that the SFD is indeed a fast dryer as described in the introduction.

6.5. Particle Motion

Particle movement through the dryer is governed by the flow profile of the drying air and the particle mass. In order to produce proper dried product the particle residence time has to exceed the particle drying time.

In this chapter, the particle motion through the SFD will only be discussed theoretically. With the performed experiments no definite statement can be given nor can calculations be performed.

6.5.1. Solid Unit Operations

In this chapter the SFD will be regarded as a combination of unit operations for handling solid particles. For that SFD can be abstracted as following:

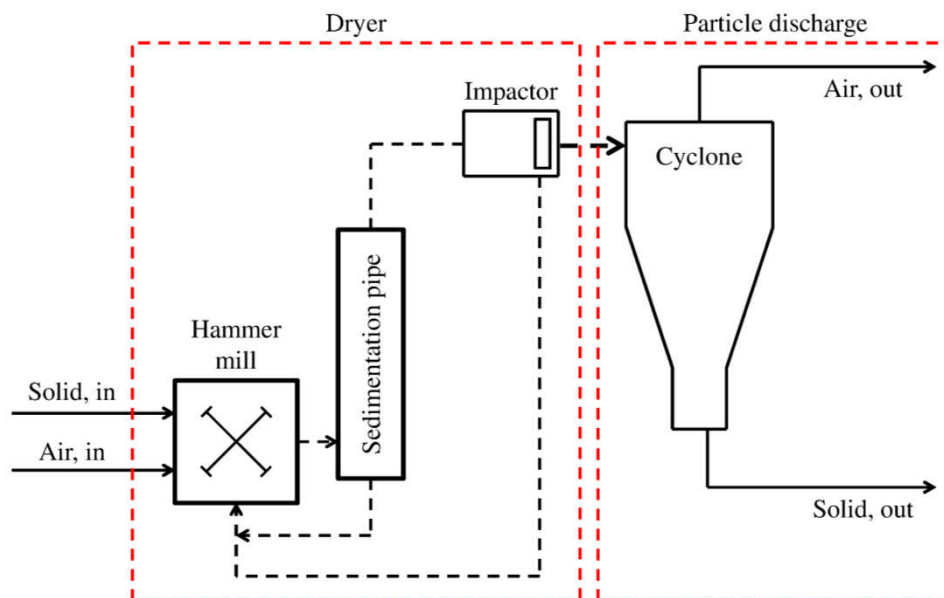


Figure 6-13: SFD as solid unit operation.

Hammer mill

The feed is conveyed into the dryer above the agitator blades and falls into the dryer as big lumps of agglomerates. Passing the agitator blades these agglomerates are disintegrated. The operation principles are similar to the operation function of a hammer mill. There particles are tumbling around being accelerated by spinning blades. Particle breakage occurs when particles impact with the blade, wall or other particle.

Sedimentation pipe

Being small enough to become air-borne, particles follow the air stream and leave the dryer. Particle movement is similar to transport in pneumatic conveying systems [36]. Smaller particles with lower settling velocity rise faster and easier than bigger particles. In addition particles move to the wall due to centrifugal forces. In the fluid boundary layer at the wall air velocity decreases and particles fall back into the dryer. Due to their greater mass bigger particles accumulate on the wall. Summing up, depending on the particle size and shape particles segregate in a pipe.

Impactor

The classifier in the SFD system acts similar to an impactor. The air flow in the region of the impactor changes quickly, resulting in high air velocity gradients. The bigger the particles the more unlikely it is that they follow the air stream and they will fall back into the dryer. For that Anhydro/SPX regards the classifier to determine the flow profile.

Cyclone

The cyclone actually is not intended as drying equipment but is installed to remove the particles from the air stream. However the particles are still distributed in the hot air stream and for that particles can dry if no equilibrium moisture content is achieved in the dryer.

6.5.2. Critical particle size $d_{p,crit}$

The critical particle size $d_{p,crit}$ describes the biggest particle being fluidized in an air stream. Theoretical particles of that size float in the air stream. Bigger particles will fall down whilst small particles follow the air stream.

Particles in the SFD are intended to remain in the drying zone until they are dry. However the feed material can be of wide particle size distribution and smaller particles of the feed might be carried out still wet whilst bigger particles remain in the dryer even being dry. Larger particles will accumulate in the dryer and will be ground down by the agitator. Figure 6-14 compares the gas velocity in the SFD to the terminal settling velocity of particles. The gas temperature is 70°C and the gas pressure is 990 mbar. Single particles of spherical and homogenous water distribution on their surface are assumed. The additional weight and size of the water changes the terminal velocity only a little. It can be seen, that particles smaller than 100 µm would follow the drying air once they are dispersed. The critical particle

diameter for dry particles is 575 μm at an air throughput of 400 kg/h and 310 μm for an air throughput of 200 kg/h.

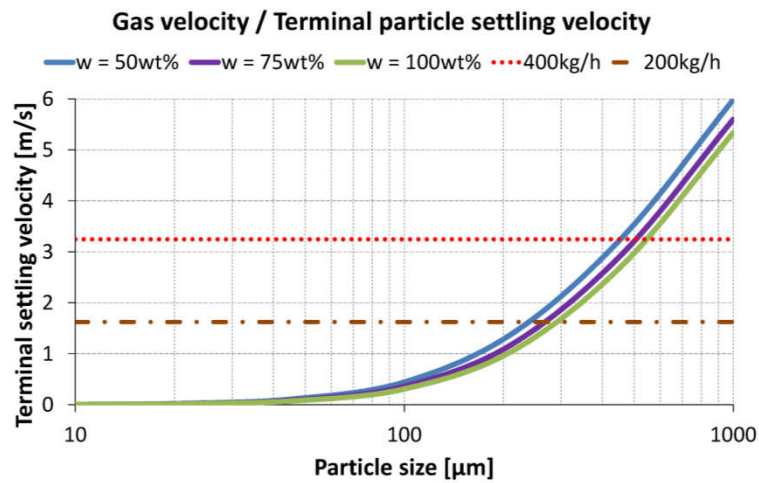


Figure 6-14: Gas velocity (dotted line) and terminal settling velocity (solid line) as function of particle size.

Compared to the results, especially for adipic acid, it can be seen that bigger particles left the dryer, in addition to the smaller ones (table 10-4). Reasons for this are a particle shape different from spherical particles and a different flow profile in the dryer.

It however explains why, for example, adipic acid or salicylic acid experienced a greater material breakage than the smaller ibuprofen. For them the big particles could not leave until they have been broken into smaller fragments.

7. Summary and Outlook

With information about the SFD from literature a statistical experimental plan DoE was set up to investigate the SFD 47 from Anhydro/SPX.

In an experimental approach the drying capacity and the dryer performance have been investigated. Materials differing in particle size distribution, particle shape and affinity to the evaporated fluid have been used. Slurries made from these materials were dried in the experiment.

In an early experiment it could be shown, that the dryer as equipped in this study is not capable of handling pumpable feed as stated in the description. The feed concentration for the experiment was constrained to not pumpable slurry feeds of higher particle concentration.

Performing the experiments it was seen that especially during start-up significant deposits of material were built up on the dryer wall in the region of the agitated bed. Depending on the material and the feed conditions the deposits remained for the entire drying operation. Remaining in the dryer at high temperature for longer time could cause changes in the material properties which could have a negative impact on product quality and purity. To minimize the residues on the dryer wall changes in the agitator concept have been suggested. Agitator concepts actively cleaning the dryer wall by wiping could have the capability to significantly decrease the amount of material residues. Material residues were found for some cases in the upper part of the dryer consisting of dried particles adhering on the wall. For them it could be shown that increasing the air throughput and hence the air velocity solves the problem. The cause of the adherence of dried particles on the dryer wall is not yet investigated. However it is assumed that tribo-charging of dry particles might play a role in this case. For that, surface treatment of the dryer wall can reduce the chance of particle adherence even for a small air throughput.

For heat sensitive materials it was shown that it is crucial to keep the drying temperature below critical material temperatures. Particles in the dryer don't have a protective fluid layer and are exposed to the temperature of the drying air. For ibuprofen slurry contaminated with surfactants, an increase of drying temperature above the melting point led to melting of the material. Drying around the melting point proved to be difficult as the particles became stickier. Successful experiments could only be performed for low feed rate.

As stated in the thesis aims the residual moisture of the product had to be below 2wt%. For the performed DoE experiments the residual moisture was well below the limit in all cases. In the statistical analyses no significant dependence on the process factors or settings was found. In the theoretical description the drying capacity of the SFD was calculated using mass and energy balances and sorption isotherms. It was found, that with the chosen feed rate and feed concentration the result is theoretical in the area of residual moisture lower than the limit. The operational area describing feasible feed rate with given solid concentration depended on the air throughput and initial water load of the air. The operational area increased with an increase in the air throughput and decrease of the initial water load. For dry air the resulting residual moisture level was lower. For that an air dehumidifier can increase the drying performance. The presented calculation can also be used for calculating and planning drying operations with more difficult substances as long as sorption data are available.

For material dissolvable in the fluid the influence of the drying heat energy was investigated. For them agglomeration occurs as small particles are precipitated out of the solution. The size and number of these precipitated particles depends on drying heat energy. It could be shown that with a change in drying temperature and air throughput different sizes of agglomerates can be produced.

The evaporation rate was calculated with standard equations from the literature and compared to literature data available for the SFD. The drying problem was stated as heat-transfer governed. The Nusselt number for the problem can be calculated with the known equation by Ranz formulated for fluidized bed. The evaporation rate increases with an increase in drying temperature and a decrease in initial water load of the air. The drying time was calculated with the evaporation rate assuming single particles of varying size. The average drying time has been several seconds. The real drying time will be larger as the calculated problem was simplified. However the results show that the SFD is indeed a fast dryer.

The downside of a pneumatic dryer such as the SFD is the presence of particle attrition and breakage. Especially in the agitated zone particles are accelerated and impact with each other or the dryer wall. PSD analyses and SEM showed a reduction in particle size. Thereby the intensity seemed to depend on particle size and material. In the DoE it could be found for adipic acid that the material damage depends on the agitator speed, the air throughput and the feed rate. With an increase of agitator speed the particle speed in the agitated zone increases and hence the collision impact force. The role of the air throughput is not that straight forward to explain. The air throughput has an impact on the lift force but also on the internal particle

recirculation. At higher air throughput the size of particles becoming air borne increases. Particles are transported upwards along the wall. There the particle concentration on the wall increases with the air throughput. At the end of the dryer the particles have to pass through a classifier, whose working principles are similar to an impactor. Higher air throughput means higher air velocity causing greater velocity gradients. At increased velocity gradient the size of particles retained by the classifier decreases. Applying this information on the results of adipic acid and ibuprofen can help to explain the difference in the material breakage. For adipic acid having larger particles than ibuprofen the number of particles too big to be discharged from the dryer is higher. For them the possibility is higher to be broken than for particles being discharged after drying.

Concluding it can be said, that the Spin-Flash dryer has the capability to be used in the pharmaceutical industry. Particles could be dried with little difficulty in short time even at low drying temperature. The residual moisture level was well below the acceptable limit of 2wt%. However some adoption should be made to the agitation concept. Regarding the material breakage the SFD 47 should be used for drying of small particles. For big particles breakage has to be accounted. For drying of bigger particles the air throughput has to be adapted to the maximum particle size. To keep material breakage at a minimum drying should be performed at low agitator speed.

For a detailed description of the particle motion and material damage in the SFD residence time distributions have to be calculated. According to RTD experiments described in [10] colored particles can be fed in after establishing a steady-state process. The output particles could be measured using optical spectroscopy giving the material residence time. To investigate the milling behavior of the agitator colored particles can be separated in classes and introduced separately. Results are the residence time for each size fraction and the degree of milling for large particles.

In addition the flow profile of the drying air can be simulated. Information gained from the simulation can be the influence of the classifier which could not be quantified in this work and the actual velocity around the agitator and in the upper part of the drying cylinder. The results could quantify the influence of the air throughput and give a first hint about particle movement in the dryer. In addition the fluid simulation can be coupled with a simulation of particle motion to give a full picture about the SFD.

Literature

- [1] EvaluatePharma, „World Preview 2018 - Embracing the Patent Cliff,“ EvaluatePharma, 2012.
- [2] J. L. Kukura und M. P. Thien, „Current Challenges and Opportunities in the Pharmaceutical Industry,“ in *Chemical Engineering in the Pharmaceutical Industry*, New Jersey, Wiley, 2011.
- [3] G. Reklaitis, J. Khinast and F. Muzzio, "Pharmaceutical engineering science - New approaches to pharmaceutical development and manufacturing," *Chemical Engineering Science*, vol. 65, no. 21, pp. iv-vii, 2010.
- [4] T. J. Watson und R. Nosal, „Scientific Opportunities Through Quality by Design,“ in *Chemical Engineering in the Pharmaceutical Industry - R&D to Manufacturing*, New Jersey, Wiley, 2011.
- [5] F. J. Muzzio, T. Shinbrot and B. J. Glasser, "Powder technology in the pharmaceutical industry: the need to catch up fast," *Powder Technology*, vol. 124, no. 1-2, pp. 1-7, 2002.
- [6] S. Murugesan, P. K. Sharma und J. E. Tabora, „Design of Filtration and Drying Operations,“ in *Chemical Engineering in the Pharmaceutical Industry - R&D to Manufacturing*, New Jersey, Wiley, 2011.
- [7] I. Borde and L. Avi, "Pneumatic and Flash Drying," in *Handbook of Industrial Drying*, Taylor & Francis, 2006, pp. 397-409.
- [8] APV Separations Product Group, "APV Dryer Handbook," West Sussex.
- [9] A.-G. Frank, "Anhydro Spin Flash Drying," Denmark, 2012.
- [10] A. Reyes, G. Díaz und F.-H. Marquardt, „Analysis of Mechanically Agitated Fluid-Particle Contact Dryers,“ *Drying Technology*, Bd. 19, pp. 2235-2259, 2001.
- [11] J. Kim und G. Y. Han, „Effect of agitation on fluidization characteristics of fine particles in a fluidized bed,“ *Powder Technology*, Bd. 166, pp. 113-122, 2006.
- [12] S. Watano, N. Yeh und K. Miyamoto, „Heat Transfer and the Mechanism of Drying in Agitation Fluidized Bed,“ *Chemical Pharmaceutical Bulletin*, Bd. 46, pp. 843-846, 1999.

- [13] SPX Cooperation, "Anhydro Small Scale Spin Flash Dryer - Functional Description and Operator's Instructions," AI-01.08#03 ENG Version 1, 2012.
- [14] Umetrics Academy, Design of Experiment, USA.
- [15] G. Reich, "Near-infrared spectroscopy and imaging: Basic principles and pharmaceutical applications," *Advanced Drug Delivery Reviews*, no. 57, pp. 1109-1143, 2005.
- [16] S. C. Harris and D. S. Walker, "Quantitative Real-Time Monitoring of Dryer Effluent Using Fiber Optic Near-Infrared Spektroskopie," *Journal of Pharmaceutical Science*, vol. 89, no. 9, pp. 1180-1186, 2000.
- [17] G. X. Zhou, Z. Ge, J. Dorwart, B. Izzo, J. Kukura, G. Bicker und J. Wyvratt, „Determination and Differentiation of Surface and Bound Water in Drug Substances by Near Infrared Spectroscopy,“ *Journal of Pharmaceutical Science*, Bd. 92, Nr. 5, pp. 1058-1065, 2003.
- [18] Europäisches Arzneibuch, 5. Ausgabe Hrsg., Bd. 1, Verlag Österreich, 2005.
- [19] L. R. Genskow, W. E. Beimesch, J. P. Hecht, I. Kemp, T. Langrish, C. Schwartzbach und L. F. Smith, „Chapter 12: Psychrometry, Evaporative Cooling, and Solids Drying,“ in *Perry's Chemical Engineering Handbook 8th Edition*, McGraw-Hill, 2008.
- [20] Research Center Pharmaceutical Engineering, „Zwischenbericht Modellsubstanzen,“ Graz, 2012.
- [21] Á. Kukovecz, T. Kanyó, Z. Kónya und I. Kiricsi, „Long-time low-impact ball milling of multi-wall carbon nanotubes,“ *Carbon*, Nr. 43, pp. 994-1000, 2005.
- [22] T. C. Alex, R. Kumar, A. J. Kailath, S. K. Roy und S. P. Mehrotra, „Physiochemical Changes During Mechanical Activation of Boehmite,“ Jamshedpur, 2010.
- [23] E. Berlin, P. G. Kliman, B. A. Anderson und M. J. Pallansch, „Calorimetric measurement of the heat of desorption of water vapor from amorphous and crystalline lactose,“ *Thermochimica Acta*, Bd. 2, pp. 143-152, 1970.
- [24] K. C. Patel und X. D. Chen, „Drying of aqueous lactose solutions in a single steam dryer,“ *Food and Bioproducts Processing*, Bd. 86, pp. 185-197, 2008.

- [25] S. Watano und K. Miyunami, „Image processing for on-line monitoring of granule size distribution and shape in fluidized bed granulation,“ *Powder Technology*, Bd. 83, pp. 55-60, 1995.
- [26] Research Center Pharmaceutical Engineering, „Besuchsbericht Anhydro 2012,“ 2012.
- [27] D. S. Christen, *Praxiswissen der chemischen Verfahrenstechnik*, Berlin Heidelberg: Springer, 2005.
- [28] W. Vauck and H. Müller, *Grundoperationen Chemischer Verfahrenstechnik*, Stuttgart: Deutscher Verlag für Grundstoffindustrie, 2000.
- [29] A. Mersmann, M. Kind und J. Stichlmair, *Thermal Separation Technology*, Heidelberg: Springer, 2011.
- [30] K. Fischer, I. Shulgin, J. Rarey und J. Gmehling, „Vapor-liquid equilibria for the system water + tert.-pentanol at 4 temperatures,“ *Fluid Phase Equilibrium*, Nr. 120, pp. 143-165, 1996.
- [31] Verein Deutscher Ingenieure, "E Wärmeleitung," in *VDI Heat-Atlas*, Berlin Heidelberg, Springer, 2006.
- [32] A. M. Keech, „The Determination of Drying Kinetics and Equilibrium Characterisation at Low Moisture,“ University of Canterbury, Christchurch, 1997.
- [33] W. E. Ranz und W. R. Marshall, „Evaporation from Drops,“ *Chemical Engineering Progress*, Bd. 48, pp. 141-146, 1952.
- [34] A. Wadewitz und E. Specht, „Limit value of the Nusselt number for particles of different shape,“ *Int. J. Heat and Mass Transfer*, Bd. 44, pp. 967-975, 2001.
- [35] D. Kunii und O. Levenspiel, *Fluidization Engineering*, Newton, USA: Butterworth-Heinemann, 1991.
- [36] G. Klinzing, F. Rizk, R. Marcus und L. Leung, *Pneumatic Conveying of Solids*, Springer, 2010.
- [37] Verein Deutscher Ingenieure, „D Berechnungsmethoden für Stoffeigenschaften,“ in *VDI Heat-Atlas*, Heidelberg, Springer, 2006.

- [38] A. Apelblat, „Enthalpy of solution of oxalic, succinic, adipic, maleic, malic, tartaric, and citric acids, oxalic acid dihydrate, and citric acid monohydrate in water at 298.15 K,“ *Journal Chemical Thermodynamics*, Nr. 18, pp. 351-357, 1986.
- [39] Y.-Y. Di, C.-T. Ye, Z.-C. Tan und G.-D. Zhang, „Low-temperature heat capacity and standard molar enthalpy of formation of crystalline (S)-(+)-Ibuprofen (C₁₃H₁₈O₂)(S),“ *Indian Journal of Chemistry*, Nr. 46A, pp. 947-951, 2007.

8. List of Figures

Figure 1-1: Production route of oral dosage forms [5].....	2
Figure 1-2: Pathways for producing API solids in the pharmaceutical industry.	3
Figure 1-3: Thermal energy requirement to dry 1 kg/h solid with a given amount of water.	4
Figure 1-4: Solid dryer with dispersed particle and their hand able feeds [11].	5
Figure 2-1: SFD consisting of the drying chamber, air heater, feeder and particle separator. Figure adapted from literature [7].	9
Figure 3-1: Spin-Flash Dryer SFD47 from Anhydro/SPX used for the feasibility study. According components are listed in table 3-1 [13].	11
Figure 3-2: Control panel of the SFD 47 with measurement points are indicated. Adapted from [13].	13
Figure 3-3: NIR measurement principles and NIR probe position.	20
Figure 4-1: Process set-up for drying of liquid suspension feed, experiment SFD 18.	27
Figure 4-2: In-process pictures of experiment SFD 18.	27
Figure 4-3: Feed rate calibration for adipic acid and ibuprofen.	30
Figure 4-4: Process steps.	31
Figure 5-1: Start-up phase of adipic acid experiment SFD 15 / DOE 03.	33
Figure 5-2: Adipic acid DoE experiment with dry particles adhering on the dryer wall.	34
Figure 5-3: Different particle movement according to the air throughput.	34
Figure 5-4: PSD distribution of adipic acid feed and products SFD 14 and SFD 15.	35
Figure 5-5: SEM images of adipic acid at a magnification level of 500. (A) feed, (B) SFD 14 and (C) SFD 15.	35
Figure 5-6: Specific surface area of adipic acid feed and experiments SFD 14 and SFD 15. .	36
Figure 5-7: DoE raw data evaluation with Modde. Histogram plot [14].	37
Figure 5-8: Model performance indicator for adipic acid for optimized model.	38
Figure 5-9: Raw coefficient plot for the material damage of adipic acid.	39
Figure 5-10: Coefficient plot after preparation showing only statistically significant factors.	39

Figure 5-11: Summary of statistically dependence of DoE responses on factors for adipic acid. 40

Figure 5-12: Predictive model for the material damage of adipic acid. The agitator speed is in % of maximum revolution which is 1400 rpm. The air throughput and feed rate are in kg/h. 42

Figure 5-13: Non-ideal experiments SFD40 / DOEIP07 and SFD43 / DOEIP15. Material residues built up at feed entrance and on dryer wall. 44

Figure 5-14: Ideal experiments SFD28 / DOEIP04 and SFD42 / DOEIP16. 45

Figure 5-15: PSD distribution of ibuprofen feed and products SFD 27 and SFD 39. 45

Figure 5-16: SEM images of ibuprofen at a magnification level of 500. (A) Feed, (B) SFD 14 and (C) SFD 15. 46

Figure 5-17: Specific surface area of ibuprofen feed and experiments SFD 27 and SFD 39. . 47

Figure 5-18: Summary of statistical dependence of DoE responses on factors for ibuprofen. 47

Figure 5-19: Start-up with slurry of 70% Lactose. Feed entering the dryer covers the wall. .. 49

Figure 5-20: Optical lactose particle concentration and distribution in dependence of the drying air temperature. 50

Figure 5-21: PSD distribution of lactose feed and product SFD 75 and SFD 79. 51

Figure 5-22: SEM images of lactose at magnification level of 500. (A) feed, (B) SFD 75 and (C) SFD 79. 52

Figure 5-23: Specific surface area of lactose feed and experiments SFD 75 and SFD 79..... 52

Figure 5-24: Summary of statistically dependence of DoE responses on factors for DoE drying energy (lactose). 53

Figure 5-25: Ibuprofen suspension 40wt% with surfactant. 56

Figure 5-26: SFD 46 in-process images. Residues built up on the wall and lumps of particles are stirred by the agitator. 56

Figure 5-27: Aborted experiment SFD 48. The dryer tended to flood. 56

Figure 5-28: Experiment SFD 06, drying of heat sensitive materials at different temperatures. Left: under critical; right: critical. 58

Figure 5-29: Left: Start-up phase. Material stuck to the wall. Right: Process end, little material residues are found. 59

Figure 5-30: PSD of benzoic acid feed and product.	59
Figure 5-31: SEM image of benzoic acid at a magnitude of 500. (A) feed and (B) SFD 67...	59
Figure 5-32: Experiment SFD 69 during start-up. Thin feed suspension is smeared around the agitator.....	60
Figure 5-33: Salicylic acid particles covering dryer wall (left). Particles being blown off (right).....	61
Figure 5-34: PSD of salicylic acid feed and product.	61
Figure 5-35: SEM image of salicylic acid at a magnitude of 100. (A) feed and (B) SFD 69..	61
Figure 5-36: Experiment SFD 83. Both the dryer wall (left) and the cyclone wall (right) were covered with adhering particles.....	62
Figure 5-37: PSD of acetyl salicylic acid feed and product.	63
Figure 5-38: SEM image of acetyl salicylic acid at a magnitude of 500. (A) Feed and (B) SFD 83.....	63
Figure 5-39: Start-up phase for flour slurry. The lower dryer chamber is filled by dough.....	64
Figure 5-40: Experiment SFD 68 during drying (left) and at the end (right).....	65
Figure 5-41: PSD of flour feed and product.....	65
Figure 5-42: SEM images of flour at a magnitude of 1000. (A) Feed and (B) SFD 68, fine product.....	65
Figure 6-1: Balance areas of the SFD 47.	71
Figure 6-2: Overall mass and energy balance in drying operations.....	72
Figure 6-3: Technical drawing of the SFD and its dimensions.....	76
Figure 6-4: Comparison of the experimental and theoretical outlet temperature for adipic acid.	79
Figure 6-5: Sorption isotherm for various products and temperature [29].	80
Figure 6-6: Freundlich Langmuir sorption isotherm for the system water / adipic acid. Data from literature [32].....	81
Figure 6-7: Estimation of drying capacity. Calculating the equilibrium residual moisture load	82

Figure 6-8: Results for equilibrium residual moisture using an iterative calculation. The thick line indicates the critical residual moisture level of 2wt%..... 83

Figure 6-9: Contour plots for several drying conditions. A: Influence of the air throughput at 80°C; B: Influence of the air throughput at 60°C; C: Influence air throughput for dry air and D: Influence of initial air water load. 84

Figure 6-10: Typical drying curves [19]. A: Drying rate over the dry-basis moisture content. B: Drying rate over drying time. 86

Figure 6-11: Drying of adipic acid at low agitator speed, high feed rate and different air throughput. 91

Figure 6-12: Calculation of drying time and evaporation rate. 92

Figure 6-13: SFD as solid unit operation. 96

Figure 6-14: Gas velocity (dotted line) and terminal settling velocity (solid line) as function of particle size..... 98

Figure 10-1: Model performance indicator of adipic acid. On the x-axis the responses are listed and on the y-axis the magnitude of model quality parameter. Generally high values indicate a good model. 119

Figure 10-2: Adipic acid. Coefficient plot for residual moisture. Larger error bars than green bars indicate statistically insignificance of the factor. 119

Figure 10-3: Adipic acid. Coefficient plot for material damage. Larger error bars than green bars indicate statistically insignificance of the factor. 120

Figure 10-4: Adipic acid. Coefficient plot for location parameter, spread of distribution and product output. Larger error bars than green bars indicate statistically insignificance of the factor..... 120

Figure 10-5: Model performance indicator of ibuprofen. On the x-axis the responses are listed and on the y-axis the magnitude of model quality parameter. Generally high values indicate a good model..... 121

Figure 10-6: Ibuprofen. Coefficient plot for residual moisture, material damage and product output. Larger error bars than green bars indicate statistically insignificance of the factor. . 121

Figure 10-7: Ibuprofen. Coefficient plot for location parameter and spread of distribution. Larger error bars than green bars indicate statistically insignificance of the factor..... 122

Figure 10-8: Model performance indicator of lactose. On the x-axis the responses are listed and on the y-axis the magnitude of model quality parameter. Generally high values indicate a good model. 122

Figure 10-9: Lactose. Coefficient plot for material damage and residual moisture. Larger error bars than green bars indicate statistical insignificance of the factor. 123

Figure 10-10: Lactose. Coefficient plot for production rate, location parameter and spread of distribution. Larger error bars than green bars indicate statistical insignificance of the factor. 123

9. List of Tables

Table 3-1: Main components of the drying unit SFD 47 [13].....	12
Table 3-2: 7 steps to generate a statistically predictive model by use of DoE.....	14
Table 3-3: Assumed factors for the SFD 47.....	15
Table 3-4: Factors for the SFD DoE.	16
Table 3-5: DoE worksheet for adipic acid.	17
Table 3-6: Doe worksheet "influence of the drying energy".....	18
Table 3-7: Properties of the materials used for the DoE study.	23
Table 4-1: Feed concentration. Slurries for the DoE experiments are highlighted grey.....	29
Table 5-1: Settings and results for exemplary adipic acid experiments.....	35
Table 5-2: Settings and results for exemplary ibuprofen experiments.....	45
Table 5-3: Settings and results for exemplary lactose experiments.	50
Table 5-4: SFD process settings for drying of ibuprofen/surfactant.	55
Table 5-5: Process settings for drying over the melting point.	57
Table 5-6: Process settings for drying Benzoic acid.....	58
Table 5-7: Process settings for drying salicylic acid.....	60
Table 5-8: Process settings for production of acetyl salicylic acid.....	62
Table 5-9: process setting for drying flour.....	64
Table 6-1: Antoine parameters for water [30].....	73
Table 6-2: Physical and geometrical data of wall material and insulation.....	76
Table 6-3: Liquid water content on dry basis X_{out} for dried particles of adipic acid.	78
Table 6-4: Evaporation rate using Ranz equation or Watano correlation for Nusselt number. Varying drying conditions.....	93
Table 6-5: Particle drying time in the SFD calculated for a simplified setting.....	95
Table 10-1: Physical material data for calculation of stationary drying.	113
Table 10-2: Exemplarily process data documentation. The documentation was in German.	113

Table 10-3: List of experiments.	113
Table 10-4: Result data of DoE adipic acid.	116
Table 10-5: Result data of DoE ibuprofen.	117
Table 10-6: Result data of DoE heat influence (lactose).	118
Table 10-7: Result data of influence of surfactant, benzoic acid, salicylic acid, acetyl salicylic acid and flour.....	118
Table 10-8: Calculated water load of the product particle X_{out}	124
Table 10-9: List of outlet temperature data for DOE Adipic acid.	125

10. Appendix

10.1. Data

Table 10-1: Physical material data for calculation of stationary drying.

	Value	Unit	Temperature	Source
$C_{p,air}$	1.0097	kJ/(kg*K)	80°C	[37]
$C_{p,vapor}$	2.012	kJ/(kg*K)	80°C	[37]
$C_{p,water}$	4.182	kJ/(kg*K)	25°C	[37]
$h_{vl,water}$	2501	kJ/kg	0°C	[37]
$C_{p,adipic\ acid}$	175	kJ/(kmol*K)	25°C	[38]
$C_{p,ibuprofen}$	328	kJ/(kmol*K)	55°C	[39]
H_{loss}	150	kJ/h	79°C	

10.2. Process data documentation

Table 10-2: Exemplarily process data documentation. The documentation was in German.

Versuchsprotokoll - Spin-Flash Dryer												
VersuchNr.	Datum	Substanz	Blende	Raumdaten / Temp / Feuchte								
SFD 15 / DOE 03	17.07.2012	Adipinsäure 71%	weit (80 mm)	37.4% / 25.5°C								
Probe [Ja/Nein]	Uhrzeit [hh:mm]	Luftstrom [kg/h]	Δp Zyclon [mbar]	Luft,ein [kg/h]	Luft,ein [%]	$T_{Luft,Ein}$ [°C]	$T_{Luft,aus}$ [°C]	Δp Dryer [mmWS]	Dryer Agi [%] / [A]	Screwdrive [%]	Vat Agi [%]	
Nein	11:33	202.4	4.39	200	52	80.5	70.7	120	30 / 1,5	1	50	
Ja	11:46	199.2	4.31	200	49	79.7	71.7	110	30 / 1,5	1	50	
Ja	11:56	201.0	4.27	200	64	80.0	73.0	110	30 / 1,6	1	50	
Ja	12:04	200.1	4.36	200	64	80.0	74.0	115	30 / 1,6	1	50	
Ja	12:10	199.6	4.36	200	68	79.5	73.5	120	30 / 1,6	1	50	

10.3. List of all experiments

Table 10-3: List of experiments.

Sample SFD	Date	Material	Solid conc. [wt%]	SFD settings				
				Air [kg/h]	Classifier [mm]	Agitator [rpm]	Feed [kg/h]	Temp. [°C]
SFD 01	05.07.2012	Granulac230	58	Feed was sucked into drying chamber				
SFD 02	05.07.2012	Granulac230	67	Fast variation of settings --> get to know the SFD				
SFD 03	05.07.2012	Sorbolac	30	Feedrate 30% screw velocity --> flooding				
SFD 04	06.07.2012	Sorbolac	30	Setup for pump able feed				
SFD 05	09.07.2012	Ibuprofen25	50	Feed screw calibration				

SFD 06	09.07.2012	Ibuprofen25	50	Temperature influence on Ibuprofen (80°C)				
SFD 07	10.07.2012	Granulac230	65					
SFD 08	11.07.2012	Granulac230	65					
SFD 09	12.07.2012	Granulac230	65					
SFD 10	12.07.2012	Granulac230	65					
SFD 11	13.07.2012	Sorbolac	55	Pump able feed				
SFD 12	16.07.2012	Adipic acid	71	400	60	420	1	80
SFD 13	16.07.2012	Adipic acid	71	200	60	1400	1	80
SFD 14	16.07.2012	Adipic acid	71	400	80	1400	1	80
SFD 15	17.07.2012	Adipic acid	71	200	80	420	1	80
SFD 16	17.07.2012	Adipic acid	71	Run out of feed				
SFD 17	17.07.2012	Adipic acid	59	200	80	420	1	80
SFD 18	18.07.2012	Adipic acid	45.5	Pump able feed (2)				
SFD 19	19.07.2012	Adipic acid	60	400	80	1400	1	80
SFD 20	19.07.2012	Adipic acid	60	200	80	420	1	80
SFD 21	20.07.2012	Adipic acid	71	400	80	420	3	80
SFD 22	20.07.2012	Adipic acid	71	200	80	420	3	80
SFD 23	20.07.2012	Adipic acid	71	200	60	420	3	80
SFD 24	20.07.2012	Adipic acid	71	400	60	1400	3	80
SFD 25	20.07.2012	Adipic acid	71	200	80	1400	3	80
SFD 26	23.07.2012	Ibuprofen25	35	Preparation for Ibuprofen DoE				
SFD 27	24.07.2012	Ibuprofen25	40	200	80	420	1	70
SFD 28	24.07.2012	Ibuprofen25	40	400	80	420	1	70
SFD 29	24.07.2012	Ibuprofen25	40	400	80	420	3	70
SFD 30	24.07.2012	Ibuprofen25	40	300	60	910	2	70
SFD 31	24.07.2012	Ibuprofen25	40	400	60	1400	1	70
SFD 32	25.07.2012	Ibuprofen25	40	200	60	1400	3	70
SFD 33	25.07.2012	Ibuprofen25	40	400	60	420	3	70
SFD 34	25.07.2012	Ibuprofen25	40	200	60	420	1	70
SFD 35	25.07.2012	Ibuprofen25	40	400	60	420	1	70
SFD 36	25.07.2012	Ibuprofen25	40	400	60	1400	3	70
SFD 37	25.07.2012	Ibuprofen25	40	300	60	910	2	70
SFD 38	25.07.2012	Ibuprofen25	40	200	60	420	3	70
SFD 39	25.07.2012	Ibuprofen25	40	400	80	1400	1	70
SFD 40	26.07.2012	Ibuprofen25	40	200	80	1400	1	70
SFD 41	26.07.2012	Ibuprofen25	40	200	80	420	3	70
SFD 42	26.07.2012	Ibuprofen25	40	400	80	1400	3	70
SFD 43	26.07.2012	Ibuprofen25	40	200	80	1400	3	70
SFD 44	26.07.2012	Ibuprofen25	40	200	60	1400	1	70
SFD 45	26.07.2012	Ibuprofen25	40	300	60	910	2	70
SFD 46	27.07.2012	Ibu25/Surf.	40	400	80	420	1	70
SFD 47	27.07.2012	Ibu25/Surf.	40	200	80	1400	1	70
SFD 48	27.07.2012	Ibu25/Surf.	40	400	80	1400	3	70
SFD 49	30.07.2012	Ibu25/Surf.	60	400	80	1400	3	70
SFD 50	01.08.2012	Adipic acid	71	200	60	420	1	80
SFD 51	01.08.2012	Adipic acid	71	300	60	910	2	80

SFD 52	01.08.2012	Adipic acid	71	400	60	420	3	80	
SFD 53	01.08.2012	Adipic acid	71	200	60	1400	3	80	
SFD 54	01.08.2012	Adipic acid	71	300	60	910	2	80	
SFD 55	01.08.2012	Adipic acid	71	Feed run out					
SFD 56	01.08.2012	Adipic acid	71	400	80	420	1	80	
SFD 57	01.08.2012	Adipic acid	71	200	80	420	3	80	
SFD 58	01.08.2012	Adipic acid	71	400	80	1400	3	80	
SFD 59	01.08.2012	Adipic acid	71	200	80	1400	1	80	
SFD 60	02.08.2012	Adipic acid	71	400	60	1400	1	80	
SFD 61	02.08.2012	Adipic acid	71	300	60	910	2	80	
SFD 62	02.08.2012	Adipic acid	71	200	60	420	1	80	
SFD 63	02.08.2012	Adipic acid	71	300	60	910	5	80	
SFD 64	02.08.2012	Granulac230	70	200	80	1400	5	80	
SFD 65	03.08.2012	Granulac230	70	200	80	1400	5	80	
SFD 66	06.08.2012	Ibu25/Surf.	53	300	80	1120	2	70	
SFD 67	07.08.2012	Benzoic acid	67	400	80	1400	3	80	
SFD 68	08.08.2012	Flour	54	300	80	1400		70	
SFD 69	13.08.2012	Salicylic acid	69	400	80	420	4	80	
SFD 70	14.08.2012	Adipic acid	71	200	80	420	2	60	
SFD 71	14.08.2012	Adipic acid	71	300	80	420	2	60	
SFD 72	14.08.2012	Adipic acid	71	300	80	420	2	70	
SFD 73	14.08.2012	Adipic acid	71	300	80	420	2	80	
SFD 74	14.08.2012	Adipic acid	71	300	80	420	4	80	
SFD 75	16.08.2012	Granulac230	70	200	80	910	2	60	
SFD 76	16.08.2012	Granulac230	70	400	80	910	2	60	
SFD 77	16.08.2012	Granulac230	70	300	80	910	2	70	
SFD 78	16.08.2012	Granulac230	70	300	80	910	2	70	
SFD 79	16.08.2012	Granulac230	70	400	80	910	2	80	
SFD 80	16.08.2012	Granulac230	70	200	80	910	2	80	
SFD 81	16.08.2012	Granulac230	70	300	80	910	2	70	
SFD 82	16.08.2012	Granulac230	70	300	80	1400	2	70	
SFD 83	20.08.2012	ASA	62	200	80	1400	2	80	
SFD 84	21.08.2012	Sorbolac	65	200	80	1400	4	80	
SFD 85	21.08.2012	Sorbolac	65	Injury led to experiment stop					

Orange highlighted experiments had to be stopped due drying problems or led to now valid result.

ASA ... Acetyl salicylic acid

Ibu25/Surf. ... Ibuprofen25 with surfactant

10.4. List of DoE results

10.4.1. Adipic acid

Table 10-4: Result data of DoE adipic acid.

Exp Name	Process settings				Results Mass Flow			
	Air throughput [kg/h]	Classifier opening [mm]	Agitator speed [rpm]	Feed rate [kg/h]	Residual moisture [w%]	Material output abs [g]	Experiment time [min]	Material output [kg/h]
	Process values				Results PSD			
	Actual air throughput [kg/h]	Dryer pressure drop [mmWS]	Inlet air temp. [°C]	Outlet air temp. [°C]	x ₅₀ [μm]	Material damage [-]	x' [μm]	n [-]
SFD 12 / DOE 02	400	60	420	1.19	0.07	350.3	31	0.678
	385	> 300	79.7	71.7	55.50	0.238	73.511	1.2004
SFD 13 / DOE 05	200	60	1400	1.19	0.05	367.9	30	0.736
	200	100	80.0	72.8	26.21	0.112	35.748	1.1865
SFD 14 / DOE 08	400	80	1400	1.19	0.06	457.16	38	0.722
	400	235	80.1	76.4	23.18	0.099	33.646	1.0486
SFD 15 / DOE 03	200	80	420	1.19	0.10	375.8	32	0.705
	200	115	79.8	73.1	114.24	0.477	140.912	1.2006
SFD 21 / DOE 12	400	80	420	5.34	0.06	994.1	16	3.728
	370	260	80.3	71.7	107.17	0.459	137.445	0.8837
SFD 23 / DOE 09	200	60	420	5.34	0.08	525.1	8	3.938
	200	150	80.1	71.1	194.88	0.835	225.035	1.4064
SFD 24 / DOE 14	400	60	1400	5.34	0.04	716.8	15	2.867
	350	> 300	79.9	74.0	41.81	0.179	61.511	0.9889
SFD 25 / DOE 15	200	80	1400	5.34	0.04	478.8	15	1.915
	200	70	79.3	70.0	50.92	0.227	67.233	1.1489
SFD 51 / DOE 19	300	60	910	3.26	0.07	422.1	12	2.111
	300	> 300	79.8	70.7	77.00	0.330	99.286	1.0821
SFD 52 / DOE 10	400	60	420	5.34	0.08	837.4	9	5.583
	325	> 300	79.9	72.4	143.91	0.617	173.318	1.2087
SFD 53 / DOE 13	200	60	1400	5.34	0.04	431.5	15	1.726
	200	180	80.2	71.2	28.89	0.124	37.709	1.1465
SFD 54 / DOE 17	300	60	910	3.26	0.04	638.4	15	2.554
	300	> 300	80.1	75.1	54.22	0.232	76.696	1.0398
SFD 56 / DOE 04	400	80	420	1.19	0.08	345.8	23	0.943
	308	> 300	80.0	73.8	91.70	0.393	121.364	0.8787
SFD 57 / DOE 11	200	80	420	5.34	0.10	1111.3	16	4.167
	200	230	80.1	68.3	200.17	0.858	222.577	1.6908
SFD 58 / DOE 16	400	80	1400	5.34	0.02	1055.9	17	3.727
	311	> 300	79.2	73.3	31.56	0.135	43.084	1.1673
SFD 59 / DOE 07	200	80	1400	1.19	0.03	209.7	28	0.449
	200	180	80.1	74.3	28.45	0.122	39.781	1.0745
SFD 60 / DOE 06	400	60	1400	1.19	0.06	434.8	32	0.815
	321	> 300	79.8	75.3	70.38	0.301	97.343	0.9529
SFD 61 / DOE 18	300	60	910	3.26	0.04	618.3	17	2.182
	300	> 300	79.8	74.2	59.46	0.255	85.988	0.9235
SFD 62 / DOE 01	200	60	420	1.19	0.03	290.3	24	0.726
	200	210	79.8	75.1	154.18	0.661	182.573	1.0475

10.4.2. Ibuprofen

Table 10-5: Result data of DoE ibuprofen.

Exp Name	Process settings				Results Mass Flow			
	Air throughput [kg/h]	Classifier opening [mm]	Agitator speed [rpm]	Feed rate [kg/h]	Residual moisture [w%]	Material output abs [g]	Experiment time [min]	Material output [kg/h]
	Process values				Results PSD			
	Actual air throughput [kg/h]	Dryer pressure drop [mmWS]	Inlet air temp. [°C]	Outlet air temp. [°C]	x ₅₀ [μm]	Material damage [-]	x' [μm]	n [-]
SFD 27 / DOE IP03	200	80	420	0.98	0.05	235	28	0.613
	200	60	70.0	57.8	30.32	0.888	38.690	1.6657
SFD 28 / DOE IP04	400	80	420	0.98	0.04	355.9	30	0.712
	400	195	70.1	62.5	26.69	0.782	33.543	1.7341
SFD 29 / DOE IP12	400	80	420	3	0.03	779.6	16	2.924
	400	210	70.0	50.7	26.90	0.788	33.714	1.7566
SFD 30 / DOE IP18	300	60	910	1.95	0.03	491	23	1.281
	300	190	69.6	58.4	27.49	0.805	34.594	1.7367
SFD 31 / DOE IP06	400	60	1400	0.98	0.02	302.7	26	0.699
	400	> 300	69.9	61.0	23.26	0.682	29.116	1.7408
SFD 32 / DOE IP13	200	60	1400	3	0.02	254.4	17	0.898
	200	125	69.9	40.9	28.39	0.832	35.702	1.7308
SFD 33 / DOE IP10	400	60	420	3	0.03	449.2	18	1.497
	400	> 300	69.7	52.9	22.03	0.645	27.300	1.8500
SFD 34 / DOE IP01	200	60	420	0.98	0.01	298.8	30	0.598
	200	90	70.1	60.1	26.84	1.079	34.162	1.6494
SFD 35 / DOE IP02	400	60	420	0.98	0.03	246.7	31	0.477
	400	300	70.0	64.4	20.48	0.600	25.524	1.7827
SFD 36 / DOE IP14	400	60	1400	3	0.03	713.8	22	1.947
	400	> 300	69.9	58.0	22.17	0.650	27.595	1.8197
SFD 37 / DOE IP19	300	60	910	1.95	0.02	604.2	19	1.908
	300	200	69.8	51.1	26.75	0.784	33.528	1.7606
SFD 38 / DOE IP09	200	60	420	3	0.04	510.7	11	2.786
	200	105	70.0	39.9	28.33	0.830	35.722	1.7148
SFD 39 / DOE IP08	400	80	1400	0.98	0.02	183.3	24	0.458
	400	240	70.0	65.2	20.15	0.590	25.292	1.7576
SFD 40 / DOE IP07	200	80	1400	0.98	0.02	353.3	31	0.684
	200	70	70.0	59.6	28.46	0.834	36.059	1.6963
SFD 41 / DOE IP11	200	80	420	3	0.02	662.5	18	2.208
	200	70	70.0	40.5	30.43	0.892	38.571	1.6972
SFD 42 / DOE IP16	400	80	1400	3	0.03	522.7	16	1.960
	400	230	70.0	54.3	23.70	0.694	29.732	1.7689
SFD 43 / DOE IP15	200	80	1400	3	0.15	590.8	18	1.969
	200	90	69.4	42.9	30.59	0.896	38.854	1.6874
SFD 44 / DOE IP05	200	60	1400	0.98	0.02	284.7	22	0.766
	200	120	69.5	59.0	28.99	0.849	36.677	1.7334
SFD 45 / DOE IP17	300	60	910	1.95	0.04	405.17	20	1.216
	300	245	70.0	58.4	26.41	0.774	33.063	1.7606

10.4.3. Heat Influence (Lactose)

Table 10-6: Result data of DoE heat influence (lactose).

Exp Name	Process settings				Results Mass Flow			
	Air throughput [kg/h]	Classifier opening [mm]	Agitator speed [rpm]	Feed rate [kg/h]	Residual moisture [w%]	Material output abs [g]	Experiment time [min]	Material output [kg/h]
	Process values				Results PSD			
	Actual air throughput [kg/h]	Dryer pressure drop [mmWS]	Inlet air temp. [°C]	Outlet air temp. [°C]	x ₅₀ [μm]	Material damage [-]	x' [μm]	n [-]
SFD 75 / DOE TL01	200	60	910	3	3.86	855.2	18	2.851
	200	60	59.6	48.0	26.19	1.362	33.111	1.5291
SFD 76 / DOE TL03	400	60	910	3	4.06	1242.9	21	3.551
	400	240	59.9	52.9	51.41	2.673	66.840	1.4834
SFD 77 / DOE TL 05	300	70	910	3	4.06	1218.7	25	2.925
	300	150	70.0	61.4	37.29	1.939	46.597	1.6766
SFD 78 / DOE TL 06	300	70	910	3	4.03	1140.4	21	3.258
	300	140	69.9	57.4	37.07	1.928	46.183	1.6328
SFD 79 / DOE TL04	400	80	910	3	4.14	1530.8	24	3.827
	400	235	80.0	68.4	63.23	3.288	81.919	1.5204
SFD 80 / DOE TL02	200	80	910	3	3.94	1064.2	24	2.661
	200	60	79.8	68.0	32.26	1.678	41.129	1.5571
SFD 81 / DOE TL 07	300	70	910	3	4.14	1111.8	20	3.335
	300	140	70.0	59.0	41.63	2.165	51.975	1.6609

10.5. Result Data of Additional Experiments

Table 10-7: Result data of influence of surfactant, benzoic acid, salicylic acid, acetyl salicylic acid and flour.

Exp Name	Process settings				Results Mass Flow			
	Air throughput [kg/h]	Classifier opening [mm]	Agitator speed [rpm]	Dryer pressure drop [mmWS]	Residual moisture [w%]	Material output abs [g]	Experiment time [min]	Material output [kg/h]
	Process values				Results PSD			
	Feed rate [kg/h]	Feed concentration [wt%]	Inlet air temp. [°C]	Outlet air temp. [°C]	x ₅₀ [μm]	Material damage [-]	x' [μm]	n [-]
SFD 46 Ibu/surfactant 0.8wt%	400	80	420	240	0.07	183.6	20	0.551
	0.98	40	70.0	63.6	31.43	0.921	39.898	1.6879
SFD 47 Ibu/surfactant 0.8wt%	200	80	1400	72	0.05	68.6	19	0.217
	0.98	40	70.0	62.7	27.34	0.801	34.898	1.6592
SFD 48 Ibu/surfactant 0.8wt%	400	80	1400	240	Experiment hat to be stopped. No result data.			
	3.00	40	70.0	59.3				
SFD 67 Benzoic acid	400	80	1400	230	0.03			
	3	67	80.0	66.9	35.62	0.060	49.798	1.3925
SFD 69 Salicylic acid	400	80	420	> 300	0.03			
	4	69	80.0	65.6	84.63	0.181	119.143	0.8006
SFD 83 Acetylsalicylic acid	200	80	1400	125	0.06			
	2	69	80.0	63.2	73.66	0.361	94.233	0.9363
SFD 68 flour fine flour coarse	400	80	1400	300	5.12			
	N.A.	54	70.0	46.5	134.46	0.854	191.576	1.1565
					838.27	5.323	936.253	4.3377

10.6. List of DoE analyses

10.6.1. DoE analyses adipic acid

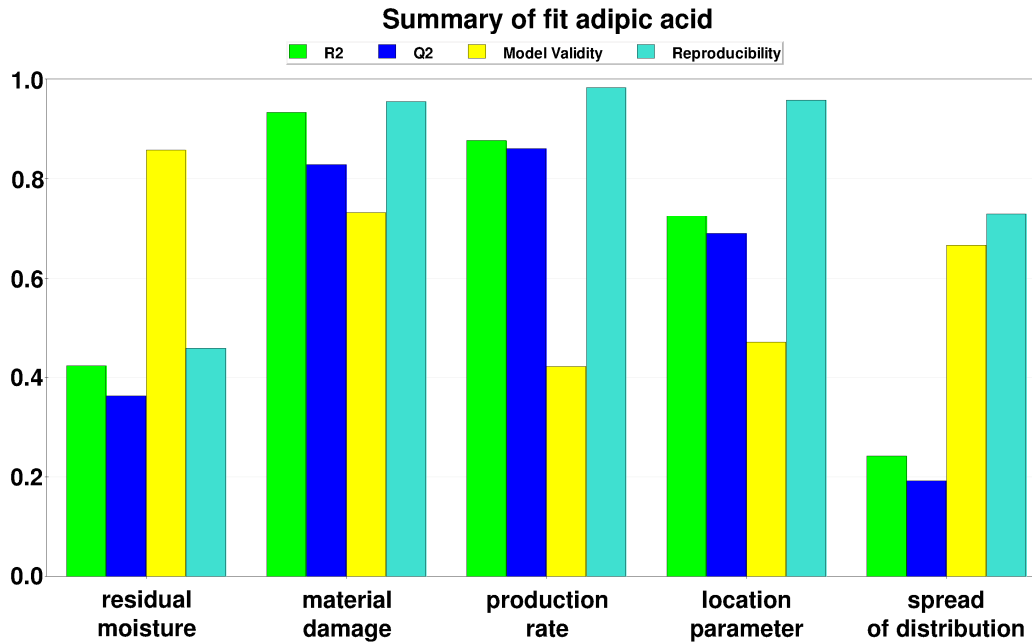


Figure 10-1: Model performance indicator of adipic acid. On the x-axis the responses are listed and on the y-axis the magnitude of model quality parameter. Generally high values indicate a good model.

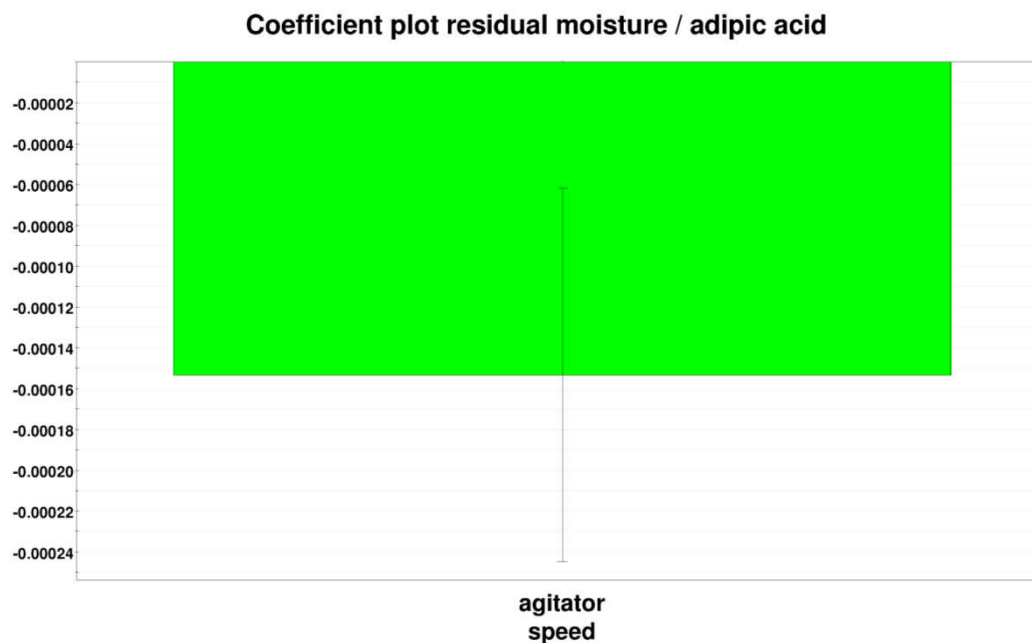


Figure 10-2: Adipic acid. Coefficient plot for residual moisture. Larger error bars than green bars indicate statistical insignificance of the factor.

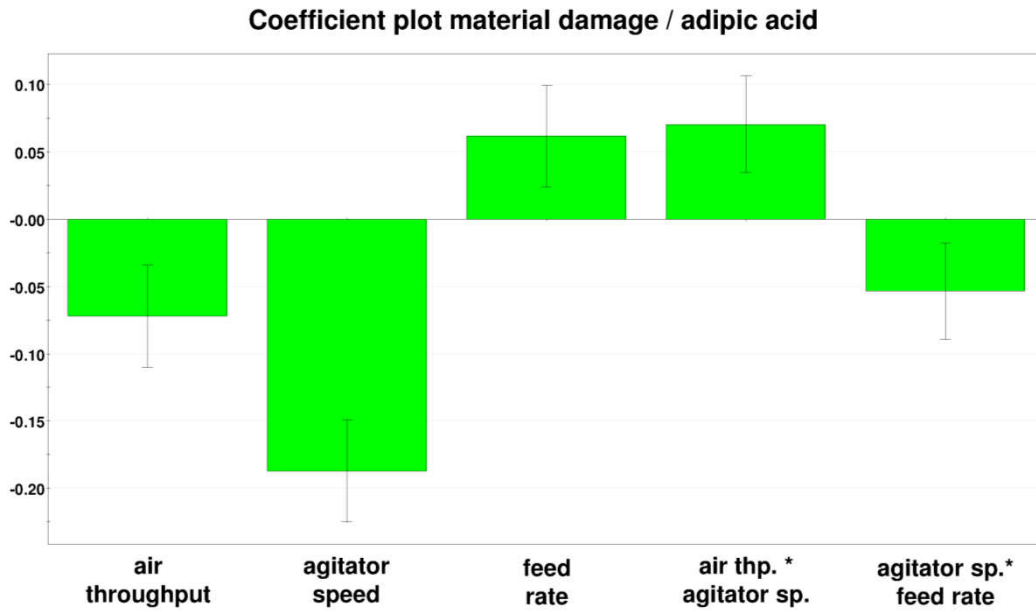


Figure 10-3: Adipic acid. Coefficient plot for material damage. Larger error bars than green bars indicate statistically insignificance of the factor.

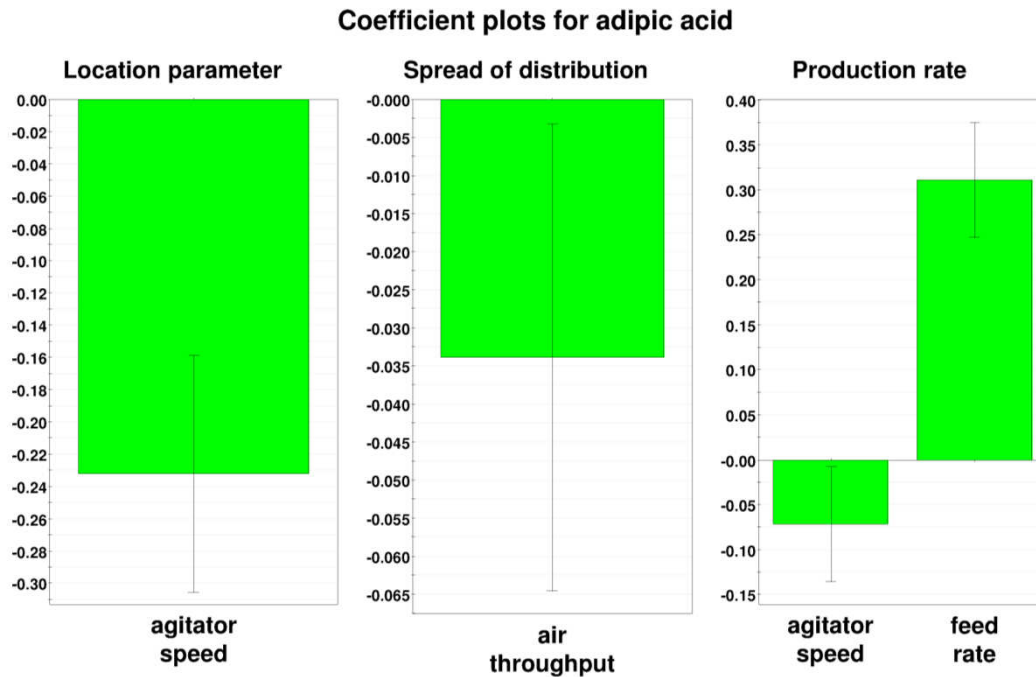


Figure 10-4: Adipic acid. Coefficient plot for location parameter, spread of distribution and product output. Larger error bars than green bars indicate statistically insignificance of the factor.

10.6.2. DoE analyses for Ibuprofen

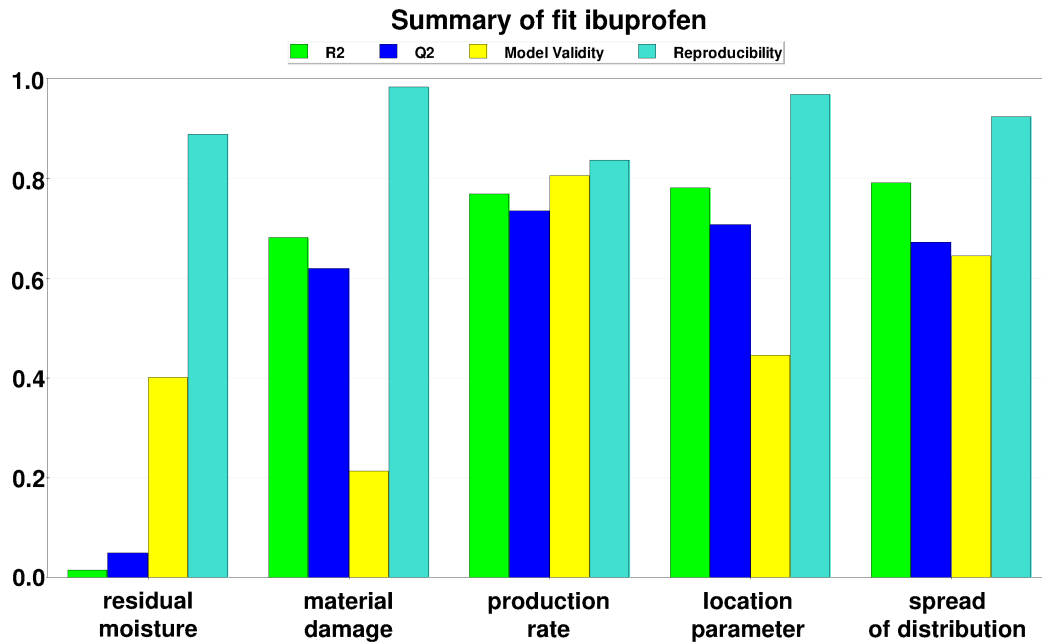


Figure 10-5: Model performance indicator of ibuprofen. On the x-axis the responses are listed and on the y-axis the magnitude of model quality parameter. Generally high values indicate a good model.

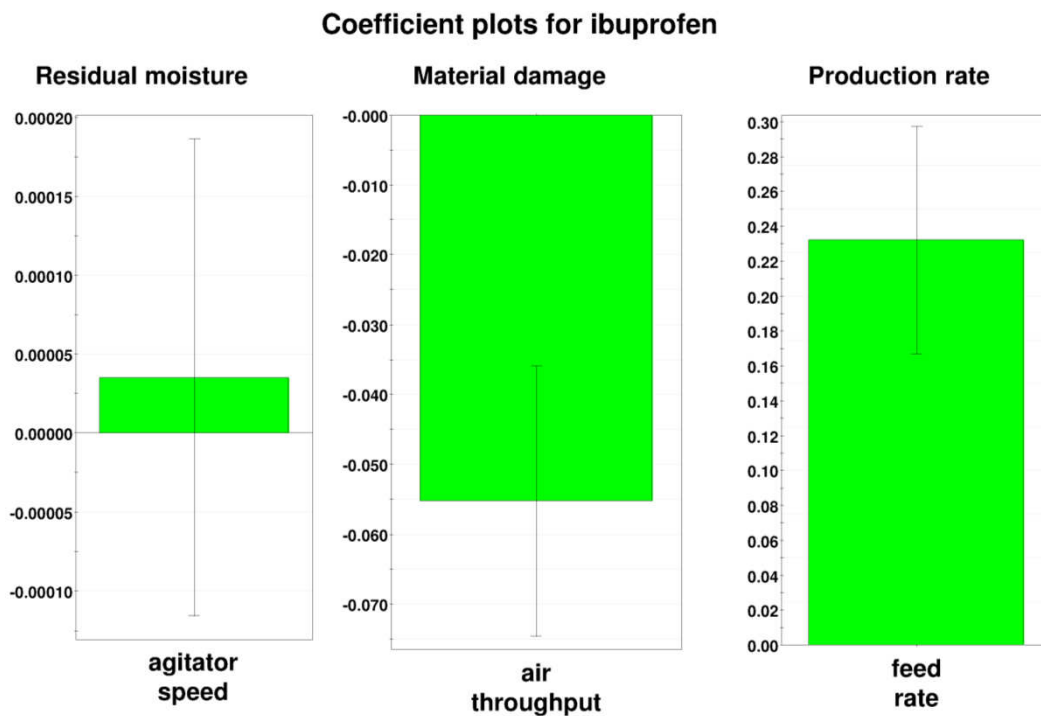


Figure 10-6: Ibuprofen. Coefficient plot for residual moisture, material damage and product output. Larger error bars than green bars indicate statistical insignificance of the factor.

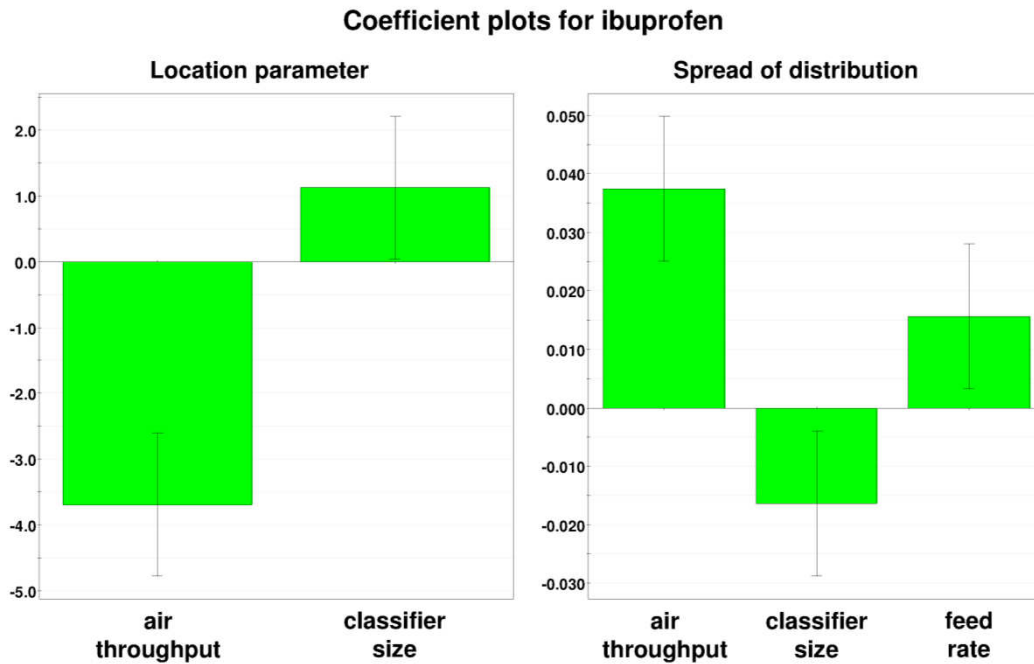


Figure 10-7: Ibuprofen. Coefficient plot for location parameter and spread of distribution. Larger error bars than green bars indicate statistical insignificance of the factor.

10.6.3. DoE analyses for heat influence (Lactose)

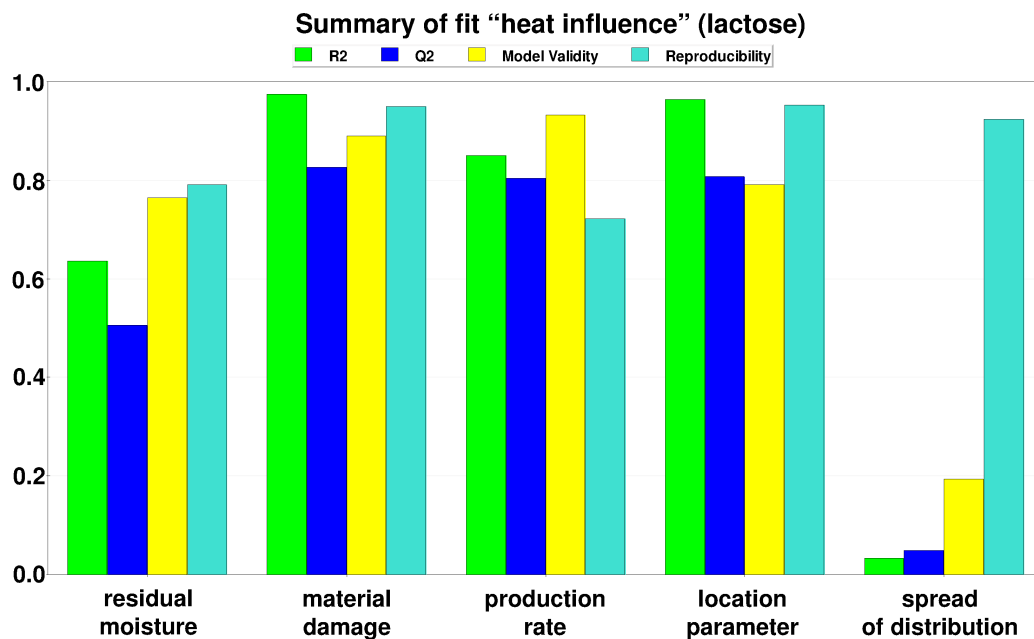


Figure 10-8: Model performance indicator of lactose. On the x-axis the responses are listed and on the y-axis the magnitude of model quality parameter. Generally high values indicate a good model.

Coefficient plots for lactose

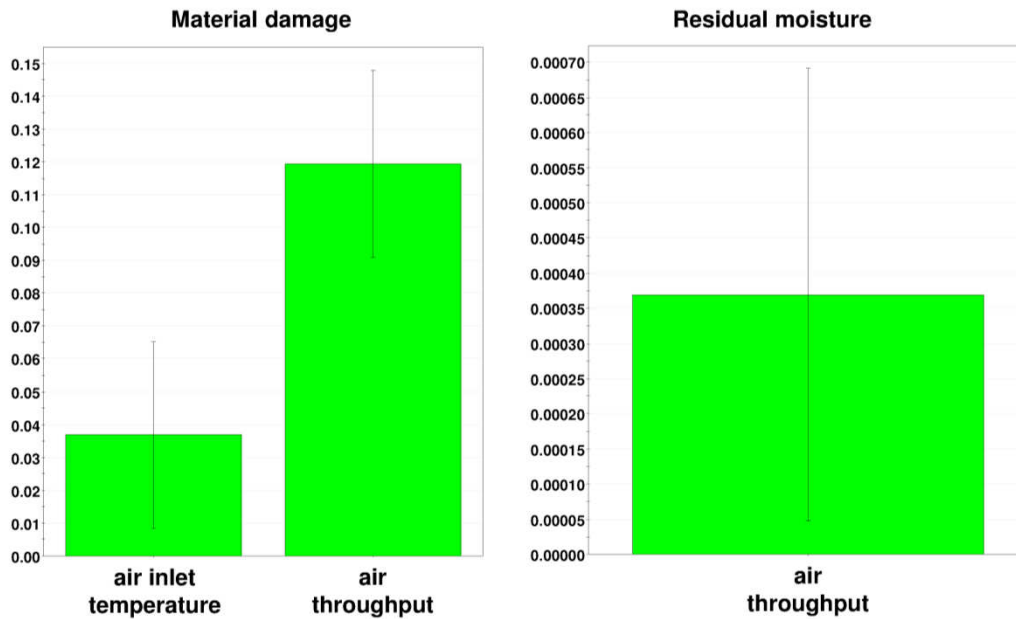


Figure 10-9: Lactose. Coefficient plot for material damage and residual moisture. Larger error bars than green bars indicate statistical insignificance of the factor.

Coefficient plots for lactose

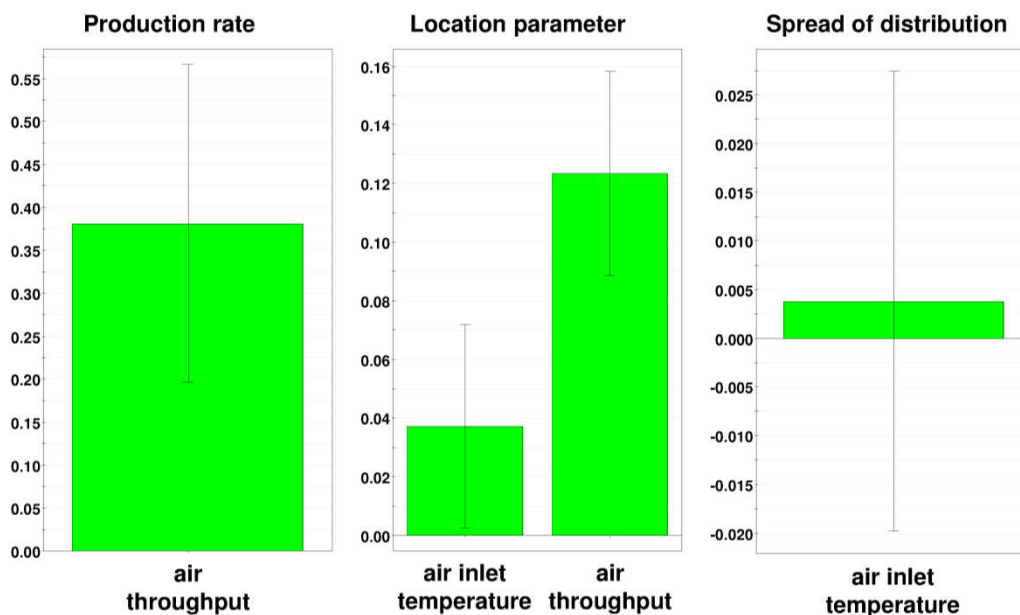


Figure 10-10: Lactose. Coefficient plot for production rate, location parameter and spread of distribution. Larger error bars than green bars indicate statistical insignificance of the factor.

10.7. Comparison of Calculated Outlet Temperature to Experimental Data

Table 10-8: Calculated water load of the product particle X_{out} .

Case	$T_{Environment}$ [°C]	ϕ [%]	m_{Air} [kg/h]	m_{Feed} [kg/h]	w_{Solid} [wt%]	T_{in} [°C]	T_{out} [°C]	X_{out} [-]
SFD62/DOE01	27.1	49.5	200	1.19	90	79.8	75.1	-0.179
SFD12/DOE02	24.3	40.8	385	1.19	77	79.7	71.7	-1.035
SFD15/DOE03	25.5	37.4	200	1.19	77	79.8	73.1	-0.221
SFD56/DOE04	25.6	48.5	308	1.19	77	80.0	73.8	-0.494
SFD13/DOE05	26.2	35.7	200	1.19	84	80.0	72.8	-0.324
SFD60/DOE06	24.8	54.3	321	1.19	77	79.8	75.3	-0.277
SFD59/DOE07	28.0	42.3	200	1.19	90	80.1	74.3	-0.274
SFD14/DOE08	25.5	37.4	400	1.19	90	80.1	76.4	-0.401
SFD23/DOE09	26.6	49.9	200	5.34	90	80.1	71.1	-0.006
SFD52/DOE10	26.0	50.6	325	5.34	84	79.9	72.4	0.016
SFD57/DOE11	27.1	44.5	200	5.34	84	80.1	68.3	0.019
SFD21/DOE12	25.1	55.9	370	5.34	77	80.3	71.7	0.025
SFD53/DOE13	26.6	49.1	200	5.34	90	80.2	71.2	-0.006
SFD24/DOE14	26.0	52.3	350	5.34	90	79.9	74.0	-0.027
SFD25/DOE15	26.6	49.7	200	5.34	90	79.3	70.0	-0.013
SFD58/DOE16	27.1	44.0	311	5.34	90	79.2	73.3	-0.008
SFD54/DOE17	26.7	46.4	300	3.26	90	80.1	75.1	-0.055
SFD61/DOE18	26.7	49.6	300	3.26	84	79.8	74.2	-0.008
SFD51/DOE19	24.9	52.6	300	3.26	77	79.8	70.7	-0.096

Table 10-9: List of outlet temperature data for DOE Adipic acid.

Case	T _{Environment} [°C]	φ [%]	m _{Air} [kg/h]	m _{Feed} [kg/h]	w _{Solid} [wt%]	T _{in} [°C]	T _{out} measured [°C]	T _{out} calculated [°C]
SFD62/DOE01	27.1	49.5	200	1.19	90	79.8	75.1	77.2
SFD12/DOE02	24.3	40.8	385	1.19	77	79.7	71.7	77.4
SFD15/DOE03	25.5	37.4	200	1.19	77	79.8	73.1	75.4
SFD56/DOE04	25.6	48.5	308	1.19	77	80.0	73.8	77.2
SFD13/DOE05	26.2	35.7	200	1.19	84	80.0	72.8	76.5
SFD60/DOE06	24.8	54.3	321	1.19	77	79.8	75.3	77.1
SFD59/DOE07	28.0	42.3	200	1.19	90	80.1	74.3	77.6
SFD14/DOE08	25.5	37.4	400	1.19	90	80.1	76.4	78.9
SFD23/DOE09	26.6	49.9	200	5.34	90	80.1	71.1	71.6
SFD52/DOE10	26.0	50.6	325	5.34	84	79.9	72.4	72.0
SFD57/DOE11	27.1	44.5	200	5.34	84	80.1	68.3	67.5
SFD21/DOE12	25.1	55.9	370	5.34	77	80.3	71.7	71.2
SFD53/DOE13	26.6	49.1	200	5.34	90	80.2	71.2	71.6
SFD24/DOE14	26.0	52.3	350	5.34	90	79.9	74.0	74.9
SFD25/DOE15	26.6	49.7	200	5.34	90	79.3	70.0	70.8
SFD58/DOE16	27.1	44.0	311	5.34	90	79.2	73.3	73.7
SFD54/DOE17	26.7	46.4	300	3.26	90	80.1	75.1	76.4
SFD61/DOE18	26.7	49.6	300	3.26	84	79.8	74.2	74.4
SFD51/DOE19	24.9	52.6	300	3.26	77	79.8	70.7	72.6

10.8. MatLab Code for equilibrium residual moisture

```

%% Mass and Energybalance for Dryer
% Using this program the equilibrium residual moisture of drying goods can
% be calculated.
% To calculated physical properties Antoine and Langmuir equation are used.
%% Input Variables
clear

% Parameter:
% Parameter can either be a discreet value or a vector a values
GasFlux = [400 300 200 100]; %[kg/h], Air throughput, Flux of drying air
InletTemp = 60; %[°C], Inlet temperature of drying air
MinConc = 20; %[wt%], Minimum solid concentration
MaxConc = 100; %[wt%], Maximum solid concentration
MinFeed = 0; %[kg/h], Minimum feed flow
MaxFeed = 10; %[kg/h], Maximum feed flow
crit = 2; %[wt%], Critical moisture level
resolution = 2;
SolidConc = linspace(MinConc, MaxConc, resolution*(MaxConc-MinConc+1));
%[wt%],Solid concentration of feed
FeedFlux = linspace(MinFeed, MaxFeed, resolution*(MaxFeed-MinFeed+1));
%[kg/h],Feed flux
Hloss = 150; %[kJ/h] Heat loss of dryer
TF = 1; %Temperature Faktor = TSolid/TGas describes the temperature ratio of
product streams
GasMM = 28.9; %[g/mol] Molar mass of the Gas ... Air
FluidMM = 18; %[g/mol] Molar mass of the evaporative Fluid ... Water

% Environment Data:
% Environment data or sate of room air
RoomHum = 50; %[%], Relative humidity at room temperature
RoomTemp = 24; %[°C], Room temperature
RoomPres = 990; %[mbar] or [hPa], Static air pressure in room

% Properties of Gas, Liquid and Solid
cpSolid = 1.197; %[kJ/(kg*K)], Heat capacity of adipic acid
cpLiquid = 4.182; %[kJ/(kg*K)], Heat capacity of water
cpVapor = 2.012; %[kJ/(kg*K)], Heat capacity of water vapor
cpGas = 1.0069; %[kJ/(kg*K)], Heat capacity of air
hlv = 2501; %[kJ/kg], Latent heat of evaporication at 0°C of water

% Equation of State
% Vapor pressure by Antoine
% log(PS[kPa]) = A-B/(C+T[K])
AT1 = [7.19622 1730.63 -39.724]; %Antoine parameter at room temperature
AT2 = [7.19951 1730.63 -39.724]; %Antoine parameter at 70.10°C
% Equilibrium distribution of evaporative by Langmuir
% X[kg/kg] = X0*(K*ExHum*PS)/(1+K*ExHum*PS)
% ExHum = Relative humidity of exhaust gas, X0 and K are system parameter.
% Values are for pressure in Pascal
X0 = 0.103186753085414;
08.02.13 16:27 H:\ML_drying_capacity.m 2 of 5
K = 0.000124313770396854;

%% Calculation
SolidFlux = FeedFlux.*(SolidConc/100);
Xin = 100./SolidConc-1;
PSRoom = 10^(AT1(1)-AT1(2)/(AT1(3)+RoomTemp+273.15))*1000; %[Pa]
RoomHum = RoomHum/100; %[1]
RoomPres = RoomPres*100; %[Pa]
Yin = FluidMM/GasMM * (RoomHum*PSRoom)/(RoomPres-RoomHum*PSRoom);
for at = 1:length(GasFlux);
for mf = 1:length(FeedFlux);
for sc = 1:length(SolidConc);
Xout1 = 1; %Start condition
Xout2 = 0; %Start condition
count = 0;
while abs((Xout1-Xout2)/Xout1) > 0.00001
Xout1 = Xout2;
hxlin = cpSolid*RoomTemp+Xin(sc)*cpLiquid*RoomTemp;
hylin = cpGas*InletTemp+Yin*(hlv+cpVapor*InletTemp);
Hin = hxlin*SolidFlux(mf,sc)+hylin*GasFlux(at)-Hloss;

```

```
dW = SolidFlux(mf,sc)*(Xin(sc)-Xout1);
Yout = Yin+dW/GasFlux(at);
OutletTemp = (Hin-GasFlux(at)*Yout*hlv)/(SolidFlux(mf,sc)*TF*(cpSolid-
Xout1*cpLiquid)+GasFlux(at)*(cpGas+Yout*cpVapor));
PSEx = 10^(AT2(1)-AT2(2)/(AT2(3)+OutletTemp+273.15))*1000; %[Pa]
ExHum = (RoomPres/PSEx)*(Yout*GasMM)/(FluidMM+Yout*GasMM);
Xout2 = X0*(K*ExHum*PSEx)/(1+K*ExHum*PSEx);
count = count+1;
end
RM = Xout2/(Xout2+1);
result(mf,sc,at) = RM;
end
end
end

%% Graph: Plot 3D figure
gf = 1; %Chosen gas flux from input array
X=SolidConc;
Y=FeedFlux;
V = [crit crit];
ColorSet = varycolor(length(GasFlux));
TitleFontSize = 30;
AxisFontSize = 28;
FigFontSize = 24;
figure
08.02.13 16:27 H:\ML_drying_capacity.m 3 of 5
subplot(1,2,1)
Z=result(:, :,1)*100; %RM content in [%]
mesh(X,Y,Z)
hold on
[C,H]=contour3(X,Y,Z,V);
set(H, 'LineStyle', '-', 'LineWidth', 3)
hold off
XLIM([MinConc, MaxConc]);
YLIM([MinFeed, MaxFeed]);
set(gca, 'FontSize', FigFontSize);
title('Residual moisture level', 'FontSize', TitleFontSize);
xlabel('Solid conc. [wt%]', 'FontSize', AxisFontSize);
ylabel('Feed rate [kg/h]', 'FontSize', AxisFontSize);
zlabel('Residual moisture content [wt%]', 'FontSize', AxisFontSize);
subplot(1,2,2)
Z=result(:, :,3)*100; %RM content in [%]
mesh(X,Y,Z)
hold on
[C,H]=contour3(X,Y,Z,V);
set(H, 'LineStyle', '-', 'LineWidth', 3)
hold off
XLIM([MinConc, MaxConc]);
YLIM([MinFeed, MaxFeed]);
set(gca, 'FontSize', FigFontSize);
title('Residual moisture level', 'FontSize', TitleFontSize);
xlabel('Solid conc. [wt%]', 'FontSize', AxisFontSize);
ylabel('Feed rate [kg/h]', 'FontSize', AxisFontSize);
zlabel('Residual moisture content [wt%]', 'FontSize', AxisFontSize);
```

10.9. MatLab Code for evaporation rate and drying time

```
%% Evaporation Rate and Drying Kinetics
%Using mass and energy balances as well as equations of state the drying
%conditions are calculated.
%In that environment the average drying rate and the drying kinetics are
%calculated using Nu correlations formulated by Ranz and Watano.
%% Input Variables
% Input Data in SI Units
clear
% Parameter:
% Parameter can either be a discreet value or a vector a values
GasFlux = 400; %[kg/h], Air throughput, Flux of drying air
InletTemp = 80; %[°C], Inlet temperature of drying air
AgRev = 1400; %[rps], Agitator speed
```

```

SolidConc = 70; %[-], Solid concentration of feed
FeedFlux = 1; %[kg/h], Feed flux
Hloss = 150; %[kJ/h] Heat loss of dryer
g = 9.81; %[m/s2], Earth gravity
TF = 1;
% Environment Data:
% Environment data or sate of room air
RoomHum = 50; %[%], Relative humidity at room temperature
RoomTemp = 24; %[°C], Room temperature
RoomPres = 990; %[mbar] or [hPa], Static air pressure in room
% Properties of Gas, Liquid and Solid
cpSolid = 1.197; %[kJ/(kg*K)], Heat capacity of adipic acid
RhoP = 1400; %[kg/m3], Density of adipic acid
cpLiquid = 4.182; %[kJ/(kg*K)], Heat capacity of water
hlv = 2501; %[kJ/kg], Latent heat of evaporation at 0°C of water
FluidMM = 18; %[g/mol] Molar mass of the evaporative Fluid ... Water
cpVapor = 1.950; %[kJ/(kg*K)], Heat capacity of water vapor
cpGas = 1.0078; %[kJ/(kg*K)], Heat capacity of air
GasMM = 28.9; %[g/mol] Molar mass of the Gas ... Air
CondGas = 30.225; %[mW/(m*K)], Conductivity of air
ViscGas = 21.009; %[μPa*s], Dynamic viscosity of air
PrAir = 0.7018; %[-], Prandtl Number for air
% Equation of State
% Vapor pressure by Antoine
% log(PS[kPa]) = A-B/(C+T[K])
AT1 = [7.19622 1730.63 -39.724]; %Antoine parameter at room temperature
AT2 = [7.19951 1730.63 -39.724]; %Antoine parameter at 70.10°C
% Equilibrium distribution of evaporative by Langmuir
% X[kg/kg] = X0*(K*ExHum*PS)/(1+K*ExHum*PS)
% ExHum = Relative humidity of exhaust gas, X0 and K are system parameter.
% Values are for pressure in Pascal
X0 = 0.103186753085414;
K = 0.000124313770396854;
% Unit of input data is changed into SI Unit
SolidConc = SolidConc/100;
19.02.13 12:16 H:\matlab\ML_DryingKinetic.m 2 of 4
RoomHum = RoomHum/100;
RoomPres = RoomPres*100;
CondGas = CondGas/103;
ViscGas = ViscGas/106;
cpSolid = cpSolid*103;
cpLiquid = cpLiquid*103;
hlv = hlv*103;
cpVapor = cpVapor*103;
cpGas = cpGas*103;
Hloss = Hloss*103;
AgRev = AgRev/60;
% Particle size, particle size distribution and particle surface
% for sperical particles
MinSize = 1; %[μm]
MaxSize = 1000; %[μm]
Points = 50; % Number of points of log size class vector
PSD = logspace(log10(MinSize),log10(MaxSize),Points);
sizePSD = length(PSD);
PSD = PSD';
% Calculation of PSD q3 and Q3 by RRSB distribution / PSD in [μm]
% Location parameter x' and spread of distribution n are from adipic acid
% feed. Parameters are fitted by least sugare sum.
% Q3(x) = 1 - exp(-(x/x')^n)
location = 264.948; %[μm]
spread = 2.0953; %[-]
PSD(:,3) = 1-exp(-(PSD(:,1)./location).^spread);
PSD(2:Points,2) = PSD(2:Points,3)-PSD(1:Points-1,3);
PSD(1,2) = PSD(1,3);
PSD(:,1) = PSD(:,1)/106;
% Particle surface for sperical particle [m2]
PSD(:,4) = PSD(:,1).^2*pi;
%% Drying conditions
SolidFlux = FeedFlux*SolidConc;
Xin = 1/SolidConc-1;
PSRoom = 10^(AT1(1)-AT1(2)/(AT1(3)+RoomTemp+273.15))*1000; %[Pa]
Yin = FluidMM/GasMM * (RoomHum*PSRoom)/(RoomPres-RoomHum*PSRoom);
Xout1 = 1; %Start condition
  
```

```

Xout2 = 0; %Start condition
while abs((Xout1-Xout2)/Xout1) > 0.00001
Xout1 = Xout2;
hxlin = cpSolid*RoomTemp+Xin*cpLiquid*RoomTemp;
hylin = cpGas*InletTemp+Yin*(hlv+cpVapor*InletTemp);
Hin = hxlin*SolidFlux+hylin*GasFlux-Hloss;
dW = SolidFlux*(Xin-Xout1);
Yout = Yin+dW/GasFlux;
OutletTemp = (Hin-GasFlux*Yout*hlv)/(SolidFlux*TF*(cpSolid-
Xout1*cpLiquid)+GasFlux*
(cpGas+Yout*cpVapor));
PSEx = 10^(AT2(1)-AT2(2))/(AT2(3)+OutletTemp+273.15))*1000; %[Pa]
19.02.13 12:16 H:\matlab\ML_DryingKinetic.m 3 of 4
ExHum = (RoomPres/PSEx)*(Yout*GasMM)/(FluidMM+Yout*GasMM);
Xout2 = X0*(K*ExHum*PSEx)/(1+K*ExHum*PSEx);
end
hylout = cpGas*OutletTemp+Yout*(hlv+cpVapor*OutletTemp);
Tcalc = OutletTemp;
Hum = ExHum;
while Hum < 1;
Ycalc = (hylout-cpGas*Tcalc)/(hlv+cpVapor*Tcalc);
PScalc = 10^(AT2(1)-AT2(2))/(AT2(3)+Tcalc+273.15))*1000;
Hum = (RoomPres/PScalc)*((Ycalc*GasMM)/(FluidMM+Ycalc*GasMM));
Tcalc = Tcalc-0.001; %Stepwise reduction of Tsat
end
Tbulb = Tcalc;
Xout = Xout2;
%% Properties of exhaust gas
% Gas velocity VelG
VolFlux = (((GasFlux/3.6)/GasMM)*8.314*(OutletTemp+273.15))/(RoomPres);
CrossA = 0.205^2*pi/4;
VelG = VolFlux/CrossA;
% Gas density
RhoGas = (GasFlux/3600)/VolFlux;
%% Nusselt number Ranz
% Calculation of terminal settling velocity --> PSD Column 5
for it1 = 1:sizePSD;
dpref = PSD(it1,1)*(RhoGas*(RhoP-RhoGas)*g/ViscGas^2)^(1/3);
tvref = (18/dpref^2 + (2.335-1.744)/dpref^0.5)^(-1);
tv = tvref/((RhoGas^2/(ViscGas*(RhoP-RhoGas)*g))^(1/3));
PSD(it1,5) = tv;
end
% Reynolds number --> PSD Column 6
PSD(:,6) = PSD(:,1).*PSD(:,5)*RhoGas/ViscGas;
% Prandtl number --> Column 7
for it2 = 1:sizePSD;
PSD(it2,7) = PrAir;
end
% Nusselt number according to Ranz
for it3 = 1:sizePSD;
PSD(it3,8) = 2 + 1.8 * PSD(it3,6)^(1/2)*PSD(it3,7)^(1/3);
end
% Heat-Transfer coefficient according to Ranz
PSD(:,9) = CondGas*PSD(:,8)./PSD(:,1);
%% Nusselt number Watano
% Nusselt number according to Watano, PSD in μm
for it4 = 1:sizePSD;
PSD(it4,10) = (29.96*PSD(it4,1)*10^6-0.027)*(VelG*exp(-
0.1*AgRev)*RhoGas/ViscGas)
19.02.13 12:16 H:\matlab\ML_DryingKinetic.m 4 of 4
^0.475;
end
% Heat-Transfer coefficient according to Ranz
PSD(:,11) = CondGas*PSD(:,10)./PSD(:,1);
%% Evaporation rate
HeatRanz = 0;
EvapRanz = 0;
MassRanz = 0;
HeatWatano = 0;
EvapWatano = 0;
MassWatano = 0;
for it5 = 1:sizePSD;
PSD(it5,12) = (PSD(it5,9)*(OutletTemp-Tbulb)/hlv); %Evaporation Rate Ranz [kg/

```

```

(m2*s)]
PSD(it5,13) = PSD(it5,12)*PSD(it5,4); %Mass Flux Ranz [kg/s]
PSD(it5,14) = (PSD(it5,11)*(OutletTemp-Tbulb)/hlv); %Evaporation Rate Watano
[kg/
(m2*s)]
PSD(it5,15) = PSD(it5,14)*PSD(it5,4); %Mass Flux Watano [kg/s]
HeatRanz = HeatRanz+PSD(it5,9)*PSD(it5,2);
EvapRanz = EvapRanz+PSD(it5,12)*PSD(it5,2);
MassRanz = MassRanz+PSD(it5,13)*PSD(it5,2);
HeatWatano = HeatWatano+PSD(it5,11)*PSD(it5,2);
EvapWatano = EvapWatano+PSD(it5,14)*PSD(it5,2);
MassWatano = MassWatano+PSD(it5,15)*PSD(it5,2);
end
%% Drying time
PSD(:,16) = (PSD(:,1).^3*pi)/6*RhoP;
PSD(:,17) = PSD(:,16).*Xin; %Mass of water for particle size fraction
PSD(:,18) = PSD(:,17)./PSD(:,13);
TimeRanz = 0;
for it6 = 1:sizePSD;
TimeRanz = TimeRanz+PSD(it6,18)*PSD(it6,2);
end
%% Printing the values
Tbulb %[°C]
HeatRanz %[W/(m2*K)]
HeatWatano %[W/(m2*K)]
EvapRanz*3600 %[kg/(m2*h)]
EvapWatano*3600 %[kg/(m2*h)]
TimeRanz %[s]

```